Janne Sorsanen

Assessment of realistic solar electricity production potential of grid-connected photovoltaic systems in Tapiola district

School of Electrical Engineering

Thesis submitted for examination for the degree of Master of Science in Technology.

Espoo 20.5.2015

Thesis supervisor:

Prof. Matti Lehtonen

Thesis advisors:

M.Sc. (Tech.) Osmo Huhtala

M.Sc. (Tech.) Risto Laurila

Aalto University
School of Electrical
Engineering

AALTO UNIVERSITY
SCHOOL OF ELECTRICAL ENGINEERING

ABSTRACT OF THE
MASTER'S THESIS

Author: Janne Sorsanen

Title: Assessment of realistic solar electricity production potential of grid-connected photovoltaic systems in Tapiola district

Date: 20.5.2015 Language: English Number of pages:10+96

Department of Electrical and Automation Engineering

Professorship: Power Systems Code: S-18

Supervisor: Prof. Matti Lehtonen

Advisors: M.Sc. (Tech.) Osmo Huhtala, M.Sc. (Tech.) Risto Laurila

The objective of this thesis was to assess realistic solar electricity production potential of grid-connected photovoltaic systems in Tapiola district. Furthermore, the goal was to model the energy balance of the buildings in the area. The thesis was carried out as part of the EUE (Energizing Urban Ecosystems) project founded by RYM Oy. The thesis was made for the new business unit of Fortum Oyj.

The realistic solar electricity production potential was evaluated based on solar radiation data provided by the city of Espoo. Three filters were generated in order to eliminate roof surface areas unsuitable for solar electricity production. The energy balance examinations were carried out based on the results of solar electricity production potential by exploiting load curves and index series calculation. Moreover, a model for solar electricity production in southern Finland was utilized in the thesis.

In the light of the results it turned out that almost one-sixth of the current electricity consumption in the Tapiola district could be satisfied by the solar electricity production. In addition, it was shown that especially shopping centres and office buildings are highly potential targets to be exploited for the solar electricity production.

Keywords: photovoltaic, solar, production, potential, grid-connected, energy balance

AALTO-YLIOPISTO
SÄHKOTEKNIIKAN KORKEAKOULU

DIPLOMITYÖN
TIIVISTELMÄ

Tekijä: Janne Sorsanen

Työn nimi: Realistisen aurinkosähkön tuotantopotentiaalin evaluointi verkkoonkytketyille aurinkosähköjärjestelmille Tapiolan aluella

Päivämäärä: 20.5.2015 Kieli: Englanti Sivumäärä:10+96

Sähkötekniikan ja automaation laitos

Professuuri: Sähköjärjestelmät Koodi: S-18

Valvoja: Prof. Matti Lehtonen

Ohjaajat: DI Osmo Huhtala, DI Risto Laurila

Tämän diplomityön tavoitteena oli määrittää realistinen aurinkosähkön tuotantopotentiaali verkkoonkytketyille aurinkosähköjärjestelmille Tapiolan alueella. Aurinkosähkön tuotantopotentiaaliin perustuen oli tavoitteena myös mallintaa alueen rakennusten energiatasetta. Työ tehtiin osana RYM Oy:n EUE-projektia (Energizing Urban Ecosystems) ja työn tilaajana oli Fortum Oyj:n New Business -yksikkö.

Realistista aurinkosähkön tuotantopotentiaalia selvitetiin Espoon kaupungilta saadun auringonsäteilydatan perusteella. Työn aikana realistista aurinkosähkön tuotantopotentiaalin määrittämistä varten kehitettiin kolme erillistä suodatinta eliminoimaan aurinkosähkölle kelpaamatonta kattopinta-alaa. Energiabalanssitarkastelut toteutettiin saatujen aurinkosähköpotentiaalitulosten perusteella kuormituskäyriä ja indeksisarjalaskentaa hyödyntäen. Lisäksi työssä sovellettiin Etelä-Suomen alueelle tehtyä aurinkosähkön tuotantomallia.

Tulosten valossa osoittautui, että lähes kuudesosa Tapiolan alueen tämänhetkisestä sähkönkulutuksesta kyettäisiin tuottamaan aurinkosähköjärjestelmillä. Lisäksi osoittautui, että etenkin kauppakeskukset ja toimistorakennukset ovat erittäin potentiaalisia kohteita hyödynnettäviksi aurinkosähkön tuotantoa varten.

Avainsanat: aurinkosähkö, tuotanto, potentiaali, verkkoonkytketty, energiatase

Preface

Firstly, I would like to thank my supervisor Matti Lehtonen for his guidance and support during the process. I would also like to express my gratitude to my advisors Osmo Huhtala (Fortum Oyj) and Risto Laurila (Fortum Oyj) for their advice and interest towards the topic of this thesis. In addition, I am thankful for all the help and expertise I received from the interviewees Eero Vartiainen (Fortum Oyj), Markus Andersén (Naps Solar Systems Oy) and Robert Eriksson (City of Espoo).

Completion of the thesis has required a lot of effort, but it has all been worth it. I would like to give a special word of thanks to my beloved wife Jenny for an endless amount of love and support along the journey. Finally, I want to express my most humble thanks to my parents Juhani and Anita and my twin brother Joni for always encouraging me to continue challenging myself in life.

Espoo, 17.5.2015

Janne Sorsanen

Contents

Symbols and abbreviations

Symbols

A	Curve fitting constant
α	Solar altitude angle / Temperature coefficient / Albedo (0,15)
$AM(number)$	Air mass
b	Subscript for buildings
β	Temperature coefficient / Temperature dependence coefficient of electricity use
$\cos(\varphi)$	Power factor
D	Diffuse radiation
δ	Solar declination
E_{AC}	Actual electrical energy delivered to the power grid
E_r	Annual energy of user group r
η	Photoconversion efficiency / Altitude angle above horizon
η_{inv}	Inverter conversion efficiency
FF	Fill factor
Φ	Solar zenith angle
G^*	Ideal global irradiation
G	Global radiation
$G_y(\beta, \alpha)$	Global irradiation at given orientation α and tilt angle β
h	Hour angle
I	Current / Load current / Direct radiation
i	Moment
I_{ac}	Output current of AC side
I_d	Diode current
I_D	Saturation current of diode
I_{dc}	Input current from DC side
I_L	Photo current
I_{MP}	Maximum power point current
I_O	Operating current
I_{SC}	Short-circuit current
I_{SH}	Shunt-leakage current
k	Boltzmann constant ($1,38 \times 10^{-23}\,\mathrm{J/^\circ K}$)
$K_\downarrow$	Incoming short-wave radiation
$K_r(n)$	Coincidence factor of user group r with n amount of objects
L	Local latitude
L_C	Capture losses
L_S	System losses
ω	Incidence angle of the sun
P	Power
P_in	Input power
$P_k(t)$	Power of user k at moment t

P_M^*	Maximum power of photovoltaic array under Standard Test Conditions
P_{MP}	Maximum power point power
PR	Performance ratio
P_{ri}	average hourly power of user group r at moment i
Ψ	View factor
Q	Charge of an electron ($1,6 \times 10^{-19}$ C)
$q_0(t)$	Use of electricity in normal outdoor temperature
Q_{ri}	External index of user group r at moment i
q_{ri}	Internal index of user group r at moment i
$q_{tod}(t)$	Measured electricity use at time t
r	User group
R_S	Series resistance
R_{SH}	Shunt resistance
S	Shadow (absence=1, presence=0)
T	Temperature
t	Time / Moment (1,..,8760)
τ	Transmissivity of shortwave radiation through vegetation
$\mathrm{t_{ssh}}$	Sunshine hour value
V	Voltage
v	Subscript for vegetation
V_{ac}	Output voltage of AC side
V_{dc}	Input voltage from DC side
V_{MP}	Maximum power point voltage
V_O	Operating voltage
V_{OC}	Open-circuit voltage
W_p	Peak watts
Y_a	Array yield
Y_f	Final yield
Y_r	Reference yield
z	Solar azimuth angle

Abbreviations

AC	Alternating current
AMR	Automatic Meter Reading
ASCII	American Standard Code for Information Interchange
CdS	Cadmium sulfide
CdTe	Cadmium telluride
CE	Conformité Européenne (European Conformity)
CEC	California Energy Commission
CO_2	Carbon dioxide
c-Si	Single-crystal silicon
$Cu(InGa)Se_2$	Copper indium gallium (di)selenide
$CuInSe_2$	Copper indium diselenide
DC	Direct current
EIA	U.S. Energy Information Association
ESRI	Environmental Systems Research Institute
EU	The European Union
EUE	Energizing Urban Ecosystems program
GaAs	Gallium arsenide
GaInP	Gallium indium phosphide
Ge	Germanium
GIS	Geographic Information System
GNU	Recursive acronym for "GNU's Not Unix"
H	Hydrogen
H_2O	Water
He	Helium
IEA	International Energy Agency
IEC 62109	Safety of power converters for use in photovoltaic power systems
IEEE-1547	Standard for Interconnecting Distributed Energy Resources with Electric Power Systems
LAS	Log ASCII Standard
LID	Light-induced degradation
MATLAB	Matrix laboratory
multi-Si	Multicrystalline silicon
NREL	National Renewable Energy Laboratory
O_2	Oxygen (dioxygen)
O_3	Ozone (trioxygen)
OECD	The Organisation for Economic Co-operation and Development
OSGeo	Open Source Geospatial Foundation
PR	Performance ratio
psh	Peak sun hours
PV	Photovoltaic
SEES	Solar Energy from Existing Structures
SRC	Standard reporting conditions

STC	Standard test conditions
S-W	Staebler-Wronski degradation
UL-1741	Standard for Safety Inverters, Converters Controllers and Interconnection System Equipment for Use with Distributed Energy Resources

1 Introduction

Solar energy forms the largest available energy source of all energy sources on the earth. The total energy input from the sun that reaches the ground surface is more than enough to meet the energy demand of the world. It is predicted that the total amount of insolation exceeds the global energy demand by a factor of 10 000. On the other hand, according to International Energy Agency (IEA) the whole energy demand of the world could be satisfied if only 4 % of the very dry desert areas of the world were utilized for solar electricity production. Moreover, generating electricity from solar radiation does not actually waste a finite source as is the case when for instance fossil fuels are burned for electricity generation. Figure 1 illustrates how the annual solar energy potential relates to other potentials of common established energy sources and global annual energy consumption. [1] [2]

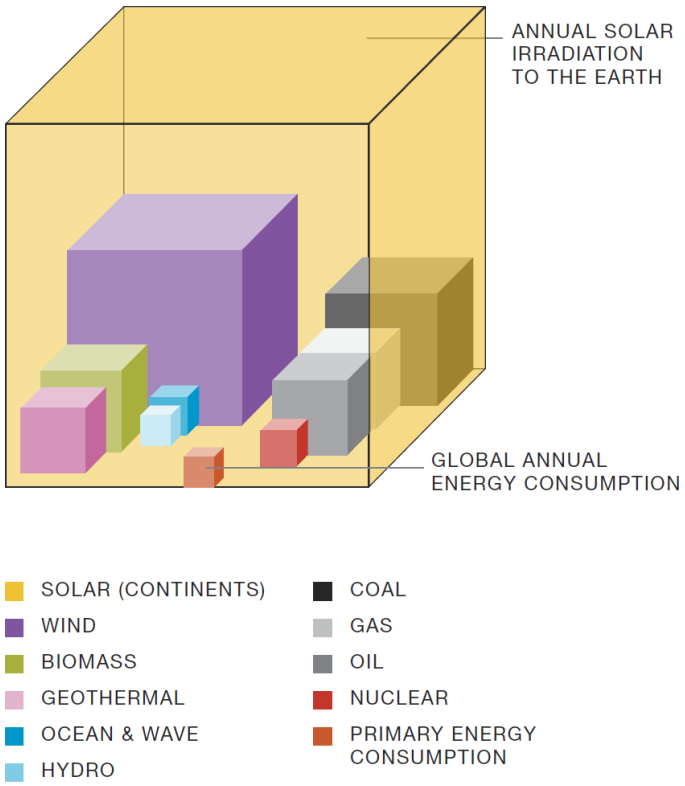

Figure 1: Annual solar irradiation potential in relation to established global energy resources and global annual energy consumption. [1]

Electricity is the world's fastest-growing form of energy, and the net electricity generation of the world is projected to increase from 20,2 trillion kilowatthours in 2012 to 39,0 trillion kilowatthours in 2040. Moreover, the electricity delivered to end users is predicted to grow by 2,2 percent annually from 2010 to 2040, whereas the average annual growth of all delivered energy sources is 1,4 percent. [3]

In 2010 non-OECD nations consumed 49 % of the world's total electricity supply. However, in 2040 the share of non-OECD nations is predicted to be 64 %. This

means that the share of OECD nations will decrease from 51 % to 36 % of the world's electricity consumption. The increased energy demand will create phenomenal opportunities to exploit renewable energy sources such as solar energy. Figure 2 shows the growth of net electricity generation and total delivered energy consumption from 1990 to 2010 and forecast till 2040 for both. Year 1990 is considered as a reference year, and it represents the index 1 in the graph. [3]

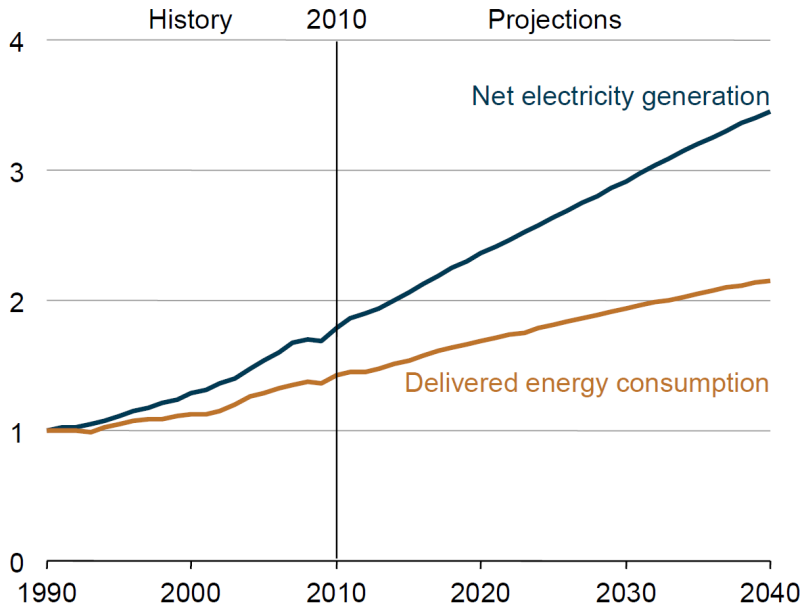

Figure 2: Growth in world electricity generation and total delivered energy consumption during years 1990–2035. Year 1990 is used as a reference year (index 1). [3]

Concerns about greenhouse gas emissions, their environmental impacts and security of energy supplies have driven governments around the world in decision-making in order to support renewable energy sources. As a result, renewable energy sources are projected to be the fastest-growing form of energy in the future. According to U.S. Energy Information Association (EIA) the share of renewable energy sources will grow an average of 2,8 % per year from 2010 to 2040. As a consequence of this, the share of renewable energy sources from the world's electricity generation will increase from 21 % in 2010 to 25 % in 2040. Hydropower and wind power will constitute approximately 80 % of the growth of renewable energy sources. However, the net solar electricity generation of the world is forecasted to grow from 34 billion kilowatthours in 2010 to 452 billion kilowatthours in 2040 which is equivalent to the average annual growth of 9,1 % [3]

As part of the Europe 2020 strategy, the European Commission has set the general objectives of the EU countries to combat climate change and increase energy efficiency. EU's overall objective is to reduce greenhouse gas emissions by 20 % below 1990 levels, and by up to 30 % if conditions are right. Share of renewable energy sources is to be increased by 20 %, and energy efficiency is to be increased by 20 %, which corresponds to a reduction in energy consumption of 368 Mtoe. Each EU

country has its own goals to reduce emissions and increase energy efficiency. The aim of Finland is to reduce CO2 emissions by 16 %, increase the share of renewable energy to 38 %, and to increase energy efficiency so that it corresponds to a reduction in energy consumption of 4,21 Mtoe. [4]

In order to be able to fully exploit the potential of solar radiation in electricity generation, the relationships between solar electricity generation and electricity consumption must be thoroughly understood. Moreover, the potential of solar electricity generation available is an essential part of the examination of these relationships. This thesis is intended to answer some of the questions that this approach might draw. The focus of this thesis is particularly in the grid-connected photovoltaic power systems.

Objective and scope of the thesis

This thesis is intended to provide basic information for the analysis of future urban energy systems, and it is made for the new business unit of Fortum Oyj. In addition, this thesis is done as a part of Energizing Urban Ecosystems program (EUE) developed by RYM Oy which was founded as the Strategic Centre for Science, Technology and Innovation of built environment in Finland in 2009. RYM Oy is a private equity firm of the real estate and building construction excellence, which has 53 shareholders. Research consortium of EUE program consists of many big and well-known companies and organizations such as Fortum Oyj, KONE Oyj, SRV Yhtiöt Oyj and the city of Espoo. [5]

The purpose of the EUE program is to construct an internationally recognized and multidisciplinary hub of excellence for urban development in Finland. The program is intended to provide a globally networked collaboration platform for urban planning and development for various research and development projects. The urbanization will bring challenges for which this program tries to apply operating models and solutions. In particular, the program focuses on the future of urban development and urban infrastructure development. The program itself is carried out during the years 2012–2015, with a budget of approximately 20 million euros. Concepts developed in the EUE program are supposed to be modelled, simulated and tested for example in Espoo T3 area. Espoo T3 area consists of the center of Tapiola, Otaniemi and Keilaniemi. [5]

Energy systems are treated as a part of the urban infrastructure analysis in the Smart Cities theme of the EUE program. In this sense, this thesis aims to support research related to energy systems by examining how solar energy generation is going to affect the urban energy system in the future. The main objective of this study is to provide basic information about the potential of grid-connected solar electricity production in an urban environment. The results of the potential examination are utilized in energy balance examination in order to receive information on the influences of the added grid-connected solar electricity production and existing electricity consumption. In addition, based on the results of the energy balance examination a brief analysis is made in order to find out how the size of the photovoltaic system in relation to the annual electricity consumption affects the ratio of own usage of

the produced solar electricity when the storage is not in use. All the examinations made in this thesis are carried out by using the above mentioned Espoo T3 area as a reference region. The energy systems are examined at the levels of building, block of buildings and district in order to better understand the behaviour of energy systems at these levels.

Structure of thesis

Firstly, chapter two introduces the characteristics of the sun as a source of energy to be exploited in solar electricity production. In chapter three the focus is on the photovoltaic effect and the equipment relating to the solar electricity production, as well as the availability of solar radiation. In the fourth chapter the realistic solar electricity production potential is evaluated. In addition, the fifth chapter deals with the energy balance features of different building types in Tapiola area based on the results of chapter four. Finally, the sixth chapter pulls together the most important results and conclusions of the thesis.

2 The sun as an energy source

This chapter introduces the sun as an energy source. To begin with, solar radiation and characteristics of the sun are presented. In addition, the availability of solar radiation globally and especially in Finland is introduced.

2.1 Characteristics of the sun

The sun is a hot sphere of gas that is heated by reactions of nuclear fusion at its center. The nuclear reactions consume hydrogen (H) to form helium (He) in the central region of the sun which is called the core. In addition, the core is the part of the sun where the temperature and the density are the highest. Moving outwards from the center of the sun, both the temperature and the density decrease. The temperature at the core is approximately 15 000 000 °C and the density is about 150 g/cm^3, which is approximately ten times the density of lead or gold. When moving beyond the outer edge of the core, about 175 000 km (25 % of the radius) from the center of the sun, the nuclear burning almost completely ends. The temperature at this point is approximately half of the temperature of the center of the sun. In addition, the density decreases approximately to a value of 20 g/cm^3. [6] [7]

The interior of the sun can be separated into four regions by different processes. All four regions are presented in Figure 3. All energy is generated in the core. The generated energy diffuses through radiative zone by gamma-rays and x-rays. After that the energy diffuses through the convective zone by convective fluid flows. The magnetic field of the sun is generated between the radiative zone and the convective zone. This thin interface layer is called Tachocline. The surface of the sun is called photosphere. This region is 500 km thick and the layer where most of the radiation of the sun is escaped into the space. [6] [7]

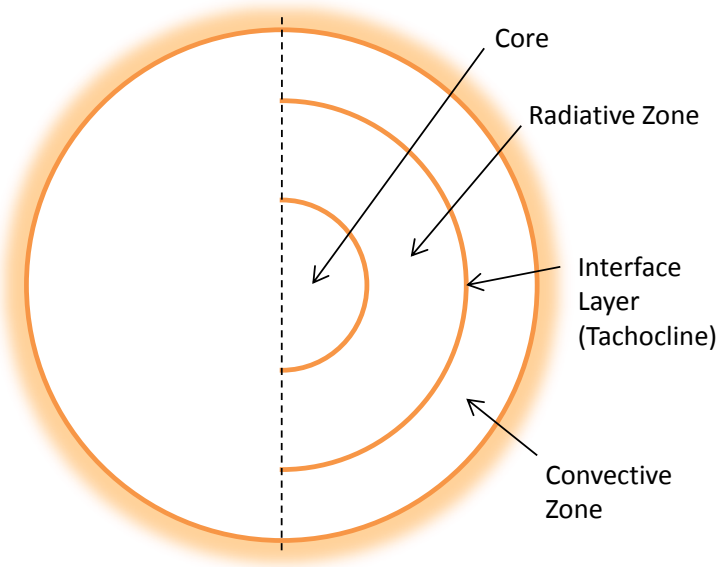

Figure 3: Regions of the sun. [7]

The total power output of the sun is $3,8 \times 10^{20}$ MW, and it radiates outwards in all directions. This power equals to 63 MW/m^2 of the surface of the sun. The distance between the sun and the earth is approximately $1,5 \times 10^8$ km, and therefore it takes approximately 8 min and 20 s for the energy of the sun to reach the surface of the earth. Approximately $1,7 \times 10^{14}$ kW of the total energy output of the sun reaches the earth. This amount of power equals to approximately 106 million times the power of Olkiluoto 3 nuclear plant [8]. Relationships between the sun and the earth are illustrated in Figure 4. As can be seen from Figure 4, the sun disk forms an angle of 32 min of a degree when the sun is observed from earth. This information is important especially in concentrator optics. [9]

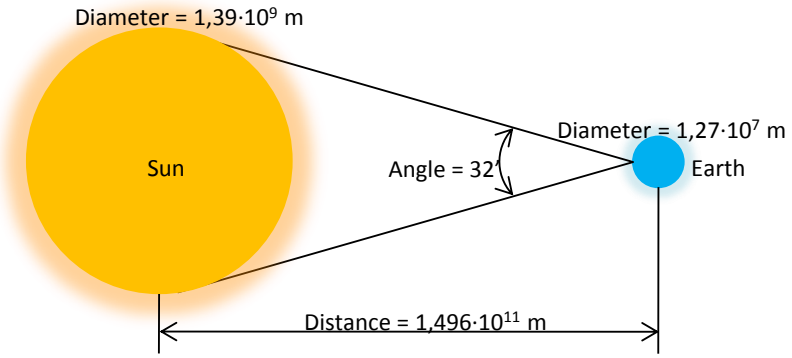

Figure 4: Relationships between the sun and the earth. [9]

2.2 Solar radiation in general

Irradiance refers to the power of the sunlight that strikes the surface of the earth, and it is usually measured in units of Watts per square meter of surface [W/m^2] [10] [11]. The irradiance value outside the atmosphere of the earth is 1 365 W/m^2. This value is called the solar constant. Before the irradiance reaches the surface of the earth, several portions of solar spectrum diminish, and peak solar irradiance decreases to a value of approximately 1 000 W/m^2. [12] This amount of irradiance is typical on a surface or a plane if the surface is directed perpendicularly to the rays of the sun on a sunny day at noon. However, the power of the sun can surpass this level for a short period of time under certain conditions. [10]

The energy contained in the sunlight striking a unit area of surface over a specified period of time is called insolation. The insolation is usually measured in units of Watt-hours per square meter [Wh/m^2]. [10] Another term for energy density of sunlight is irradiation which is measured in kWh/m^2. In many cases, irradiation is expressed as peak sun hours (psh) which means the time in hours needed to produce the daily irradiation obtained from integration of irradiance over all daylight hours at an irradiance of 1 kW/m^2. [11]

The solar radiation experienced by the receiver at the surface of the earth can be divided into three main components: direct or beam radiation, diffuse radiation and albedo radiation. Direct radiation (also known as beam radiation) is the solar

radiation that reaches the surface of the earth in a straight line from the sun without scattering or reflecting. Diffuse radiation is the radiation which is scattered towards the receiver from the whole sky apart from the disk of the sun. The radiation reflected from the ground towards the receiver is called albedo radiation. The sum of all three components is called global radiation, and it stands for the total solar radiation experienced by the receiver at the ground surface. [13]

The rays of the sun are decreased by approximately 30 % as they pass through the atmosphere. The three main factors for solar radiation deterioration are:

- rayleigh scattering by molecules in the atmosphere
- scattering caused by aerosols and dust particles
- absorption by atmospheric gases such as carbon dioxide, water vapor, ozone and oxygen. [14]

A significant factor for attenuation and scattering of solar radiation is cloud cover. Especially cumulus clouds (low altitude clouds) are effective in blocking the solar radiation. Approximately half of the solar radiation blocked by the cumulus clouds strikes the ground surface in the form of diffuse radiation. However, cirrus clouds (high altitude clouds) do not block the solar radiation as effectively as cumulus clouds. Approximately two thirds of the amount of solar radiation that is blocked by the cirrus clouds is converted in the form of diffuse radiation. Figure 5 illustrates the effects of the atmospheric scattering and cloud cover on the solar radiation approaching the atmosphere [14]

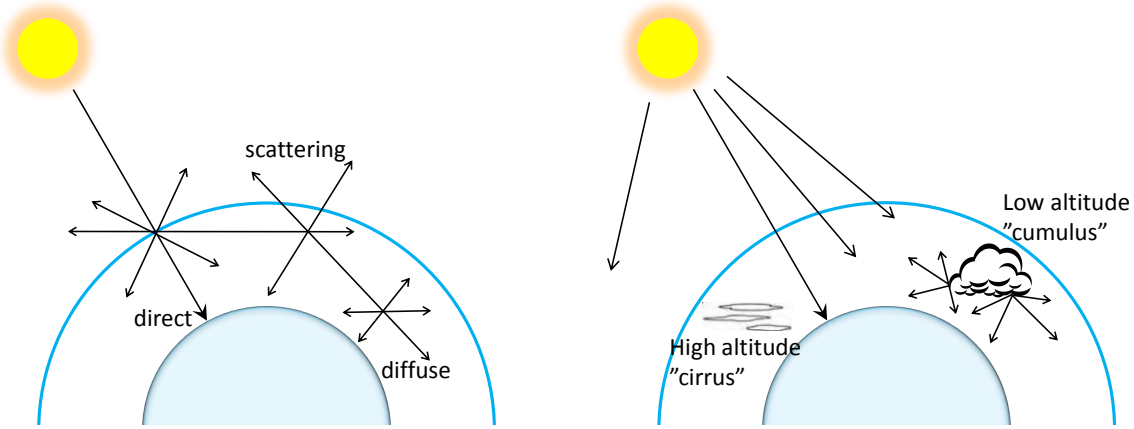

Figure 5: On the left is an example of how the atmospheric scattering leads to diffuse radiation. On the right is an example of the effect of cloud cover on the solar radiation. [14]

On a cloudy day, when the cloudiness totally blocks the sunshine, approximately 80 % of the radiation reaching the ground surface can be diffuse radiation. On the other hand, on a clear sunny day the amount of diffuse radiation can be 20 % on a

horizontal plane. For instance, in Finland approximately half of the total radiation measured on horizontal plane is diffuse radiation. [15]

When the sun is directly overhead and the sky is clear, the rays of sun have the shortest path length to reach the ground surface. Air mass refers to the amount of air that a sunbeam must penetrate before reaching the ground surface. In other words, the air mass scale is utilized to express the thickness of the atmosphere. A thicker layer of atmosphere blocks more solar radiation even if the weather is clear and cloudless. The air mass is defined by Equation

$$AM(number) = \frac{1}{\cos\phi}\,, \tag{1}$$

where ϕ represents the angle between the point directly overhead and the sun. The definition for the angle ϕ and air mass is illustrated in Figure 6. [10] [12] [14]

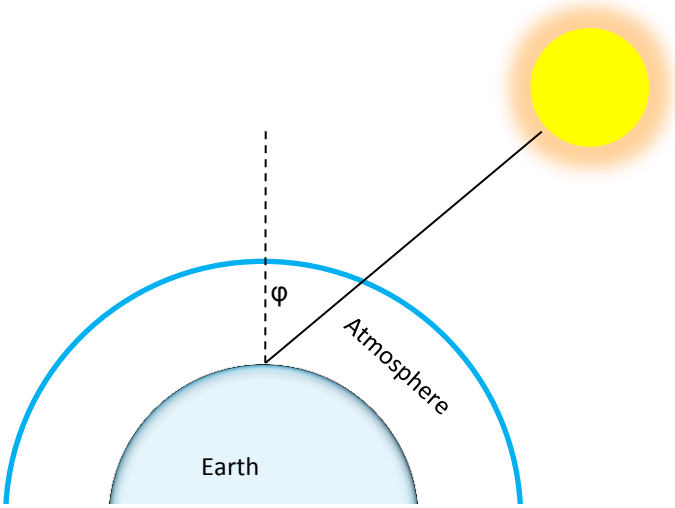

Figure 6: Definition for air mass. The position of the sun has an influence on the amount of atmosphere (air mass) through which rays of the sun must pass. [9]

In a situation where the sun is directly overhead ($\phi = 0\,^\circ$), a value of 1 for air mass (AM1) refers to the thickness of the atmosphere through which the rays of the sun must go. Figure 7 illustrates a typical AM1 clear sky absorption and scattering of incident sunlight. When the sky is clear and the sun is directly overhead, approximately 70 % of the direct solar radiation reaches the ground surface. Approximately 7 % of the solar radiation reaches the ground after scattering down from the molecules and particles in the atmosphere. About 18 % of the sunrays are absorbed in different parts of the atmosphere, and 3 % is scattered back into space.

An AM1,5 atmosphere which corresponds to an angle of $\phi = 48,19\,^\circ$ can be used as an average solar spectrum for standard solar cell measurements. For instance, a value of AM2 corresponds to a situation where the sun is 30 ° above the horizon ($\phi = 60\,^\circ$). This means that the amount of air through which the solar radiation must pass is twice as much as in the situation where the sun is directly overhead (AM1).

In northern altitudes the air mass index can be as high as 4 which corresponds to a situation where the sun is 15 ° above the horizon [16]. [10] [12] [14]

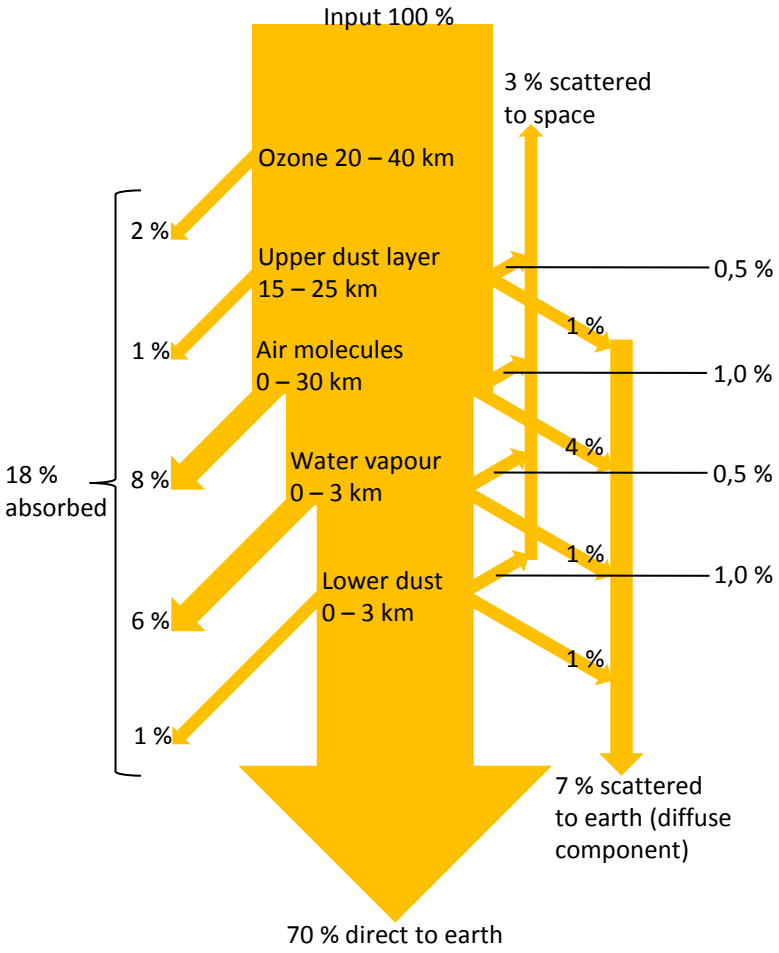

Figure 7: A typical AM1 clear sky absorption and scattering of incident sunlight. [14]

When the solar radiation is detected just outside the atmosphere the air mass is zero (AM0), and the solar spectrum is close to the value of 5 743 K black body radiation spectrum. In this case the irradiance is 1 365 W/m^2 (the solar constant). Even on clear days the amount of dust and water vapor in the atmosphere is not constant. Therefore both the direct and scattered photon fluxes vary with time and location. Figure 8 demonstrates the spectral power density of sunlight outside the atmosphere at an air mass of AM0, and both direct and diffuse radiation components at AM1,5 for an irradiance of 1 000 W/m^2. [12] [14]

The cut-outs in the Figure 8 are caused by absorption bands of several atmospheric gases such as O_3, O_2, H_2O, CO_2. The sunlight is effectively absorbed into the atmosphere at a wavelength of less than $0,3\,\mu$m. A visible and relatively high reduction at a wavelength below $0,8\,\mu$m is caused by the scattering of particulates and molecules. Ozone absorbs a significant amount of radiation in the ultraviolet region of the spectrum. However, carbon dioxide and water vapor absorb the radiation mainly in the visible and infrared region of the radiation.

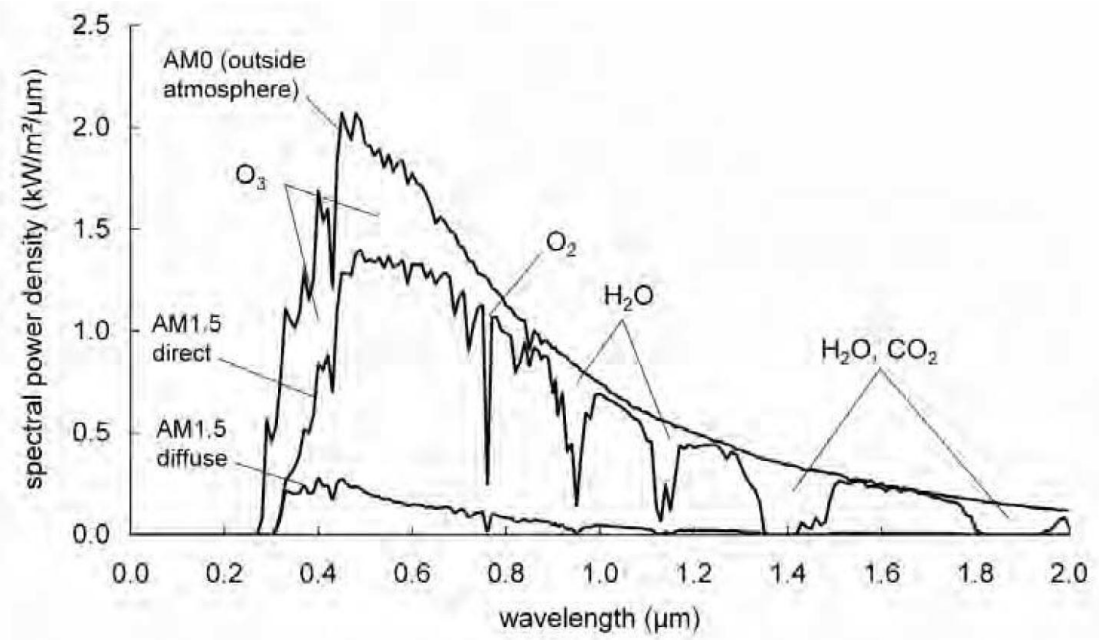

Figure 8: The spectral power density of sunlight both outside the atmosphere (AM0) and at the ground surface (AM1,5). Both direct and diffuse radiation components are illustrated in the situation of AM1,5. In addition, absorption from various atmospheric components at different wavelengths is included. [14]

It has been found that the processes of scattering deteriorate at longer wavelengths. When looking at the spectrum of the diffuse radiation it can be detected that it is richer than the direct radiation in the blue section of the spectrum. The blue color can be found in wavelength interval of 0,45–0,49 μm [17]. The cell output of solar cell systems is usually assumed to change in proportion to changes in the intensity of solar radiation when performance of solar cell systems is being analyzed. Due to this, a completely accurate evaluation for solar conversion efficiency is difficult, but the accuracy is sufficient for engineering. [12] [11] [14]

2.3 Apparent movement of the sun

For solar energy applications it is important to be able to make reasonable predictions of the location of the sun at any given time of the year. As mentioned above the amount of solar radiation on the ground surface depends on gases and air molecules that absorb and scatter sun rays. However, the amount of solar radiation also depends on the movement of the earth with respect to the sun. Common knowledge is that the earth spins around its axis every 24 hours. In addition, the earth circulates the sun on an elliptical orbit, and it lasts approximately 365,25 days for the earth to revolve around the sun. The axis of the earth is inclined at $23,5\,^\circ$ to the plane of the earth's orbit. These characteristics together cause the seasons. Because of the seasons the amount of solar radiation varies greatly around the globe. Figure 9 illustrates the movement of the earth with respect to the sun during one

year. [9] [10]

The length of daylight hours varies by location across the globe. For instance, at the equator day and night are both 12 hours long regardless of the season. However, at the poles the sun circulates 186 days a year without landing below the horizon (polar day), and 179 days a year without getting up from the horizon (polar night). At the Antarctic circle (66, 5 ° S) and Arctic circle (66, 5 ° N, which is approximately the latitude of Rovaniemi in Finland) both the polar day and the polar night last 24 hours per year. [9] [10]

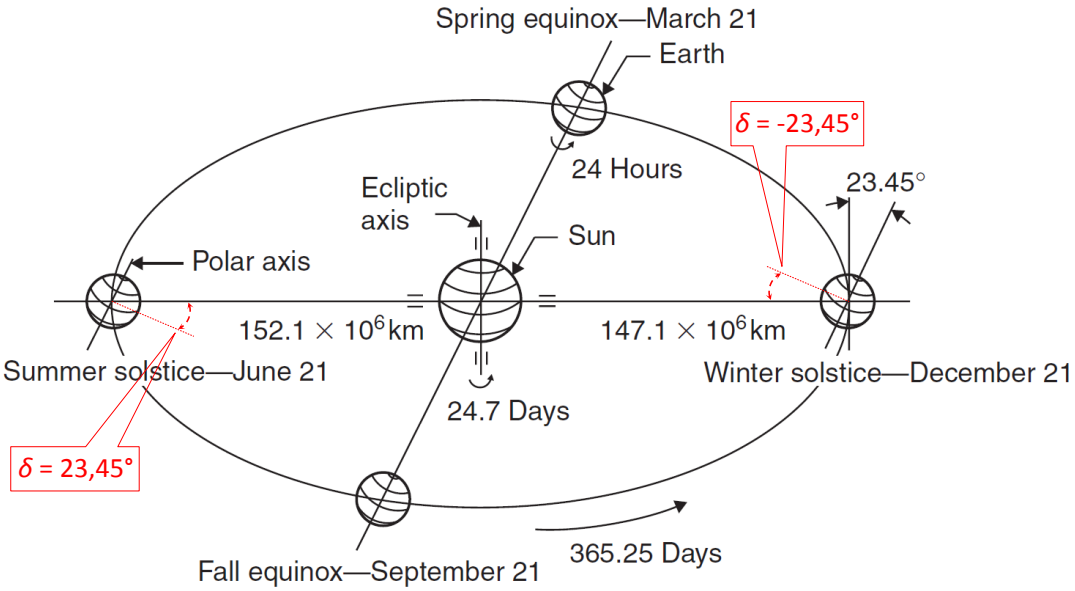

Figure 9: Annual motion of the earth about the sun. [9]

For solar energy applications the most visible movement of the sun is the movement relative to the horizon, achieving its highest location at midday. The path of the sun over the horizon during the year varies according to the seasons. At the equator the sun rises almost precisely from the east, is at noon perpendicular to the above, and sets approximately to the west. Instead, outside the equator, the sun will spend half the year rising in the southern sky and half the year rising and setting in the northern sky. As winter turns into spring in the northern hemisphere and finally into summer the points of sunrises and sunsets move northward along the horizon. The gradual movement of the sunrise and sunset points of the sun and apparent position of the sun is illustrated in Figure 10. On summer solstice the day time is at its maximum, and the sun is at its northernmost position. In turn, on winter solstice the sun is at its southernmost position, and the day time is at its shortest. However, on spring and fall equinoxes the length of the day is equal to the length of the night. [9] [10]

The position of the sun with respect to an observer at a given time can be predicted by utilizing two astrological angles: solar altitude α and solar azimuth z. These angles depend on solar declination δ and hour angle h. The solar declination is defined as the angle between the equator plane and the sunrays (sun-earth center

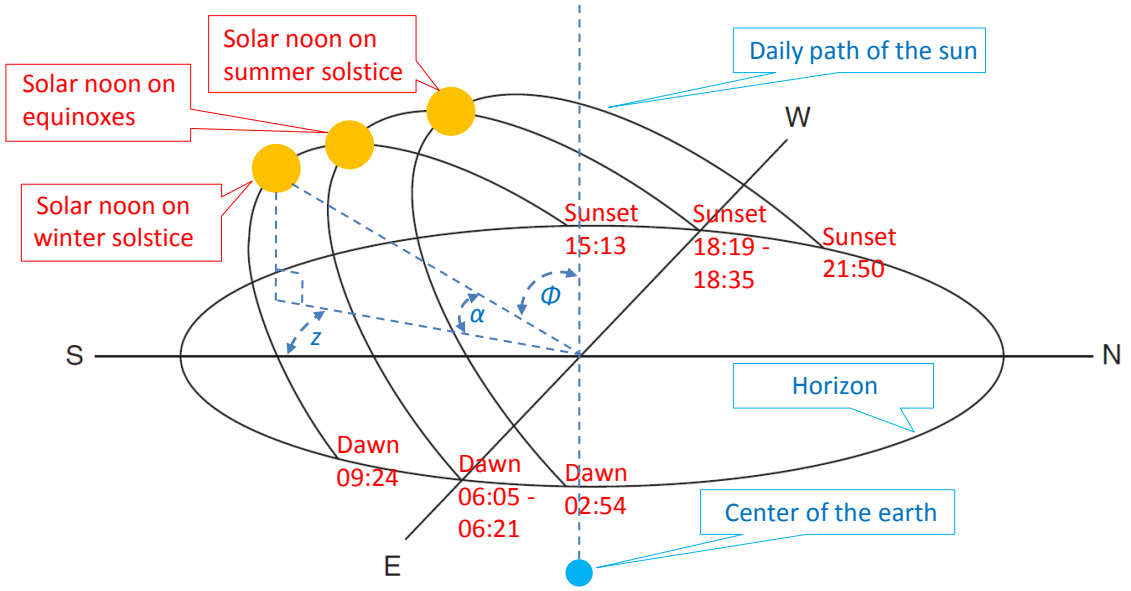

Figure 10: Apparent position of the sun during a year in Helsinki, Finland. The Figure includes times for dawns and sunsets at winter solstice, summer solstice and equinoxes in year 2012. In addition, definitions for solar altitude angle α, solar azimuth angle z and solar zenith angle Φ are included. [9] [10] [18]

line). The angle can be to north or to south from the equator. Declination north from the equator is designated as positive, and declination south from the equator is designated as negative. The definition of the solar declination and the variation of the solar declination during a year can be seen from Figure 9. The solar declination is $23,45\,^\circ$ at the summer solstice and $-23,45\,^\circ$ at the winter solstice. At the spring and fall equinoxes the solar declination is $0\,^\circ$. The solar declination δ in degrees for a desired day of a year N can be calculated by using Equation [9]

$$\delta = 23,45 \sin\left[\frac{360}{365}(284+N)\right]. \tag{2}$$

The hour angle h is expressed as the angle through which the earth would turn to bring the meridian of the point directly under the sun. At local solar noon the hour angle is $0\,^\circ$. Every hour towards either morning or afternoon is equivalent to $15\,^\circ$. Hours towards the afternoon are designated as positive. The hour angle in degrees can be expressed by Equation [9]

$$h = \pm 0,25(Number\,of\,minutes\,from\,local\,solar\,noon). \tag{3}$$

The above mentioned solar altitude angle α is defined as the angle between the horizontal plane and the sunrays. Solar zenith angle Φ, in turn, is the angle between the sunrays and the vertical plane. Thus, the sum of the solar angle α and the solar zenith angle Φ is $90\,^\circ$ $(\pi/2)$. The solar altitude angle can be expressed by Equation

$$\sin(\alpha) = \cos(\Phi) = \sin(L)\sin(\delta) + \cos(L)\cos(\delta)\cos(h), \tag{4}$$

where L represents the local latitude. [9]

For the Northern Hemisphere the solar azimuth angle z is defined as the angle of the sunrays measured in the horizontal plane from due south. For the Southern Hemisphere it is defined as the angle of the sunrays measured in the horizontal plane due north. The azimuth angle that curves westwards is designated as positive. The opposite direction is designated as negative. [9] [10] The solar azimuth angle can be calculated by Equation

$$\sin(z) = \frac{\cos(\delta)\sin(h)}{\cos(\alpha)}. \tag{5}$$

If the above mentioned Equation 5 does not provide $cos(h) > tan(\delta)/tan(L)$ the sun is behind East-West line. Graphical definitions for the solar declination δ, the solar zenith angle Φ and the solar azimuth angle z are all represented in Figure 10. [9]

3 Solar photovoltaics

This chapter introduces different technologies of solar electricity production and gives a short cross-section about photovoltaic electricity production. In addition, the impacts of tilt angles and weather conditions are covered.

3.1 Photovoltaic effect and photovoltaic cells

The operation of solar electric panels and solar cells is based on photovoltaic (PV) effect. The photovoltaic effect refers to the electrical potential that develops between two different materials when their common junction is exposed to photons or radiation. As a result, the photovoltaic cells convert solar radiation into electricity. The photovoltaic effect was discovered by a French physicist Becquerel in 1839 when he discovered that certain materials imported electric current when exposed to light. Later, in 1954, Bell Laboratories produced the first silicon cell. Solar cells are made of semiconductor materials, which operate at lower temperatures as insulation, and as conductor when exposed to energy or heat. Most solar cells are currently manufactured of silicon. [16] [14]

Semiconductor cells of several square centimetres are generally used in photovoltaic power technology. From physics point of view, the cell is basically a large pn diode where a junction point is located close to the top surface. The main purpose of the cell is to convert the solar radiation into DC power, and to produce the required power by a number of cells installed in a module. [16]

The choice of solar cell material depends significantly on the cost of manufacturing and the absorption characteristics of the material compared to the solar spectrum. Although solar cells are most commonly manufactured from crystalline, polycrystalline, and amorphous silicon, they can be manufactured from many semiconductor materials such as gallium arsenide (GaAs), gallium indium phosphide (GaInP), copper indium gallium (di)selenide ($Cu(InGa)Se_2$) and cadmium telluride CdTe. The absorption characteristics of silicon match reasonably good to the solar spectrum. In addition, since silicon is a very common material in the semiconductor industry, its manufacturing technology is well developed. For these reasons silicon has become a common solar cell material. [13]

The physical properties of a photovoltaic cell are very similar to those in classical diode with a pn junction. As the photovoltaic cell gets illuminated, the interaction of the incident photons with the atoms of the cell produces electron-hole pairs. In other words, as the junction absorbs sunlight, the energy of absorbed photons is transferred to the electron-proton system of the material. At the same time the electron-hole pairs generated by the photons are separated by the electric field created by the cell junction. The holes drift into the p region of the cell, and the electrons, respectively, drift into the n region of the cell. That is to say, the energy creates charge carriers, which are separated at the junction. The charge carriers can be electron-hole pairs in the semiconducting material or electron-ion pairs in the liquid electrolyte. The charge carriers create a potential gradient in the junction region, get accelerated by the effect of the electric field and circulate through an

external circuit as current. The power converted into electricity is the square of this current multiplied by the resistance of the circuit. All the remaining power from photons increases the temperature of the cell, and finally evaporates in the surroundings. [16] [11] [13]

The photovoltaic potential is based on the difference in the chemical potential of the electrons which are situated in two isolated materials. This difference is called the Fermi level. As these two are linked the junction moves closer to a new thermodynamic equilibrium. This equilibrium takes place only by the flow of electrons from one material to another. This flow continues as long as a voltage difference is established between the two materials. The established voltage difference has a potential which is equal to the original difference of the Fermi level. Photocurrent in the photovoltaic circuit is driven by this particular potential. [16]

The basic construction of a photovoltaic cell is illustrated in Figure 11. The cell is mechanically protected by a cover glass, which is attached with a transparent adhesive. In order to minimize the reflections and to maximize the absorption of light, the front part is equipped with an anti-reflective coating. Electrical current induced by the impinging photons is collected by metallic contacts that are located on both sides of the junction. On the top surface a thin conducting mesh of silver fibers is provided. Its task is to let the light through and collect the current. The spacing of conducting fibers is a compromise between maximum electrical conductivity and maximum passage of sunlight. On the underside of the cell and on one end of the top surface, a conducting- foil contact is provided. [16]

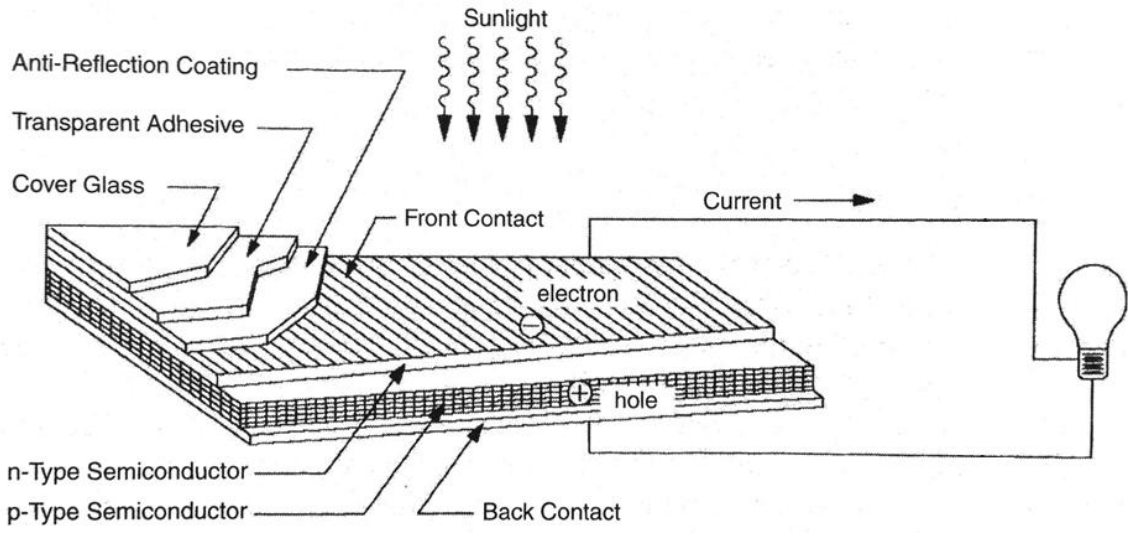

Figure 11: Basic construction of a photovoltaic cell. [16]

3.2 Electrical behaviour of photovoltaic cells

In order to represent electrical properties of the photovoltaic cell, an equivalent electrical circuit can be utilized. Equivalent circuit of the PV cell can be seen in Figure 12. In the circuit the series resistance R_S stands for the internal resistance to

the current flow. The amount of this resistance depends on impurities, pn junction depth and contact resistance. In an ideal photovoltaic cell there is no series loss, and therefore $R_S = 0$. However, in a typical high-quality silicon cell series resistance R_S varies from $0,05\,\Omega$ to $0,1\,\Omega$. Shunt resistance R_{SH} is inversely related to the shunt-leakage current I_{SH}. In the ideal PV cell there is no leakage to ground, and the shunt resistance $R_{SH} = \infty$. Typically the shunt resistance R_{SH} varies from $200\,\Omega$ to $300\,\Omega$ in the high-qualilty silicon cell. [16]

Even a small increase in series resistance R_S can cause a significant decrease in the photovoltaic output. However, the photovoltaic conversion efficiency is insensitive to variations in shunt resistance R_{SH}. Illumination creates the current I_L. As can be seen from the equivalent circuit in Figure 12, load current I equals the current I_L less the sum of the diode current I_d and the shunt-leakage current I_{SH}. [16]

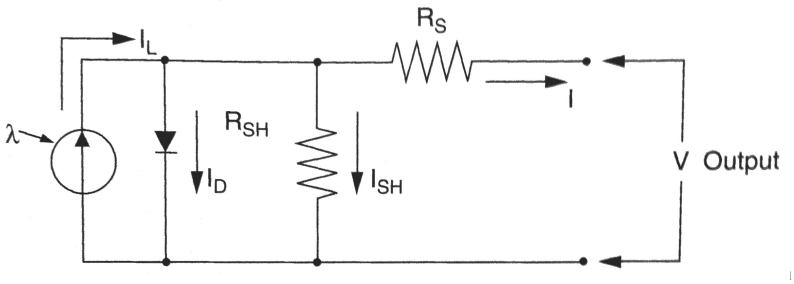

Figure 12: Equivalent electrical circuit of a photovoltaic module. [16]

The electrical characteristics of a cell are usually described under full illumination by using parameters short-circuit current I_{SC} and open-circuit voltage V_{OC}. These are the two most important parameters. When the output terminals are short-circuited and the terminal current is measured, the short circuit current I_{SC} can be determined. Short circuit current I_{SC} equals photo current I_L when the minor ground leakage and diode currents are ignored under zero terminal voltage. In the case where the load current I equals to zero, the open-circuit voltage can be expressed as:

$$V_{OC} = V + IR_{sh}. \tag{6}$$

The diode current is as follows:

$$I_d = I_D \left[e^{\frac{QV_{OC}}{AkT}} - 1 \right], \tag{7}$$

where T is the temperature on absolute scale [°K], k is the Boltzmann constant $(1,38 \times 10^{-23}\,\mathrm{J/°K})$, A is a curve fitting constant, Q is the charge of an electron $(1,6 \times 10^{-19}\,\mathrm{C})$, and I_D is the saturation current of the diode. Finally the load current I is given by the expression:

$$I = I_L - I_D \left[e^{\frac{QV_{OC}}{AkT}} - 1 \right] - \frac{V_{OC}}{R_{sh}}, \tag{8}$$

where the term $\mathrm{V_{OC}/R_{sh}}$ stands for the leakage current which in practical cells is generally ignored since it is insignificant compared to the light-generated current I_L

and the saturation current of the diode I_D. By measuring the current going into the cell when the open-circuit voltage V_{OC} is applied to the cell, the diode-saturation current can be determined. The current going into the cell is often referred as the dark current or the reverse diode-saturation current. [16]

When the load current I equals zero, and the ground leakage current is ignored the open-circuit voltage is given as

$$V_{OC} = \frac{AkT}{Q} \log_n \left(\frac{I_L}{I_D} + 1 \right), \tag{9}$$

where the term kT/Q stands for the voltage of $0,026\,\mathrm{V}$ at $300\,^{\circ}\mathrm{K}$. In practice, the open-circuit voltage turns out to be many times the value of the term kT/Q since the photocurrent is much greater than the reverse saturation current. In addition, when the cell is under constant illumination, the cell shows a negative temperature coefficient of the open-circuit voltage, and the term I_L/I_D is an adequately strong function of the cell temperature. [16] [14]

3.3 I-V characteristics

The photovoltaic cell produces direct current (DC) as its output, and it could be described as an imperfect current source since in practise it acts contrary to a voltage source such as a car battery which produces nearly stable voltage regardless of the current required by the starter motor. At a certain radiation level, the voltage of the cell will vary while the current of the cell remains relatively stable up to a certain voltage. The electrical characteristics of the photovoltaic cell can be represented by using so called I-V curve which shows the characteristic relationship between current I and voltage V. The I-V curve can be made when all possible combinations between current and voltage are drawn in the chart where X axis represents voltage V and Y axis represents current I. [10]

Figure 13 illustrates an I-V curve both in dark and sunlight conditions. From this Figure the short-circuit current I_{SC} can be found in the area of the first quarter where the voltage in the X axis is zero. The short-circuit current I_{SC} is the maximum possible current of the cell in the ideal temperature and radiation circumstances. The open-circuit voltage V_{OC}, however, can be found in the lower right corner where the current in the Y axis is zero. Therefore, when the current is zero, the open-circuit voltage V_{OC} reflects the maximum attainable voltage value of the solar cell in the ideal radiation and temperature conditions. On the right-hand side of the Y axis in the left-hand ruled section, the cell operates as a constant current source generating a voltage equivalent to the load resistance. However, in the ruled area on the right-hand side, the cell acts like a constant voltage source with an internal resistance. In this area, the current drops rapidly and voltage increases only slightly. [16] [10]

For example during a system fault transient a voltage can be externally applied in the reverse direction. During this type of external negative voltage the power is absorbed by the cell. The current is positive and continues to be flat. As in a diode, after a certain negative voltage the junction breaks down. This leads to a high value of current which can be seen from Figure 13. In the dark the breakdown voltage is

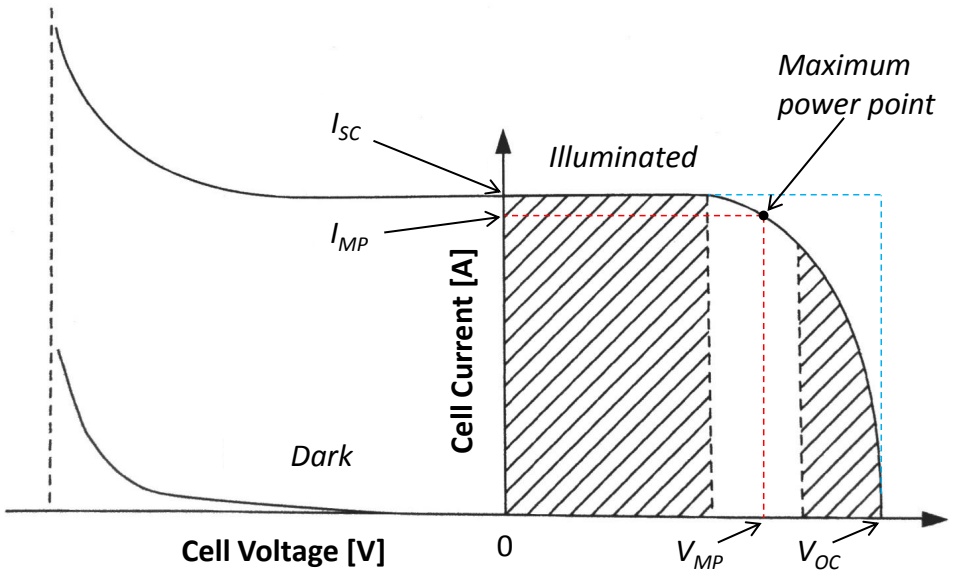

Figure 13: I-V curve of a photovoltaic cell both in dark and sunlight conditions. [16] [13]

the same as in illuminated conditions. In addition, the current is zero up until the breakdown voltage. [16]

What is particularly interesting in Figure 13 is the point in the I-V curve where the cell produces the maximum power. This point is called the maximum power point or "knee point" where $V = V_{MP}$ and $I = I_{MP}$. The maximum power point is located between the ruled areas. The power output at this point under forceful sunlight is called peak power of the cell, and it is commonly rated in terms of peak watts (W_p). From the Figure 13 it can be seen that this point defines a rectangle which is the largest rectangle of any point on the I-V curve, and it is defined as

$$P_{MP} = V_{MP} I_{MP}. \tag{10}$$

This particular maximum power point can be found by solving

$$\left.\frac{\partial P}{\partial V}\right|_{V=V_{MP}} = \left.\frac{\partial (IV)}{\partial V}\right|_{V=V_{MP}} = \left.\left[I + V\frac{\partial I}{\partial V}\right]\right|_{V=V_{MP}} = 0 \tag{11}$$

for $V = V_{MP}$. From there, the current of the maximum power point I_{MP} can be found by evaluating Equation 11 at $V = V_{MP}$. [16] [13] [14]

Fill factor (FF) is used to measure the series resistance and junction quality of a solar cell. Fill factor measures the squareness of the I-V curve, and it is defined as the ratio between the two rectangles illustrated in Figure 13:

$$FF = \frac{V_{MP} I_{MP}}{V_{OC} I_{SC}} = \frac{P_{MP}}{V_{OC} I_{SC}}. \tag{12}$$

Hence, FF will always result less than one. The nearer the FF is to one, the higher the quality of the cell. [13] [14] [11]

Figure 14 illustrates P-V characteristics where the power is plotted as a function of voltage. If either voltage or current is zero the power output of the cell is zero. However, when the voltage has a value corresponding to the maximum power point (knee point) in the I-V curve, as in Figure 13, the cell operates at the maximum power. For the before mentioned reasons, photovoltaic power circuit is always designed to operate close to the maximum power point. In the electrical analyses the photovoltaic circuit is modelled approximately as a constant current source. [16]

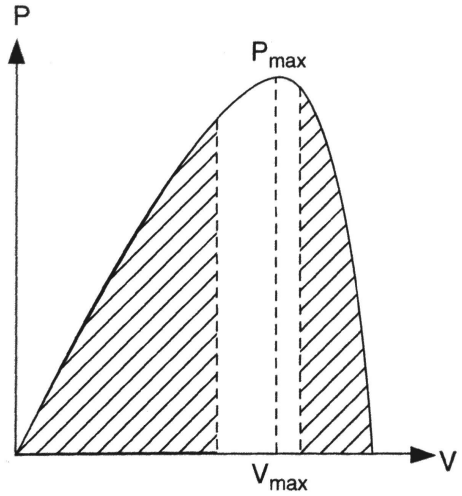

Figure 14: Power and voltage (P-V) characteristics of a photovoltaic cell. Power as a function of voltage in sunlight. [16]

Various conditions around the solar cell have an effect on the electrical properties of the cell. Such factors include the intensity of solar radiation, size of the solar cell, solar cell technology and temperature. In order to objectively evaluate the performance of the photovoltaic cell, the before mentioned factors should be standardized. For this purpose a set of standard test conditions (STC) have been defined by international convention. When the cell is at standard test conditions, the cell has a temperature of 25 °C, it is illuminated by an irradiance of 1 000 $\mathrm{W/m^2}$, and the air mass has been set at AM1,5. In addition, the maximum power output of photovoltaic devices at standard test conditions is commonly used in order to rate different devices. Maximum power output is measured in peak watt output ($\mathrm{W_p}$). In some publications the STC is also referred to as standard reporting conditions (SRC) [13]. A typical I-V curve of a crystalline silicon cell under STC conditions is illustrated in Figure 15. [10] [13]

One of the most important indicators of performance of a photovoltaic cell is its power conversion efficiency η. The power conversion efficiency of a photovoltaic cell can be calculated from the relation between the maximum power output of a cell and the solar power impinging the cell. The photoconversion efficiency is defined as follows: [10] [16] [13]

$$\eta = \frac{P_{MP}}{P_{in}} = \frac{FFV_{OC}I_{SC}}{P_{in}}. \tag{13}$$

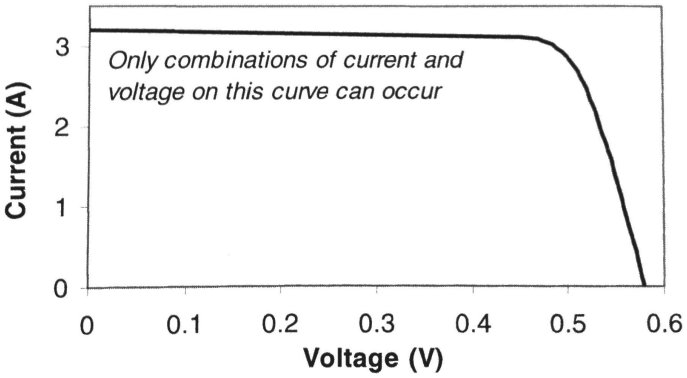

Figure 15: A typical current voltage curve (I-V curve) of a crystalline silicon cell under standard test conditions. [10]

3.4 Electrical design of photovoltaic cells

Since the surrounding conditions have an effect on the operation of the cell, these conditions and external factors need to be taken into account already in the electrical design phase of the cell. The major factors affecting the electrical design of a photovoltaic cell are sun intensity, operating temperature, sun angle and load matching for maximum power. [16]

3.4.1 Sun intensity

The intensity of the sunlight has an effect on the power output of the photovoltaic cell. This effect can be seen on the I-V curve. As the intensity of the sunlight varies the I-V characteristic starts to move in the vertical direction and the shape of the I-V curve remains approximately the same. When the intensity of the sunlight increases, the whole I-V curve moves upwards. Correspondingly, as the intensity of the sunlight decreases, the I-V curve shifts downwards. Photocurrent I_L diminishes in direct proportion to the intensity of sunlight. Therefore, the short circuit current I_{SC} diminishes significantly on a cloudy day. However, the reduction of the open-circuit voltage V_{OC} is small. Hence, the short-circuit current I_{SC} is directly proportional to the intensity of sunlight, and the open-circuit voltage V_{OC} varies only marginally. The influence of the light intensity on the I-V curve is shown in Figure 16. [10] [16] [11]

Different-sized cells have different I-V curves. Short-circuit current I_{SC} of the cell is directly proportional to the size of the cell. Therefore, a bigger photovoltaic cell produces more power. The size of the cell does not have an effect on the open-circuit voltage. Generally the size of the cell is approximately $100\,\mathrm{cm}^2$. [10]

In addition to power output, irradiation has an impact on the photoconversion efficiency. The changes in the photoconversion efficiency caused by amount of irradiance are visualized in Figure 17. As can be seen from Figure 17, the photoconversion efficiency remains practically the same both at irradiances of $500\,\mathrm{W/m}^2$ and $1\,000\,\mathrm{W/m}^2$. Thus, inside the practical working range the photoconversion efficiency is insensitive to small changes in irradiance. Therefore, the conversion efficiency re-

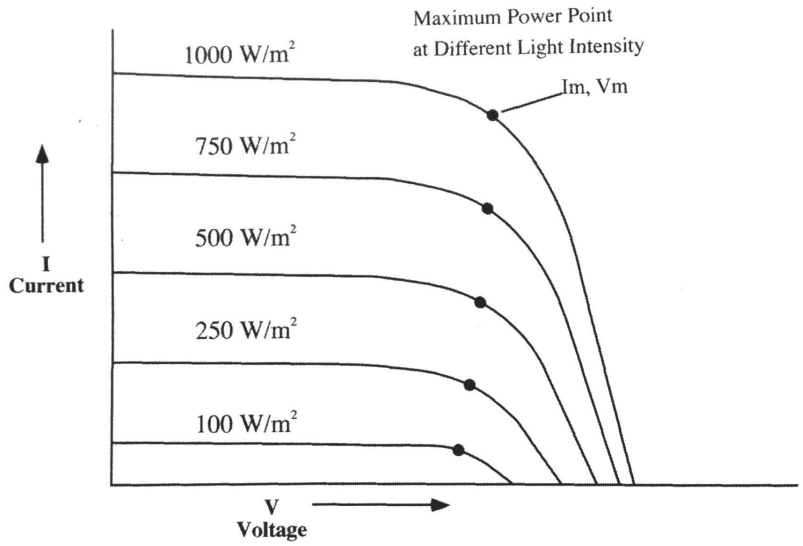

Figure 16: Behaviour of the I-V curve at different levels of irradiance. [10]

mains practically similar both on a cloudy day and on a sunny day. Even though the conversion efficiency is the same on a cloudy day as on a bright sunny day, the power output is lower on a cloudy day. Basically, the lower power output on a cloudy day compared to a sunny day is a consequence of the smaller solar energy impinging on the cell. [16]

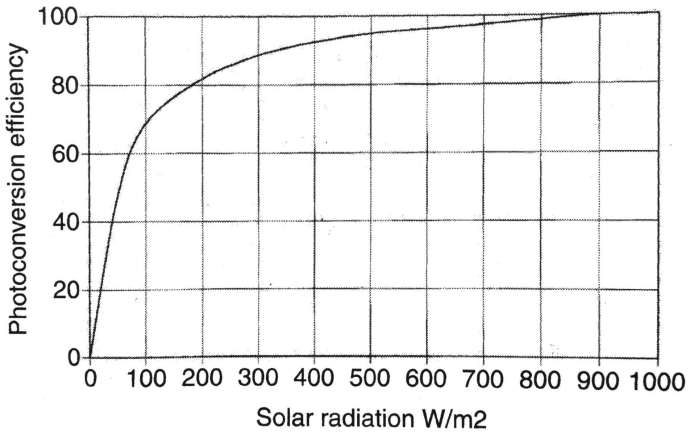

Figure 17: Photoconversion efficiency as a function of irradiance. [16]

3.4.2 Operating temperature

When the temperature rises the short-circuit current of the cell increases. Respectively, the open-circuit voltage diminishes. In order to determine the effect of temperature on power output of the photovoltaic cell, voltage and current are studied separately. With V_O being operating voltage and I_O operating current at reference temperature T, β and α are their temperature coefficients respectively. When u

stands for unit, for a single-crystal silicon cell α is approximately $20\,\mu$u/°C and β about $5\,\mu$u/°C. New voltage and current can be calculated by using following Equations when the temperature is shifted by ΔT:

$$V_{OC} = V_O\,(1 - \beta \cdot \Delta T) \tag{14}$$

and

$$I_{SC} = I_O\,(1 + \alpha \cdot \Delta T)\,. \tag{15}$$

Therefore, the new power can be defined as:

$$P = VI = V_O\,(1 - \beta \cdot \Delta T)\,I_O\,(1 + \alpha \cdot \Delta T)\,. \tag{16}$$

[16]

The effect of temperature changes on the I-V curve can be seen from picture 18. When the temperature increases the open-circuit voltage decreases by $2,3\,$mV/°C. From the above mentioned Equations it can be interpreted that the power output of the silicon cell decreases approximately by $0{,}5\,\%$ for every degree centigrade increase in the operating temperature above the reference temperature. In other words, the power output is greater at a colder operating temperature since the decrease in current is significantly less than the increase in voltage. [16] [11]

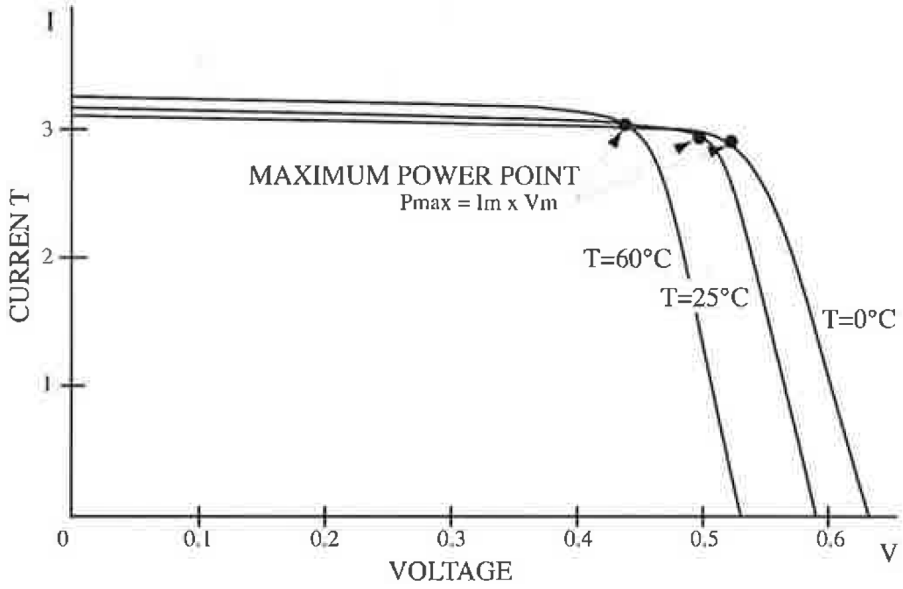

Figure 18: Influence of temperature on I-V curve. Decrease in temperature from 25 °C to 0 °C increases the maximum power output of the cell by 10 %. [10]

The characteristics of power output and voltage of the photovoltaic cell are shown in Figure 19. From this Figure it can be seen that the power output is clearly higher at a colder operating temperature compared to power outputs achieved at higher temperatures. For this reason, cold weather is better in terms of power outlet of the cell. It is worth noting that the maximum power points in Figure 19 are achieved at different stages of voltage, which must be taken into consideration in the designing phase of PV systems. [16]

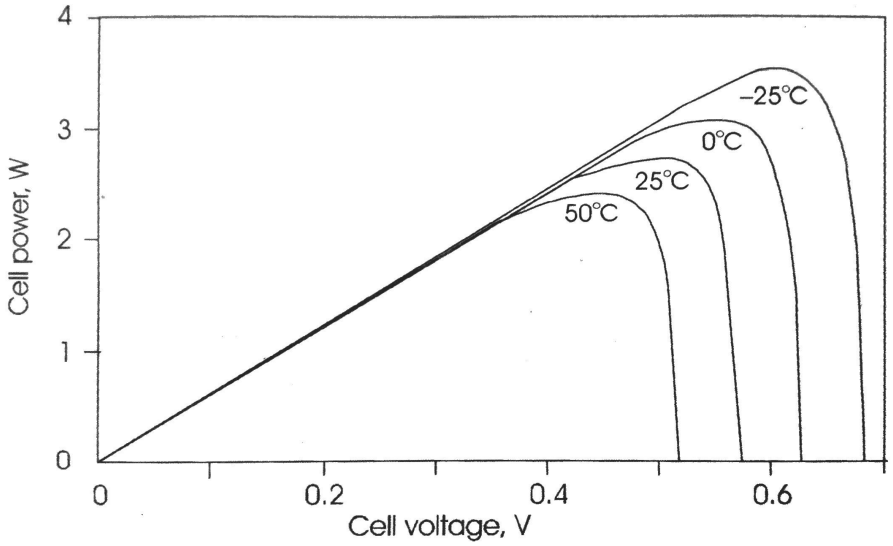

Figure 19: Influence of temperature on power output and voltage of the photovoltaic cell. Maximum power points are at different voltages. [11]

3.5 Modules and arrays

Flat-plate type modules constitute over 99 % of the PV module markets and the rest are concentrator photovoltaics. The major constituent for PV modules are wafer-based silicon cells that have the highest efficiencies available in commercial markets. Approximately 85 % of the all PV systems are manufactured from either single-crystal silicon (c-Si) or multicrystalline silicon (multi-Si) ingots. The rest 15 % of the commercial markets consist of various thin films of amorphous silicon or cadmium sulfide and cadmium telluride (CdS/CdTe). A big increase in the production of single crystal and multicrystalline silicon modules has caused a significant reduction in cost over the past few years. [13]

3.5.1 Types of photovoltaic technology

Crystalline silicon has an organized crystalline structure. Each atom is at a predetermined location. Therefore, it allows direct applicability of technologies developed for crystalline materials. In addition, the crystalline silicon behaves evenly and predictably. [14]

Single-crystal silicon is the most widely available cell material. The main advantage of this technology is the relatively high efficiency of energy conversion which usually ranges from 14 % to 18 %. Nowadays, the conversion efficiency for crystalline silicon is in most cases approximately 15 % [9] [19]. The main disadvantage of the single-crystal silicon is the high production cost, which results from the slow, complex and energy-demanding manufacturing process. [16] [9]

Multicrystal materials are widely used in commercial solar cells [14]. Unlike in the manufacturing process of the single-crystal silicon ingot, the multicrystalline silicon cells are produced by using several grains of monocrystalline silicon. The

molten silicon is cast into ingots and then cut into thin wafers and mounted into cells. [9] [16] The manufacturing process of the multicrystalline silicon cells is less complicated than the manufacturing process of the single-crystal silicon cells which makes the multicrystalline silicon cells cheaper to produce. [14] [9] [16] However, the efficiency of a multicrystalline silicon cell is slightly smaller being approximately 12 % [9]. Multicrystalline silicon cells are available as both thick and thin film cells, and they are increasing their market share in the area of commercial applications [16]

Amorphous silicon technology uses approximately 1 % of the material compared to the crystalline silicon technology. In addition, price per watt of the amorphous silicon technology is lower than for the crystalline silicon, but its efficiency is lower. [16] The amorphous silicon cells consist of silicon atoms in a thin homogeneous layer instead of the crystalline structure. [9] The amorphous silicon absorbs light more efficiently than the crystalline silicon which is why the solar cells can be thinner. This kind of technology is known as thin-film technology [9] [14] The thin-film technology uses considerably less material compared to the crystalline technologies. For this reason, it is also less expensive per Watt of power generated. [16] However, the life cycle of thin film products is currently lower than that of the crystalline products. [14] The amorphous silicon can be deposited on a large range of substrates of both flexible and rigid. Common options are for example a stainless steel roll or a glass. [9] [14] [16] The efficiency of the amorphous silicon cell is approximately 6 %. Panels made from amorphous silicon can be obtained in different shapes such as foor tiles. [9]

Currently the most promising materials include, for example, copper indium diselenide ($CuInSe_2$) and cadmium telluride (CdTe). The main trends seem to be heading towards the use of organic and polymer solar cells. When these technologies are compared to the crystalline silicon solar cells they suffer from degradation and stability problems and have the efficiency of approximately 4 %. However, the most interesting characteristic is that, compared to crystalline silicon technology, they can potentially offer faster production with lower cost. [9]

By using multijunction cells a better efficiency can be achieved, and a broader spectrum of sunlight can be converted into electricity. Multijunction cell technology uses multiple layers of semiconductor materials, thus enabling a wider range of band gaps that convert more wavelengths and a broader spectrum of sunlight into electricity. When the energy of the light matches the band gap of the semiconductor, the photovoltaic cell converts the sunlight into electricity most efficiently. By using normal single-junction n-on-p silicon cell only red and infrared light can be converted into electricity but utilization of blue and ultraviolet light is not possible. An efficiency of 34 % has been achieved by NREL and spectrolab with triple junction gallium indium phosphide/gallium arsenide/germanium (GaInP/GaAs/Ge) cell under concentrated sunlight. In addition, the cell captures infrared sunlight. By using triple-junction space-qualified cells efficiencies of even 40 % have been achieved by Spectrolab, Inc. [16]

3.5.2 Photovoltaic modules

The photovoltaic modules have many key characteristics that can be categorized into either physical or electrical. The key physical characteristics include mounting requirements, weight, dimensions, cover material, packaging and grounding method. The key electrical characteristics, in turn, are efficiency, nameplate power rating, temperature coefficients, V_{MP}, I_{MP}, V_{OC}, I_{SC} and fill factor. [13]

A photovoltaic cell is usually 0,1–0,4 mm thick and forms an area of approximately 10 cm x 10 cm. Alone it can produce a voltage of around 0,5 V. In order to obtain higher voltages, for example for the purpose of charging batteries of 12 V, multiple photovoltaic cells are usually connected in series. Module current, in turn, can be calculated as a product of the number of parallel-connected photovoltaic cells and the current of a single cell [13]. Together these connected photovoltaic cells form a photovoltaic module. Typical commercial modules have power ratings of 150–300 W_p, and these powers are usually produced at voltage levels of 20–40 V and currents of 5–10 A [13]. For example, depending on the circumstances (such as orientation in relation to the sun and the technology used) a small PV system of approximately 1,5–2 kW can consist of about 10–30 modules and cover an area of circa 15–25 m^2 [9]. The front of one cell and the rear side of the adjacent cell are connected by using tinned copper ribbons (tabs). A typical PV module includes several strings of 9–12 series-connected PV cells. PV modules are usually designed for PV systems that operate at multiples of 12 V. A traditional configuration for charging 12 V batteries consists of 36 series-connected PV cells and produces a voltage of approximately 15 V at maximum power. Nowadays, modules with different electrical configurations are needed since both building-integrated systems and grid-connected applications are growing. For this reason, new common configurations for PV modules are 60 cells with an area of 156 cm x 156 cm and 72 cells with an area of 125 cm x 125 cm. In practice, however, a power dissipation of approximately 3–4 % is detected resulting from optical losses, mismatch effects and ohmic losses largely in the tabs [13]. [16] [10] [13] [11] [20]

Photovoltaic modules can be installed on the roof of the building, on the ground, or even be integrated into the structure of the building. The main aspects of the design are usually wind and snow load. [9] A photovoltaic module is exposed to many environmental conditions during its life cycle, which is why a special attention should be paid to the structure of a module in the designing phase. In practice, grid-connected PV modules are designed to withstand outdoor use for over 20 years without maintenance. Both national and international standards have been developed for type approval and design qualification of crystalline and thin-film PV modules in order to ensure the reliability of the device. In order to be able to operate outdoors for more than 25 years the module should be appropriately encapsulated. The main conditions affecting the PV module are diurnal and seasonal temperature variations, ultraviolet radiation, evaporation and condensation of moisture, rain, hail, snow, wind, sand, dust, salt, atmospheric gases, pollutants and even birds. [14] [13]

In order to identify the main failure mechanism of PV modules and the conse-

quences of over 20 years of use accelerated testing methods have been developed. Despite this, successful completion of the approved tests does not guarantee the 20-year service life because all the fault mechanisms have not yet been detected, and the applied test methods do not simulate the consequences of long-term use in exactly the right way. [13]

The construction of a PV module has been designed to protect the cells from elements. The cells are situated in a plastic material between a backing material and a sheet of tempered glass. The most common backing material is plastic but glass and aluminium are used occasionally. The module should be easy to attach in a structure and have strong edges. For this reason, edges of the module are usually framed in aluminium. [10] Typically the PV module consists of parts such as frame, weatherproof junction box, rating plate, weather protection for 30-years life, photovoltaic cells, tempered high-transmittivity cover glass, outside electrical bus and frame clearance. The structure of a typical PV module is presented in Figure 20. [16]

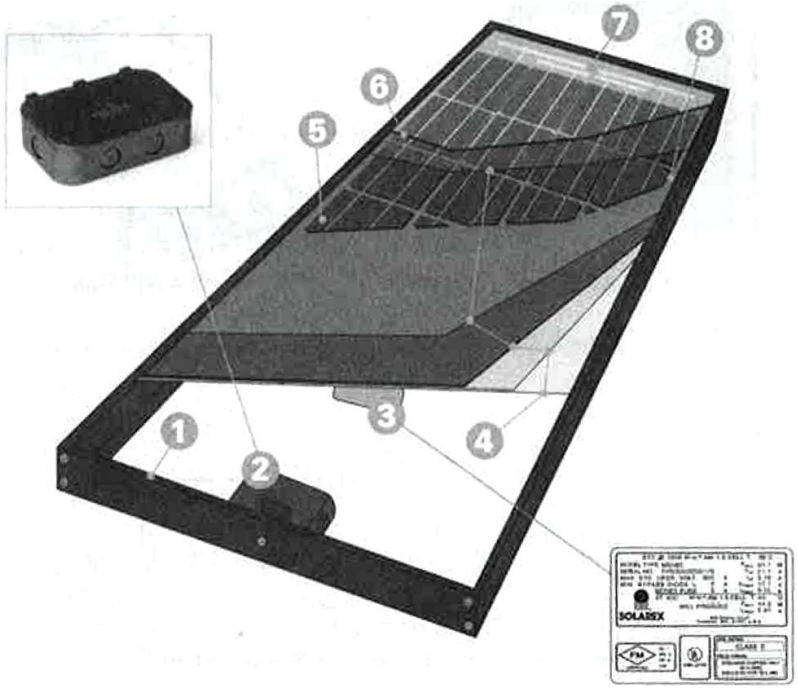

Figure 20: Structure of a typical PV module: 1) frame, 2) weatherproof junction box, 3) rating plate, 4) weather protection for 30-years life, 5) photovoltaic cells, 6) tempered high-transmittivity cover glass, 7) outside electrical bus, 8) frame clearance. [16]

3.5.3 Photovoltaic arrays

As in case of PV cells, several PV panels can also be connected together. Thus, an array consists of several PV modules. The size of a PV array in terms of power can vary between a few hundred watts and several hundreds of kilowatts. Larger systems

are usually separated into multiple subarrays that are electrically independent. If the aim is to achieve a higher voltage, the panels are coupled in series. If the goal is to achieve a higher current, panels are connected in parallel. It is important to have the maximum power production of each module occur at the same current if the modules are connected in series. However, when the modules are connected in parallel, the maximum power production should occur at the same voltage. A comparison between cell, module and array is shown in Figure 21. [20] [11] [10] [16]

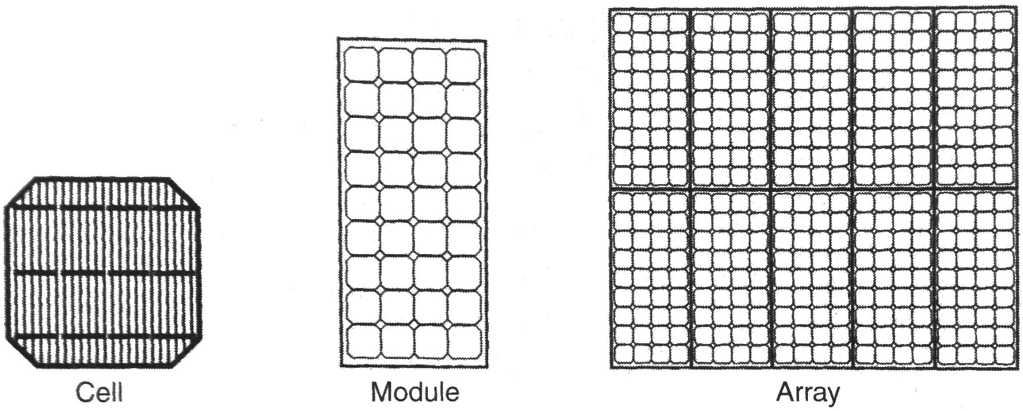

Figure 21: Illustration showing the difference between a PV cell, a PV module and a PV array. [16]

In the same way as with photovoltaic cells, a series-connected array can act as a load to the string if one module is shaded. In this kind of situation a bypass diode in parallel with the module can be exploited. Because of this, the current flows through the diode instead of flowing through the module. A blocking diode is used for blocking current from being fed through the shaded string if shading diminishes the output of one string significantly lower than the other strings. The blocking diode is connected in series with every string in order to prevent damages. Both the bypass and blocking diode protect the system but can decrease the output. [20]

The shading can have a surprising effect on the PV array output since shading of only about 5-10 % of the array can reduce the output by over 80 %. The shading can be divided into two major types in a site shading survey in order to reduce the loss caused by shading. These two types are global and near-field shadings. The global shading is sometimes referred to as horizon shading and it stands for objects that can shade either the whole or none of the array and are very large relative to the size of the PV array such as nearby buildings, rooftops or hills. As a result, the array receives only diffuse radiation. The horizon shading is usually easy to model but can be difficult or even impossible to avoid. Near-field shading, in turn, stands for objects that can shade only a portion of the PV array such as trees, rooftop equipment, walls and neighbouring rows of panels. Typically near-field shading can be hard to model but rather easy to eliminate. Electrically the near-field shading corresponds to mismatch. [13]

Many everyday matters have an effect on the production of PV array, such as leaves, bird droppings, soiling, dust, soot, snow and frost. Many of these are

dependent on the climate and the time of the year. For example, the accumulation of dust usually depends on local soil, motor and air traffic, agricultural operations and the local climate. Soiling can result in an annual loss of approximately 7 % and a monthly loss of about 25 % in production if the effects of soiling will not be lightened, for example, by washing the PV array. According to research, one wash in the middle of the dry season can reduce the annual production loss by half. Production losses caused by snow are approximately slightly above 2 % annually. The easiest way to reduce the losses caused by the snow is to set the tilt angle of the array at about 60 ° or above. This will facilitate the shedding of the snow off of the array. [13] In most cases, snow and ice are so transparent that sunlight can shine through them heating on the array which makes snow and ice begin to melt [10].

3.6 Photovoltaic systems

Photovoltaic systems can be divided into two main categories: grid-connected systems and stand-alone systems. In the grid-connected PV system the DC power produced by the PV array is converted into AC power by using an inverter, and the produced AC power can be used either on site or fed into the distribution network. The stand-alone PV system, however, can be used independently to feed dedicated loads outside the distribution network without any other power sources. In order to be able to supply electric energy even at times when the solar energy is not available, the system may also be included with energy storage feature. The system can also be connected to other energy sources such as wind power or a diesel generator in case of which the system is referred to as a hybrid PV system. Both the stand-alone and grid-connected systems can be used as a hybrid system but this is more common in stand-alone systems since the supplementary power supply allows the reduction of the storage requirement without increased loss of load probability. [20] [13] This thesis examines only the grid-connected PV systems without the storage feature. Figure 22 illustrates the structure of a grid-connected PV system by means of a simplified block diagram.

The main components of the PV system are the PV array including mounting structure, wiring and modules, power conditioning and control equipment, storage equipment if needed and load equipment. [20]. The PV systems are designed and installed so that they can withstand time. For this reason the PV systems can be expected to operate at almost initial power levels throughout the entire life cycle of over 25 years being the nominal minimum. However, there are a few recommended scheduled maintenance tasks that should ensure as fault-free operation as possible such as inspection of mechanical mounting system, inspection of wires and electrical connections, module cleaning to remove soiling, replacement of broken or damaged modules, verification of proper inverter operation and vegetation control. [13]

In general, an optimum criterion for sizing the PV system is the most profitable one. The sizing of grid-connected systems can be done according to many criteria. Below is a list of the most common criteria:

- Sized for optimal economic value.

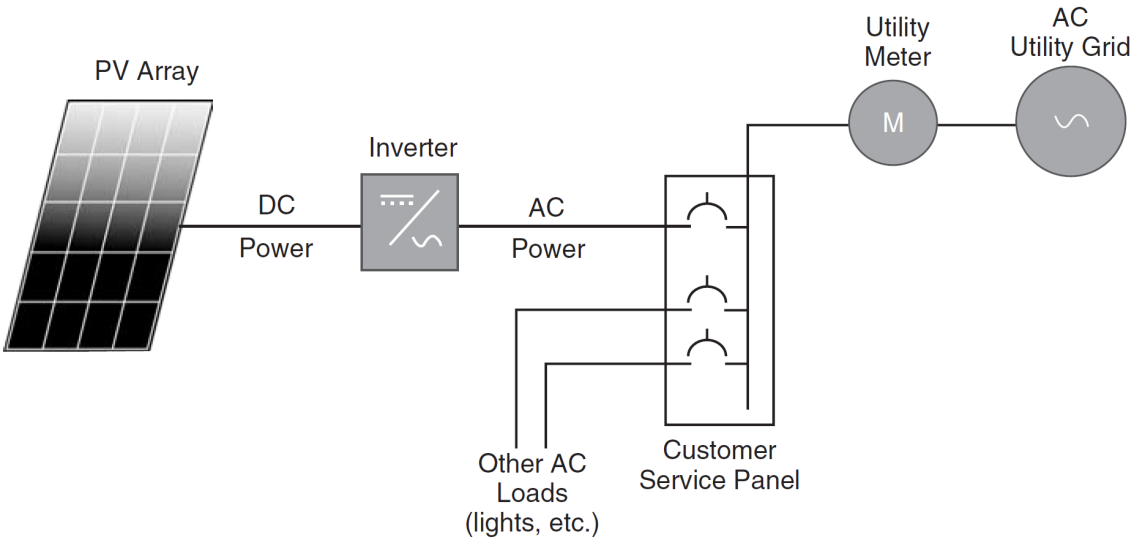

Figure 22: A simplified block diagram of a grid-connected PV system. [13]

- Sized to fit available area.
- Sized to meet 100 % or some other target fraction of annual electrical energy demand.
- Sized to meet 100 % or some other target fraction of peak power demand.
- Sized to obtain maximum incentive. [13]

In general, the PV arrays are designed to be fixed without changing the orientation angle. Nevertheless, there are PV systems with arrays that can track the movement of the sun. The tracking can be carried out either with respect to one axis or with respect to two axes. The single-axis system follows the path of the sun from east to west. Such a system has been shown to increase the electrical energy produced by approximately 30 % compared to a non-tracking PV system in a location with mainly cloudless sky. The two-axis system, in turn, follows both the north-south movement and the east-west movement of the sun. The PV system with two-axis tracking has been shown to increase the energy produced by approximately 20 % compared to the single-axis system. For example, in northern Europe the benefits of such systems, however, remain significantly lower due to weather conditions of frequent overcast. For this reason, it is more profitable to install larger arrays in conditions with less than 3 000 hours of direct sunlight annually. [20]

3.7 Inverters

Inverters are used to convert direct current into alternating current, and the output can be either single or three phase. Inverters are classified by the total power capacity and the available power range starts from hundreds of watts and ends up to the level of megawatts. [9] Whenever a photovoltaic system is used for AC load

input, the inverter is needed. Inverters can be roughly divided into two categories: stand-alone and grid-connected inverters. The latter is often referred to as line-tied inverter. [20] In addition to the power inversion the main task of the inverter is to keep the voltage of the AC side as constant [9]. The cost of the inverter represents a significant part of the total cost of the PV system. In the case of commercial grid-connected PV systems the cost of the inverter is approximately 5–10 % of the overall cost, and for the residential off-grid system the cost is approximately 15–25 %. [13]

The power inversion of a line-tied inverter is carried out by using the transistor-based power electronics circuitry. The input power of the PV array is drawn at maximum power point by switching the power transistors on and off at high frequencies of approximately 2–20 kHz. The result is alternating current waveform that is in the shape of the sinusoidal. The switching components outside the base frequency are removed by the filter component. The actual inverter is connected to the utility grid through an AC disconnect switch. The PV array is connected to the inverter through a DC disconnect switch. The switches allow the disconnection of inverter components in order to enable safe maintenance and repair actions. On both the AC and DC sides the over-current protection devices are included. The over-current protection is usually carried out by using fuses but it can also be made with circuit breakers. Usually an additional protection for transient surge suppression is included on both DC and AC sides. This kind of protection is needed for example against lightning induced voltages. The controller is the key component of the inverter. The main tasks of the controller include overall system monitoring, the system input and output metering, algorithm implementation for control of the transistors, maximum power point tracking, implementation of grid interface requirements and communication to the user. In the off-grid systems the controller is used for implementation of the charging function. An overview of the main components of the grid-connected inverter is shown in Figure 23. [13]

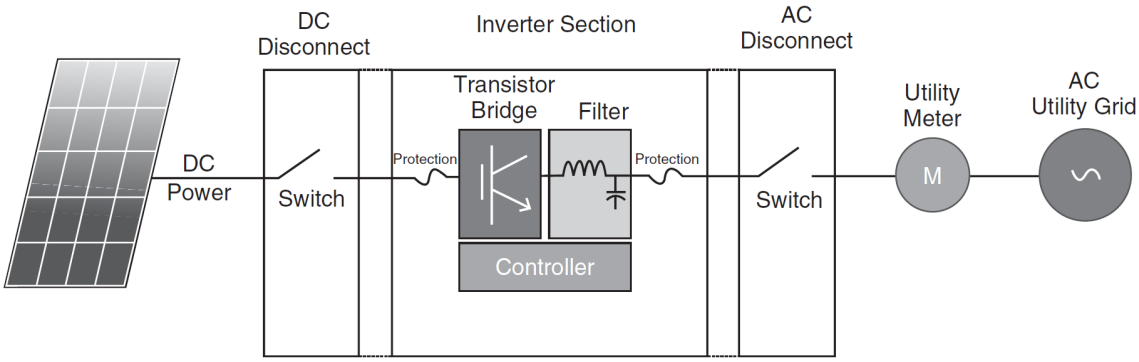

Figure 23: Inverter block diagram of the key components of the grid-connected inverter. [13]

The main factors affecting the choice of the inverter are the compatibility with the array output DC voltage characteristics and the proper interface capabilities for the loads and distribution network. [13] The designer must be able to precisely determine both the size and the type of the load [9]. The inverter in a stand-alone system

is capable to work independently outside the electricity grid. With an internal frequency generator it produces the frequency corresponding to the frequency of the loads. [20] The grid-connected inverter, however, must be fully integrated into the utility grid in terms of voltage and frequency. [20] [13] For example, in utility-scale and three-phase commercial systems a higher AC voltage is used such as 690 V in Europe and 480 V in the United States. However, inverters of some large utility-scale systems bring the voltage up to medium voltage level of approximately 12–70 kV by using transformers. [13] The inverter input voltage is determined by the type of the inverter, the type of the PV array and the requirements of the output voltage. [20]

In order to prevent the loads from overheating or damaging it is important that the waveform of the inverter output is correct. For example, a square wave output can cause this kind of problems. Grid-connected inverters must be able to produce a sine wave output with minimal harmonic components. However, stand-alone inverters can produce a modified sine wave output according to the need. [20]

It is important that the inverter is chosen optimally for each PV system. If the rated power of the PV array exceeds the rated power of the inverter, the output is limited by the rated output power of the inverter. Thus, the utilization of overall capacity of the PV system is reduced. The available power of the PV array is in practice always less than the rated power of the individual modules. For this reason, it is common that the rated power of the PV array is somewhat higher than the rated power of the inverter. In this context, a factor of 1.2 is used in many cases in the design of the PV system which would mean that, for example, a PV array with modules rated for 12 $\mathrm{kW_{DC}}$ at STC conditions would be coupled to an inverter of 10 $\mathrm{kW_{AC}}$. In a properly designed system only a small portion of the power is lost as a result of the lower rated power of the inverter. [13]

Inverter conversion efficiency η_{inv} is power-dependent and it is designed to be high. [20] [9] In addition, the inverter efficiency changes according to the voltage of the DC side [13]. The conversion efficiency η_{inv} is defined as follows

$$\eta_{inv} = \frac{P_{out}}{P_{in}} = \frac{V_{ac} I_{ac} \cos(\varphi)}{V_{dc} I_{dc}} \tag{17}$$

where P_{in} represents the input power, P_{out} is the output power, $\cos(\varphi)$ stands for the power factor, V_{dc} is the input voltage from DC side, I_{dc} is the input current from DC side, V_{ac} stands for the output voltage and I_{ac} stands for the output current. [9] Generally, the maximum efficiency is more than 90 %. The efficiency of the inverter changes as the operating point of the inverter moves. In general, the inverter reaches its maximum efficiency when the operating point is between 30 % and 50 % of the rated capacity. If the operating point rises above this range, usually the conversion efficiency drops only slightly. The efficiency decreases significantly when the operating point is less than about 10 % of the rated capacity. [20] A typical inverter efficiency curve for the grid-connected inverter with a rated output power of 250 kW and weighted-average efficiency rating of 96 % made by California Energy Commission (CEC) is illustrated in Figure 24 [13].

For the above mentioned reasons the relatively weak light conditions of the middle and north Europe can have a negative impact on the entire performance of the

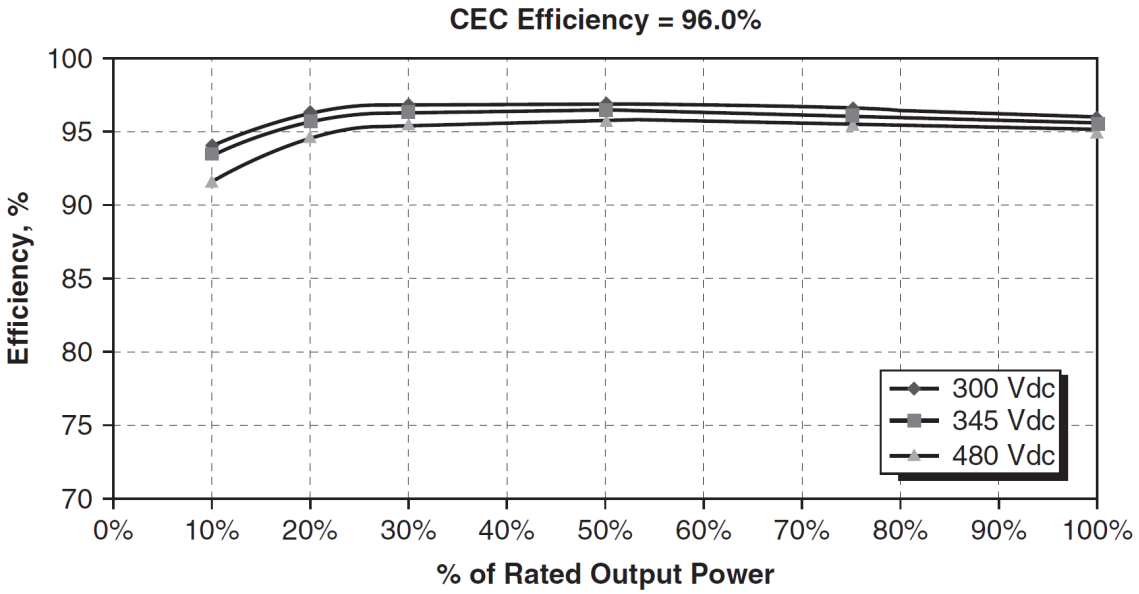

Figure 24: Inverter efficiency curve for a grid-connected inverter with a rated output power of 250 kW and weighted-average efficiency rating of 96 % made by California Energy Commission (CEC). There are three different input voltages given in the graph: 300 V_{DC}, 345 V_{DC} and 480 V_{DC}. [13]

PV system. In order to improve the overall efficiency the inverter is often dimensioned to approximately 75–80 % of the rated power of the PV array. This way, the inverter can be operated at higher efficiency region for longer periods of time although the very highest power range of the PV array is sacrificed. From performance ratio point of view this is more profitable. [20]

In the case of grid-connected PV systems the inverter is expected to meet the requirements of interaction functionality and power quality set by the utility grid [13]. It is crucial to ensure that the inverter does not supply electricity to the grid during the permanent fault of power-distribution network. Such a situation is known as islanding. For the safety of fault correction personnel and equipment it is imperative that such a situation can be avoided. [20] In order to avoid islanding country-specific and utility-specific connection regulations have been determined. For example in the USA the standards IEEE-1547 (Standard for Interconnecting Distributed Energy Resources with Electric Power Systems) and UL-1741 (Standard for Safety Inverters, Converters Controllers and Interconnection System Equipment for Use with Distributed Energy Resources) require that the inverter disconnects from the utility grid if there is a loss of AC voltage regulation by the utility grid. In addition, the inverter is not allowed to attempt to regulate the AC voltage or operate at a variable power factor angle. However, in Europe the common requirements are set by the standard IEC 62109 (Safety of power converters for use in photovoltaic power systems), and all the inverters must have a CE mark. Even so, there are many country- and utility-specific standards in use. Nonetheless, in order to support the utility grid the prevailing usage in Europe is to remain the inverters connected dur-

ing minor faults. This means operating at variable reactive power levels and staying connected through voltage dips. [13] Usually the islanding is prevented by switching off the inverter when the electrical values of distribution network move outside the predetermined limits of voltage and frequency. The limit values are country-specific but are usually about ±2 % for both the voltage and the frequency. [20]

3.8 Real world performance of photovoltaic systems

PV power conversion efficiency under standard reporting conditions (SRC) is the most common way to rate the performance of PV modules. The nameplate ratings of the PV modules are usually given in the form of peak watt or power rating in relation to SRC. However, real-world operation conditions do not usually correspond to STC conditions, they can actually differ strongly from each other since the real world situations cause efficiency loss compared to STC conditions. For this reason the standard test conditions are continuously being questioned. When a PV module is installed and used under real world conditions the efficiency is about 70 % of the STC efficiency reported by the manufacturer. The causes behind this efficiency loss between real operation conditions and STC conditions can be classified into four main categories: cell temperature, irradiance level, spectral content of light and angular distribution of light. More specifically, the real-world output of a photovoltaic system depends on various system-related losses, soiling, air temperature, wind speed, orientation, total irradiance and spectral irradiance. [13]

The nameplate value of the PV module given by manufacturer in comparison to the measured practical performance is almost always higher, and very rarely lower. [13] The module operates at many different temperatures during its lifetime. For example in good lighting conditions at ambient temperature of 25–30 °C the operating temperature of the module can usually vary in the range of 50–80 °C. [20] On a typical sunny day the PV module operates at a temperature of about 35 degrees which also makes the PV module perform worse than the nameplate rating defined at 25 degrees. This is due to the fact that the module efficiency decreases as the operating temperature rises. In addition, the nominal value does not take into account the system losses or long-term degradation. The system losses are composed of resistance losses in the wiring, orientation, shading, efficiency of the power-conditioning unit, power mismatch of different modules and ability of the power conditioner to operate at the maximum power point. [13]

Photovoltaics are supposed to operate for 20–30 years, and degradation should be under 1 % per annum. There are two elements that define the lifetime of a PV product: durability and reliability. Durability refers to slow degradation that eventually diminishes the production to unsuitable levels. Reliability, however, refers to early breaking of the system. Globally the photovoltaic systems have been working for more than 20 years and therefore a lot of information about degradation mechanics is at hand. There are manufacturers that offer over 20-year warranties and are developing their products for a 30-year lifetime as a short-term goal. A lifetime this long means that the module would keep producing the energy at an efficiency of approximately 80 % in comparison with the starting efficiency. [13]

3.8.1 Performance ratio

In order to be able to describe the global performance of a PV system the so called performance ratio (PR) has been admitted into common use. The performance ratio is defined as the ratio between the actual electrical energy delivered to the power grid E_{AC} and the energy production of a lossless PV plant with the same irradiation conditions and at temperature of 25 °C. The performance ratio may thus be used to indicate the actual capability of the PV system of producing electrical energy under ideal conditions of each production location. The performance ratio is defined as

$$PR = \frac{E_{AC}}{\frac{G_y(\beta,\alpha)}{G^*} \cdot P_M^*} \tag{18}$$

where $G_y(\beta,\alpha)$ stands for global irradiation at given orientation α and tilt angle β, G^* represents the ideal global irradiation and P_M^* is the maximum power of the PV array under STC. There are three different yields included: reference yield Y_r, array yield Y_a and final yield Y_f. These yields are defined as follows $Y_r = G_y(\beta,\alpha)/G^*$, $Y_a = E_{DC}/P_M^*$ and $Y_f = E_{AC}/P_M^*$. The parameter E_{DC} in the array yield represents the direct current energy generated by the photovoltaic array. From yield point of view the performance ratio is defined as $PR = Y_f/Y_r$. Time factor is included in all of these three components, which provides an opportunity to separate the losses caused by the operation of the system, losses of the PV array and losses due to the inverter. [13]

System losses are defined as $L_S = Y_a - Y_f$, and they are the result of the inverter inefficiencies. Capture losses, however, are losses that are resulting from array operation outside the maximum power point voltage, spectral and angular losses, module mismatch, inferior performance due to low irradiance, coverage caused by snow and ice, partial shading, cell temperatures of more than 25 °C and losses in wiring and protection diodes. Definition for capture losses is $L_C = Y_r - Y_a$. The capture losses are expressed in hours per day of PV array operation at standard test conditions (STC). For example, losses in a really good grid-connected PV system are usually approximately $L_S = 7\,\%$ and $L_C = 15\,\%$. In such a situation the performance ratio will be around 0,78. Occasionally, the performance ratio of 0.75 is used as a recommendation for rough and quick estimation of annual energy production. [13]

When talking about the grid-connected PV systems, it holds that the output of grid-connected PV system equals the output of PV array output deducted by the losses in the inverter. It has been found that the reported experimental PR values are in the range of 0,65–0,8. The reason for such low PR values is the fact that occasionally the rated output provided by the manufacturer is greater than the power of installed PV arrays in practice. From Equation 18 it can be seen that the annual solar electric energy production of the PV system can be calculated in the following manner

$$E_{AC} = P_M^* \cdot Y_r \cdot PR \tag{19}$$

where the reference yield Y_r depends substantially on the local solar conditions and the orientation of the array, and is expressed in hours per year of peak irradiation at

$1\,\mathrm{kW/m^2}$. The maximum power of the PV array under STC, P_M^*, can be calculated simply by multiplying the rated power of the PV modules by the number of the PV modules. [13]

3.8.2 Degradation

There are three types of degradation in the PV systems that cause degradation: light-induced degradation (LID), Staebler-Wronski (S-W) degradation and long-term degradation. The power loss over time is usually a result of some combination of two of the above mentioned list. The light-induced degradation takes place in wafer type silicon modules and it causes an irreversible power loss of approximately 1–3 %. This phenomenon derives from the ingot formation process where oxygen impurities get trapped. The Staebler-Wronski degradation can result in the production loss of about 15–25 % during the first 1 000 hours of exposure, and it takes place in thin film silicon modules. However, the S-W degradation is partially reversible by annealing the thin film silicon for extended periods of time at temperatures between 50–150 °C [13]

The long-term degradation applies broadly to all PV technologies and mainly it has been reported to cause a loss of approximately 0,3–1 % in the annual energy production. The lower range of 0,3–0,5 % from the above mentioned range relates exclusively to the PV modules. The upper range of 0,5–1 %, however, relates solely to the PV system level degradation. Reasons behind the module-level degradation are increased series resistance due to solder bond thermal fatigue, internal delamination and encapsulant deterioration. Daily temperature cycling of the PV module will gradually lead to an increase of series resistance which, in turn, reduces the maximum power point voltage and thus the power of the PV module even though the manufacturers are consciously trying to minimize the losses of the series resistance. The reasons behind the system-level degradation, in turn, are not yet completely unambiguous. However, it is estimated that they would be caused mainly by the following: unaddressed failures of PV modules within a larger field of PV panels, corrosion at wire terminations and degradation of inverter circuitry [13]

3.9 Availability of solar radiation

The availability of the solar radiation is divided broadly over the globe. Due to the movement of the earth with respect to the sun, the best locations for receiving solar radiation can mainly be found on sub-tropical areas of the world. Figure 25 represents the average daily solar insolation on square meter of horizontal surface. For example in Sahara the momentary solar irradiation reaches the level of $1\,\mathrm{kW/m^2}$. As can be seen from Figure 25, the average daily solar insolation can reach the level of $7\,\mathrm{kWh/m^2/day}$ on the most potential areas in Sahara. However, in the north the solar insolation varies greatly with respect to the seasons, and the average daily solar insolation can be approximately at the level of $2\,\mathrm{kWh/m^2/day}$. [1] [2]

For instance, in the Middle East the average received solar insolation varies from $1\,800\,\mathrm{kWh/m^2}$ to $2\,300\,\mathrm{kWh/m^2}$. However, in Europe the average received solar

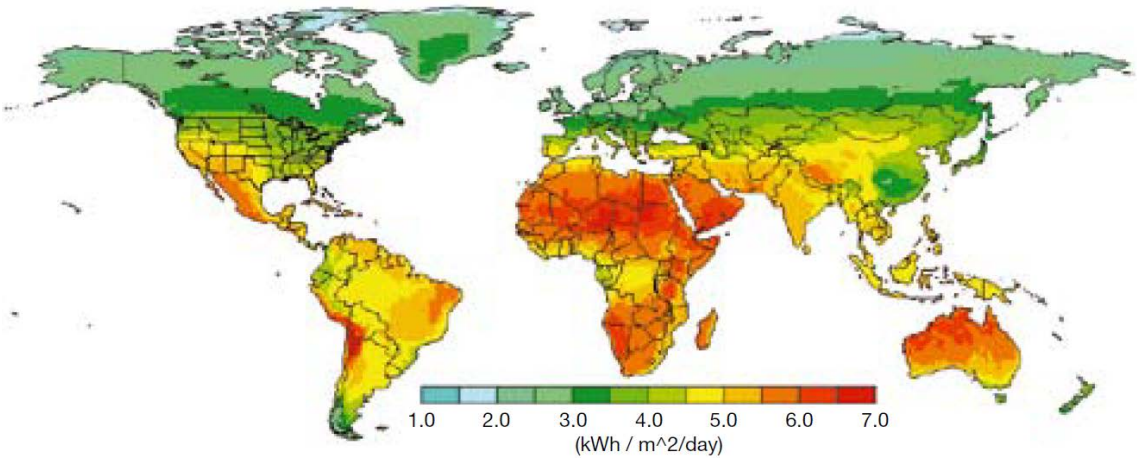

Figure 25: Average daily solar insolation on horizontal surface during years 1983–2005. [2]

insolation is approximately 1 200 kWh/m^2. As can be seen from Figure 26, the solar insolation varies greatly over the globe. [1] [2] An interesting observation from Figure 26 is that the annual solar insolation in Helsinki is approximately the same as in Hamburg even though the latitude of Hamburg is 53,6 N and the latitude of Helsinki is 60,2 N [15].

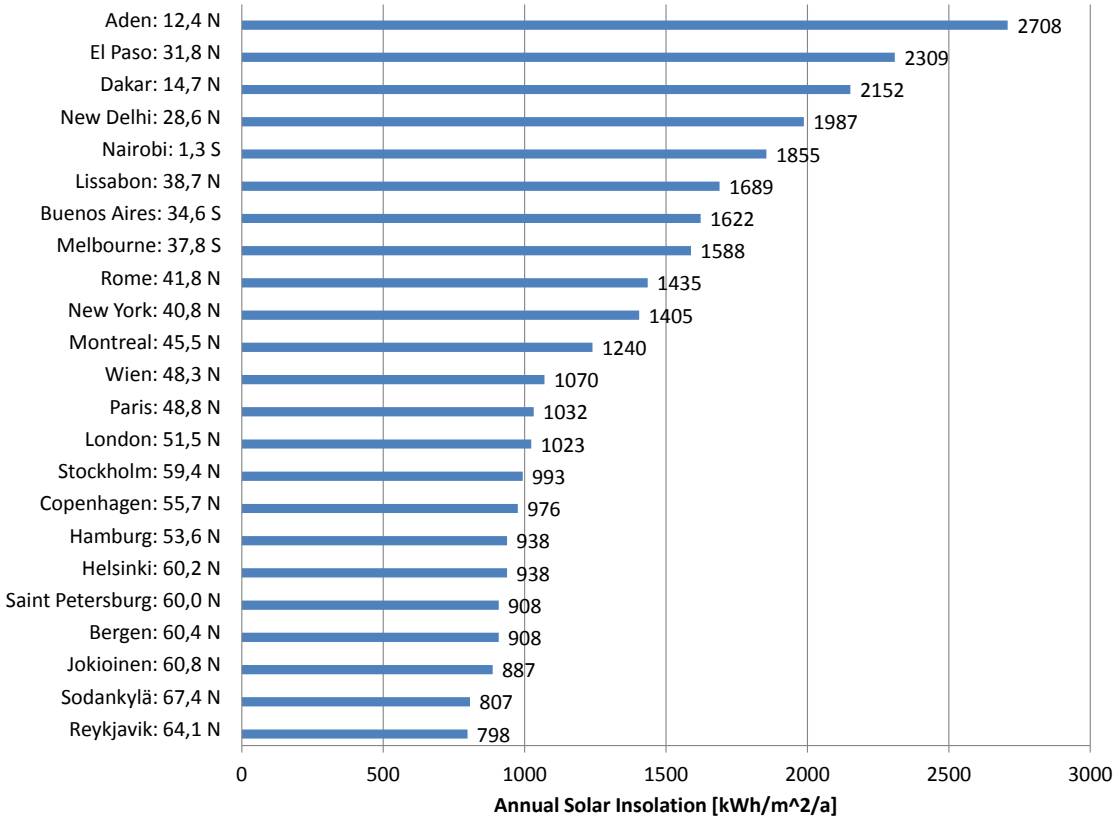

Figure 26: Annual solar insolation [kWh/m^2/a] between different cities and latitudes over the globe. [15]

Figure 27 shows the amount of solar irradiation for an optimally oriented plane in Europe. It can be seen from the Figure that the best areas in terms of annual solar irradiation can be found in the vicinity of the Mediterranean. For example, for a horizontal plane an annual irradiation of approximately 1 900–2 000 kWh/m^2/a can be received in the best locations of southern Spain. However, an optimally oriented plane can receive up to approximately 2 100 kWh/m^2/a in the same locations. [21]

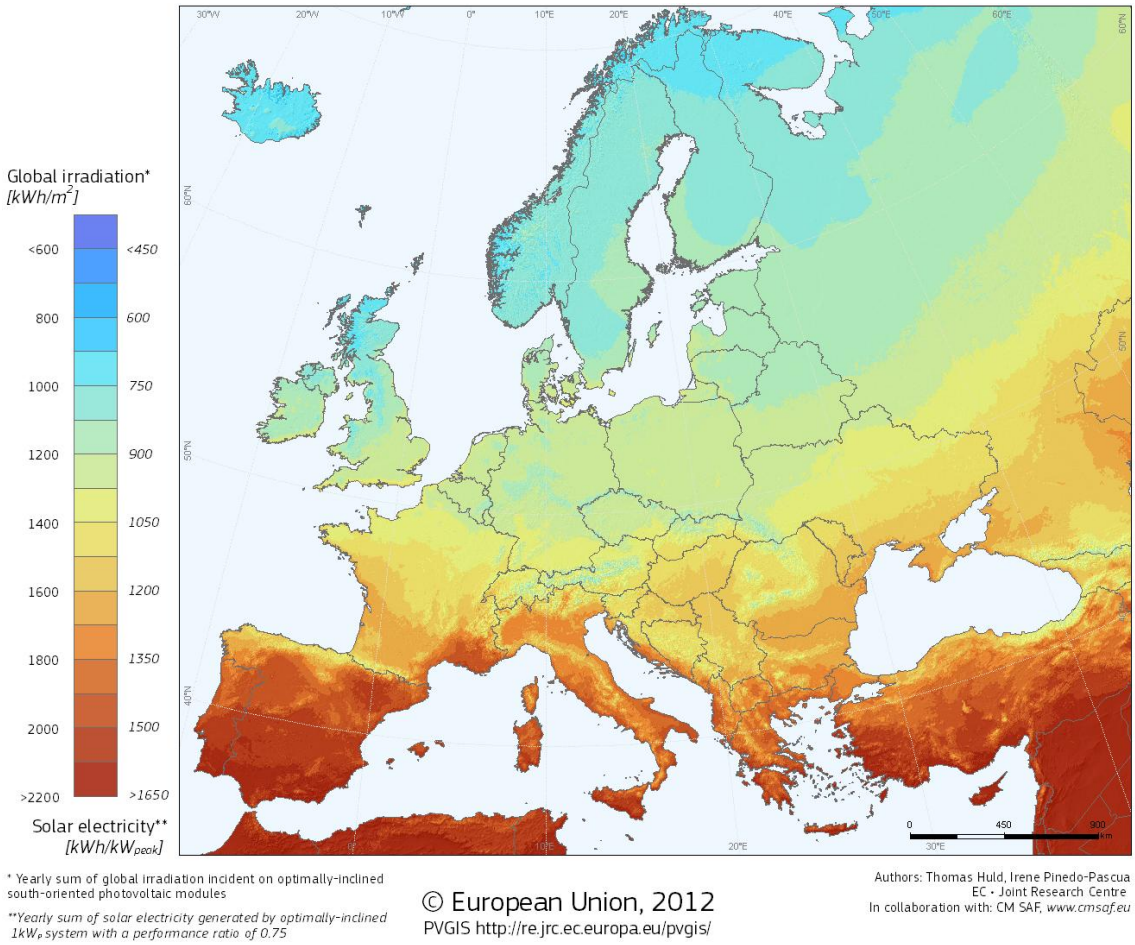

Figure 27: Photovoltaic solar irradiation and electricity potential in European countries for optimally oriented plane. [21]

In Finland the annual amount of solar irradiation to the horizontal plane in Southern Finland can be approximately 1 000 kWh/m^2/a. In Central Finland an annual irradiation of about 900 kWh/m^2/a can be achieved. [15] In the northern parts of Finland there is less sunlight available, and in the very northernmost parts of Finland the annual irradiation to the horizontal plane can be approximately 700–800 kWh/m^2/a. [21] A map in Figure 28 illustrates the annual sum of solar irradiation to the horizontal plane in Finland.

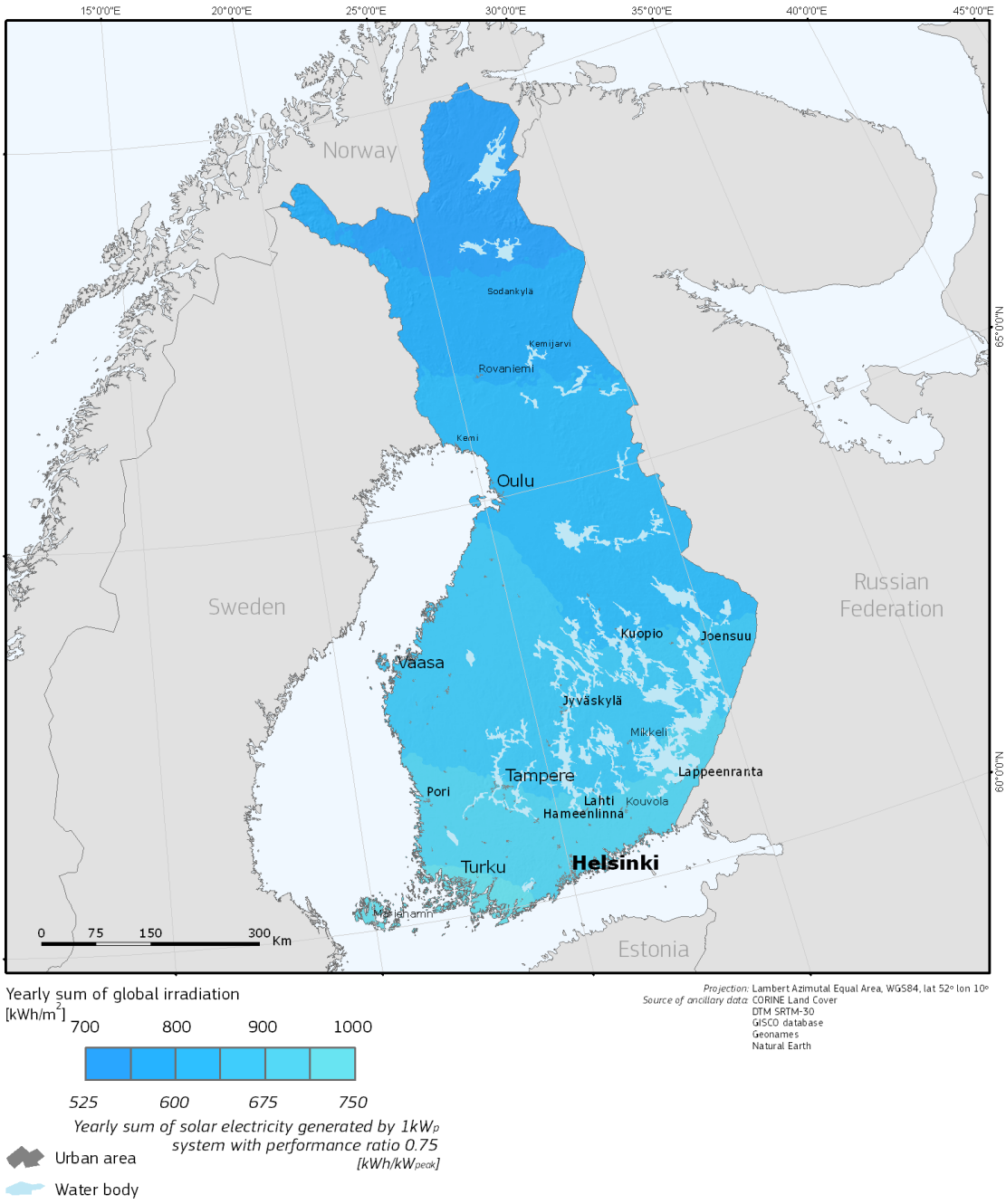

Figure 28: Yearly sum of solar irradiation for horizontal plane in Finland. [21]

3.9.1 Impacts of tilt angle on photovoltaic production

The intensity of the sunlight incoming to the plane of the array is defined by the tilt angle and the azimuth angle of the array with respect to the sun. In general, the optimum array orientation depends significantly on the load, weather conditions of the installation location and latitude. For low latitudes it is commonly accepted that the maximum output can be achieved when the tilt angle of an array is the

same as local latitude and the array is pointed towards true south in the northern hemisphere, and towards true north in the southern hemisphere. [20] [13]

At higher latitudes, for instance in the northern Europe, the maximum output can be achieved when the tilt angle is 10–15 degrees less than local latitude. However, it should be noted that the effect of tilt angle can be reduced if the location is exposed to a big amount of diffuse light. Even though the above mentioned tilt angle provides, in most cases, the maximum power output over the year the output can vary significantly because of the different lengths of daylight time between winter and summer. Especially high latitude locations like Finland are typical in this manner. Moreover, if winter load is higher than summer load, which is the case in Finland, an even bigger tilt angle can be better in order to increase the winter output. [20] [13]

The variation of the inclination angle has a surprisingly small effect on the amount of annual solar energy capture. A rough estimation is that each degree of deviation from the optimum inclination angle results in a loss of approximately 0,2 % in the annual collected solar energy. In the case of azimuthal angle, however, a rough estimation is that a loss of approximately 0,08 % in annual collected solar energy is seen for every degree of deviation from the south. Because of this, many of the existing surfaces such as roofs and car parks are suitable for the installation of the PV systems as such, even though they are not exactly at an optimal inclination and azimuthal angle from a sufficient photovoltaic production point of view. In addition, it is not necessary to carry out expensive construction works in order to level the installation site of the PV arrays. [13]

4 Evaluation of realistic maximum potential of solar electricity production in Espoo T3 area

The purpose of this chapter is to describe methods that were utilized in order to carry out evaluation of solar photovoltaic potential in Espoo T3 district area. First, the district area of T3 is introduced and defined followed by definition for potential photovoltaic energy model that was utilized in the evaluation. In addition this chapter presents all results and methods that were used in the examination.

4.1 Solar Energy from Existing Structures (SEES) Model

One of the main tasks of this work was to be able to define the potential solar electricity production that can be generated by utilizing existing roof surface areas of the Espoo T3 area. In order to define the potential solar electricity production a data package delivered by the city of Espoo was used. The data package included information about the annual insolation for all existing roof surface areas in Espoo. The data has been produced by utilizing a computer software model called SEES (Solar Energy from Existing Structures) which can be used to calculate the energy production potential of the roof installed solar panels. The SEES software model has been produced in a research project that has been conducted in collaboration between Fredrik Lindberg (University of Gothenburg) and Per Jonsson (Tyréns) in 2010 and 2011 [22]. The SEES software is written in MATLAB programming language, and its user interface has been written in Java. [23]

The insolation data of the roof surfaces in Espoo has been produced in collaboration with WSP Finland and WSP Analysis & Strategy Sweden. WSP Finland has produced all meteorology and building geometries, and WSP Analysis & Strategy has produced all the calculations. The SEES Espoo project itself was meant to produce a digital surface model of Espoo based on LAS (Log ASCII Standard) data. The SEES software model was used in the SEES Espoo project in order to define annual insolation for every existing roof surface area. The insolation data the all roof surface areas has been produced by using a spatial resolution of $0,5\,\mathrm{m} \times 0,5\,\mathrm{m}$. This means that one pixel corresponds to a roof surface area of $0,25\,\mathrm{m}^2$. The data package has been produced in a form of ESRI ASCII -grid file, and it includes information of all the buildings in Espoo such as footprint area of building, actual roof area (where all the slopes of roof surface has been taken into account) and annual insolation for the whole roof surface area of building. [24]

There are three shortwave components that are used in SEES software model: direct I, global G and diffuse D. The direct shortwave radiation I can be calculated as follows:

$$I = \frac{(G - D)}{\sin \eta}, \tag{20}$$

where η stands for altitude angle above horizon. Incoming short-wave radiation $K_{\downarrow}$ for a grid cell x, y is a function of direct I, global G, diffuse D and view factors Ψ.

Incoming shortwave radiation can be written as follows:

$$K_{\downarrow} = I[S_b - (1 - S_v)(1 - \tau)]\omega + D[\Psi_{sky\,b} - (1 - \Psi_{sky\,v})(1 - \tau)] + G\alpha[1 - (\Psi_{sky\,b} - (1 - \Psi_{sky\,v})(1 - \tau))](1 - f_s) \quad (21)$$

where α is the albedo, and it is treated as a constant value of 0,15. Parameter ω stands for the incidence angle of the sun. Parameter S stands for shadow as a boolean value (absence=1, presence=0), and subscript b stands for buildings and v for vegetation. Subscripts for Ψ indicate what aspects are being accounted for. For example subscript "sky b" stands for sky seen by building. Transmissivity of the shortwave radiation through vegetation is represented as τ. Overall the Equation 21 can be seen in three terms where the first and second terms represent direct and diffuse radiation fluxes, and the third represents reflected radiation. [24]

All the SEES calculations are based on meteorological data delivered by Espoo where all the shortwave components (direct, diffuse and global) are included as well. Originally the meteorological data has been produced by the Finnish Meteorological Institute. The data describes an average sample year in terms of weather in Espoo. A typical year with hourly irradiance in Espoo is illustrated in Figure 29. Global radiation is a sum of direct and diffuse radiations. Oscillation of irradiation in the summer months can partly be explained by a quick emergence of cumulus clouds. [24]

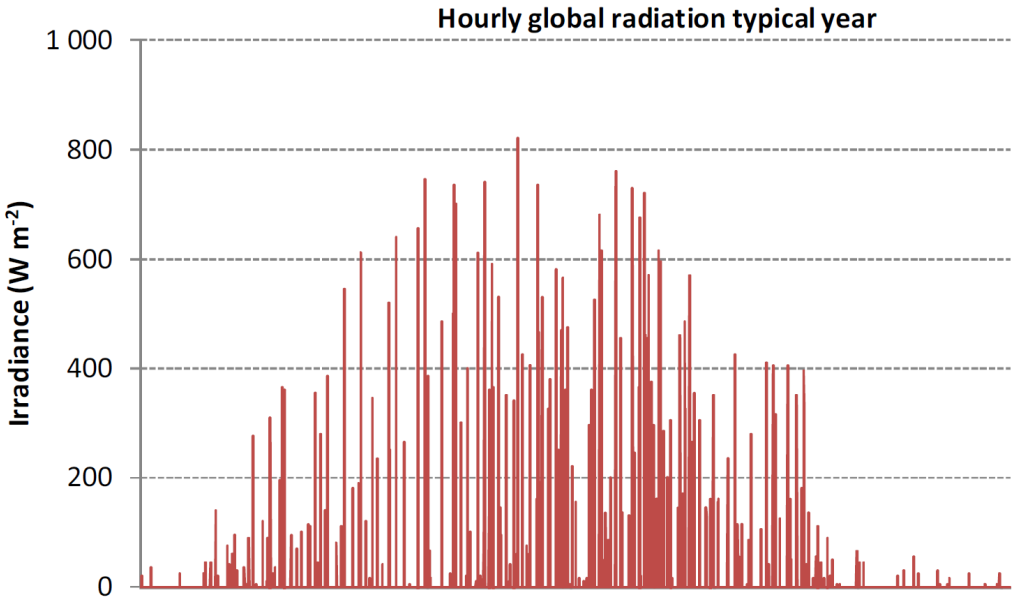

Figure 29: A typical year in terms of global radiation in Espoo. [24]

A digital surface model is needed for the SEES calculation, and it was made in ESRI ArcGIS ASCII format. The digital surface model was produced from laser scanning data delivered by Espoo. Data was classified in Terrasolid software which included point classification to several classes such as buildings, low vegetation, med vegetation, high vegetation, low points and ground points. Data covers only

buildings that have a footprint area of $20\,m^2$ at least. Altogether, the final data package covers a total footprint area of $11,3\,km^2$, which corresponds to a total actual roof area of $14,8\,km^2$ when the inclinations of the roof areas are taken into account. Overall, the data covers approximately $425\,km^2$ of land and 43 589 buildings that were identified by utilizing the above mentioned criteria. Insolation is color-coded in the pixels in the final map which enables the recognition of good insolation roof surface areas straight from the map. A map of investigated areas in Espoo is illustrated in Figure 30 where footprint areas are indicated in black color. [24]

Figure 30: An overall map of the data that was produced in the SEES Espoo project. [24]

From the results of the SEES Espoo project it can be seen that the insolation is widely divided between the roof areas of Espoo. The division of all roof surface areas as a function of insolation can be seen from Figure 31. [24]

It can be seen from the Figure 31 that the major group of the roof surface areas in Espoo can be found in the range of 900–1 000 $kWh/m^2/a$. Based on the histogram represented in Figure 31, WSP and Espoo has made a definition for a good roof surface area. A good roof surface area is an area of at least $10\,m^2$ where the entire area receives an insolation of at least $900\,kWh/m^2/a$. [24] As will be seen later in this work, this approach of a good roof surface area has been used as one filter in

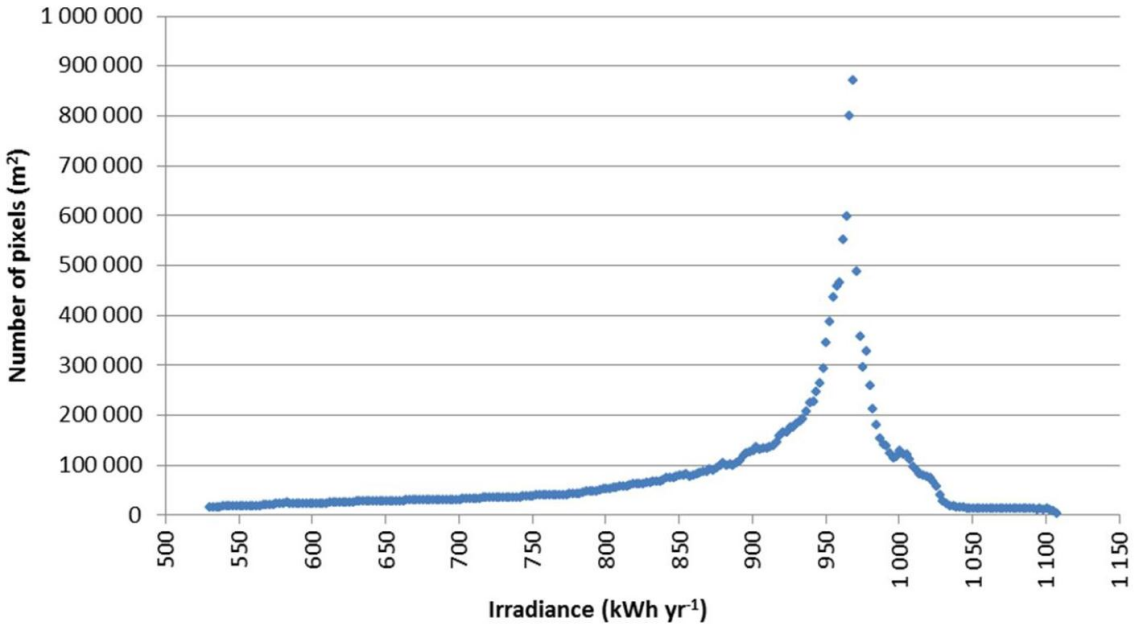

Figure 31: Division of insolation between all roof surfaces in Espoo. Chart illustrates the number of pixels (actual foor area) as a function of insolation. [24]

order to make a realistic estimation of the solar electricity production potential in the Espoo T3 area. Since the data has been received from Espoo, and this decision has been made during the working process of the SEES Espoo analysis, the decision for good roof surface area cannot be changed or varied for the purpose of this work.

4.2 Definition of T3 area

Espoo is the second largest city in Finland, and in 2012 it was a world design capital in collaboration with the cities of Helsinki, Vantaa, Kauniainen and Lahti. The world design capital is nominated every second year, and it is nominated by the International Council of Societies of Industrial Design based on the applications. World design capital for the year 2014 was Cape Town. The two previous world design capitals were Torino in year 2008 and Soul in 2010. The goal of the world design capital of the year 2012 was to be able to develop public services and business, and to improve everyday life and living environment of city dwellers. The international Council of Societies of Industrial Design, which has been established for this purpose, is responsible for all the actions related to the concept of the world design capital. [25] [26]

The Tapiola district is comprised of three different areas Otaniemi, Keilaniemi and Tapiola (also known as the Center of Tapiola) [27]. One of the main focus points of Espoo in the year of world design capital of 2012 is the T3 project which will be carried out in the areas of Otaniemi, Tapiola and Keilaniemi. These three areas are very essential for the metropolitan area which is why the T3 project aims to create new innovations in this area. The name T3 comes from three Finnish words

that all start with the letter T. All of those three words describe the corresponding district area. These three words are "Tiede" (science), "Taide" (art) and "Talous" (economy). "Tiede" refers to Otaniemi, which can be seen as a big scientific centre, where the campus area of Aalto University is located. "Taide", in turn, refers to Tapiola as it houses plenty of artistically valuable objects. Finally, "Talous" is associated with Keilaniemi since it is particularly known for the big corporate headquarters such as Microsoft and KONE. [25] The location of the T3 area in Espoo municipality can be seen from Figure 32 that has been taken from the SEES Espoo data.

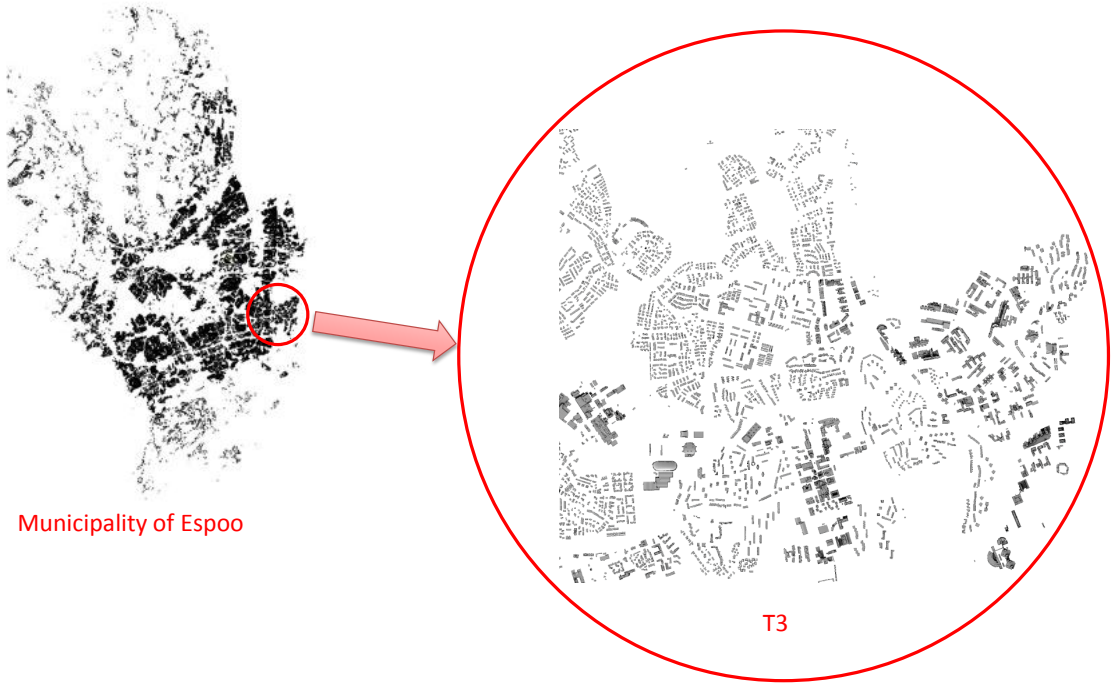

Figure 32: Location of T3 area in Espoo municipality. Pictures are taken from SEES Espoo data package. [24]

One of the main purposes of this thesis is to be able to define realistic solar electricity production potential of grid-connected PV systems in the T3 area. Borders of the T3 area were taken from the map pages of Espoo. The amount of buildings was calculated manually from the SEES Espoo data. The three areas of T3 differ considerably from each other in terms of buildings.

Tapiola is the biggest and the most multi form of these three areas. Tapiola is built as a garden town by Asuntosäätiö in the 1950s and 1960s. Tapiola residential area and residential design got a lot of fame and attention in the 1950s both at home and abroad. Tapiola has served as an example in particular in the planning of holistic living environment and community. The business center of Tapiola has later been expanded in a different way from the original garden town ideology. [28]

The buildings in Tapiola are mainly residential but there are also a lot of other building types, such as offices, commercial buildings, public buildings as well as

buildings that are related to the culture and history of Espoo. Also buildings of special architectural interest can be found in Tapiola. [27] [29] The population of the center of Tapiola was 9 335 at the turn of 2011 and 2012 [30]. The total amount of buildings in Tapiola is 606 [24].

Otaniemi, in turn, has mainly buildings related to Aalto university and its campus area that include also buildings of special architectural interest. In addition, Otaniemi includes commercial, public and residential buildings. [27] [31] The amount of buildings in Otaniemi is 187 [24]. The population in Otaniemi amounted to 3 630 at the turn of 2011 and 2012 [30].

The buildings in Keilaniemi are mainly offices and big corporate headquarters. In addition, some restaurants can be found in Keilaniemi. [27] The biggest characteristic that separates Keilaniemi from Tapiola and Otaniemi is the fact that the number of inhabitants in Keilaniemi was zero at the turn of 2011 and 2012 [30]. The amount of buildings in Keilaniemi, 29, is small compared to the two other areas [24]. A summary of T3 area with number of buildings and population information is illustrated in Figure 33.

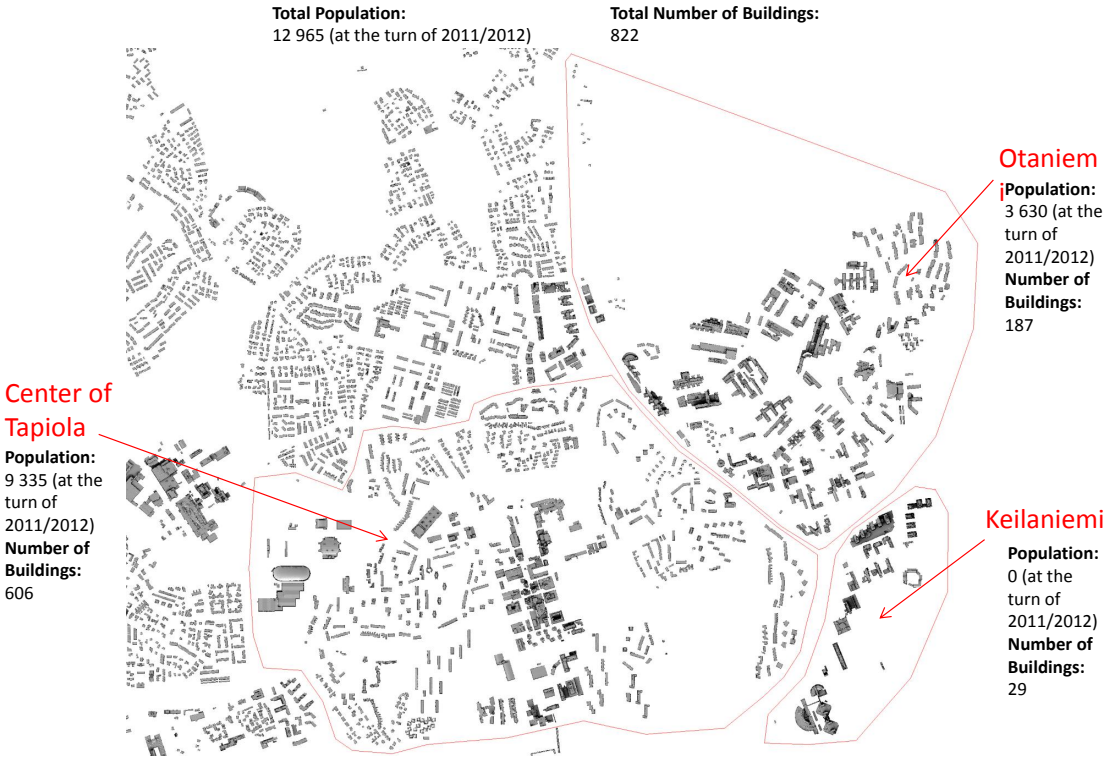

Figure 33: A map of the T3 area showing the borders of Tapiola, Otaniemi and Keilaniemi. Population, number of buildings in each area and types of buildings are also represented in Figure. Picture has been taken from the color-coded SEES map data made by WSP. [30] [32] [24]

4.2.1 Building types of T3 area

Each building of the SEES data located in the T3 area was checked manually in order to be able to categorize the buildings into building types. The chosen building types in this thesis are apartment house, detached house, row house, office, commercial, public, educational, sports center, multi-storey garage and other. The category other includes all the other buildings that cannot be classified as manned buildings such as car shelters, waste canopies, unmanned service stations, water towers, stables, small thermal power stations, bus stops, monuments and piers.

All the buildings that are not offices, commercial, educational, sports centers or parking houses, and to which everyone has access without permission, were defined as public. These include, for example, libraries, churches, health care buildings and social welfare buildings. Table 1 illustrates the division of chosen building types between Tapiola, Otaniemi and Keilaniemi.

Table 1: Division of building types in the T3 area. The table shows the amount of buildings in each chosen building types. In addition, totals for the building types and the three T3 subareas (Keilaniemi, Otaniemi and Tapiola) are included.

Building type	Keilaniemi	Otaniemi	Tapiola	Total
Apartment house		42	180	222
Detached house		28	223	251
Row house			77	77
Office	19	52	32	103
Commercial		2	17	19
Public		4	7	11
Educational		17	6	23
Sports center		1	7	8
Multi-storey garage			2	2
Other	10	41	55	106
Total	29	187	606	822

Tapiola has served as an example, in particular, in the planning of comprehensive living environment and community. Against this background, it is easy to understand why Tapiola contains the most residential buildings in the T3 region. Tapiola's business center has later been expanded from the original garden city vision in a different way which, in turn, explains the relatively large number of commercial, public and office buildings compared to other areas of T3. In addition, Tapiola comprises the most extensive region of T3, which is why a lot of public buildings, parking garages and sports centers can be found in the area. The large size and the large number of residential buildings compared to the other two areas also explain the biggest amount of the other rarer building types such as parking shelters, waste canopies, bus stop shelters, service stations etc. [28]

The nature of Otaniemi as a campus and business area can be seen from the

high quantity of office and educational buildings. A few public buildings such as the church and the library can also be found in Otaniemi. Teekkarikylä inside Otaniemi is a residential area designed for students which explains the number of residential buildings and buildings for various activities such as sports hall Otahalli albeit row houses and multi-storey carages do not exist in the area. [27]

The number of residential buildings in Keilaniemi is zero which makes it differ largely from the other two areas of T3. According to population statistics the number of inhabitants in Keilaniemi was also zero at the turn of 2011 and 2012, so the building stock consists mainly of office buildings. Keilaniemi also includes a harbour and parking areas, which makes the number of other building types approximately a third of the total number of buildings in Keilaniemi. [27]

As can be seen from Table 1 the majority of the buildings in T3 area consist of apartment houses and detached houses. Residential buildings are therefore the most common in T3. The nature of Keilaniemi as the area of business premises, the shopping centre of Tapiola and Otaniemi as the area of university campus and business premises explain the high number of office buildings in the area of T3. The amount of other buildings is relatively big but when all the included shelters and so-called unmanned buildings are taken into consideration a number this big for such a lively and busy area can be understood.

4.3 Methods of examination

The first main objective of this work was to determine the maximum realistic production potential of solar electricity for the grid-connected photovoltaic systems assembled on the roofs of existing buildings. All calculations related to solar electricity production potential were carried out based on the SEES data provided by WSP and the City of Espoo. In order to be able to utilize the data, an open-source software called Quantum GIS was used as a tool. Quantum GIS is an open-source Geographic Information System (GIS) software operating on all operating system platforms, and it is an official project of the Open Source Geospatial Foundation (OSGeo) and licensed under the GNU General Public License [33]. By utilizing the SEES data packet delivered by the city of Espoo the theoretical maximum potential of solar electricity production for the roof surfaces of the whole T3 area can be calculated. In this case, the theoretical maximum potential of solar electricity production, in practice, describes a situation in which every possible roof surface area is used for solar power generation. However, in real life all the available roof areas cannot be exploited for the production of solar electricity because of the demands of city planning, different roof structures and differences in the availability of sunlight.

In order to be able to define a more realistic maximum potential of solar electricity production from the theoretical maximum potential, three filters were defined in this thesis. The three filters are used to eliminate all the unsuitable roof surfaces areas from the total available roof surface area in order to be able to define the realistic maximum potential of solar electricity production in the T3 area. The three filters are: profitability filter, city planning filter and filter for mechanical barriers.

4.3.1 Assumptions behind the calculations

In addition to the Esri ASCII map, the SEES data delivered by the city of Espoo included information about all the buildings in Espoo area. Each building was identified by own identification number and had the following information:

- Footprint area [m^2]
- Actual roof area [m^2]
- Total irradiance [kWh/a]
- Average irradiance [$kWh/m^2/a$]
- Total good roof area [m^2]
- Irradiance on good areas [kWh/a]
- Average irradiance on good areas [$kWh/m^2/a$]

All calculations have been made based on the assumption that the PV systems are grid-connected without storage capabilities. In addition, each PV array is installed at the same level with the roof surface in each building. Therefore, the current orientation of the roof surface determines the orientation of the PV array. This assumption had to be made because the data of total annual irradiance provided by the SEES data is a sum of the solar energy that is received annually by the actual roof area of the building which includes all different orientations of the roof. Since the SEES data does not include any information about the orientations of the roof surfaces it is justified to assume that the PV arrays are also always installed at the same level with the roof surface. It is also assumed that every possible roof surface area is always used for solar electricity production.

In order to be able to utilize the SEES data in the calculations, all the buildings had to be divided into three groups (Tapiola, Otaniemi and Keilaniemi) according to the location. This could be done with the help of the selection tool of the Quantum GIS software, the building identification number provided by the SEES data and Microsoft Office Access software.

All the calculations of solar electricity production potential were carried out based on the assumption that the PV arrays are made by using crystalline silicon technology. The conversion efficiency of the crystalline silicon cell was assumed to be 17 %. [34] [19] The performance ratio, in turn, was assumed to be 0,85. These assumptions have been made based on an interview with Solar Technology Manager Eero Vartiainen of Solar Business Development at Fortum Oyj and a careful investigation of solar module database provided by PHOTON. The idea behind the assumptions is that the installation for an area as big as T3 will probably last for years. Therefore, if the present conversion efficiency of the single crystal silicon cell is approximately 15 %, as stated in the section 3.5.1, it has been thought that the average efficiency of single crystal silicon cell will slowly increase, by the effect of

technology development, to 17 % by the year of 2020. The thought behind the chosen performance ratio is to reflect the realistic performance of the PV system in the climatic conditions of Finland. These assumptions are intentionally set optimistic, so that the situation will better reflect the situation in a few years from now and the positive expectations of the development of the PV system markets in Finland. [34] Equation 19 was utilized for the calculations of annual solar electricity production potential.

4.3.2 Profitability filter

The first filter is a so-called profitability filter. The purpose of this filter is to eliminate all the unsuitable roof surface areas that do not receive enough annual solar irradiance from the theoretical maximum roof surface area of T3. As stated above in the section 4.1, this filtering was carried out by WSP and the city of Espoo in order to eliminate the risk of including several small suitable surfaces scattered across a roof [24]. In addition, this definition can be treated as the elimination of less profitable roof surface areas from the investor point of view.

The definition for a good roof surface area, and hence the definition of the profitability filter, is that a good roof surface area is an area of at least 10 m^2 where the entire area receives an insolation of at least 900 $kWh/m^2/a$ [24]. By using the profitability filter a so-called maximum production potential of profitable roof surface areas can be calculated from the theoretical maximum production potential. In this case, it is assumed in this thesis that all the roof areas that would remain unexploited for solar electricity production because of the poor availability of solar radiation can be eliminated from the theoretical maximum solar electricity production potential by the use of this above mentioned filter.

4.3.3 City planning filter

Since the city planning has a great impact on the buildings that are both possible and permissible to be exploited for solar electricity production a so-called city planning filter was used as a second filter in the calculations. The assumptions and terms of the city planning filter were determined by interviewing Robert Eriksson, architect from Espoo city planning. The terms and urban planning principles used in this thesis do not represent any official comments related to the installation of PV systems from architectural point of view, and thus should not be generalized.

The city planning aspects related to the installation of PV systems are always case-specific. The boundary conditions have been made as a private person for this thesis and an optimistic point of view has intentionally been used. Since the T3 area contains a lot of culturally and historically valuable and protected objects, also the literature about the cultural history of Tapiola was utilized in the determination of the boundary conditions of the city planning filter. The final filtering in terms of boundary conditions of city planning represents an interpretation of the author of this thesis from the results of the interview and the literature about the cultural history of Tapiola.

Both Tapiola and Otaniemi include a large number of buildings that belong to nationally significant cultural environments and therefore they need to be treated with special accuracy in terms of solar electricity production. However, regarding the buildings of Keilaniemi there are no restrictions since the area is relatively new and under major changes. [29] [31] [35]

According to the information from an interview with Robert Eriksson the most valuable and nationally significant buildings in Otaniemi and Tapiola should principally be avoided. In particular, the buildings situated in a prominent location must be avoided since their appearance is clearly visible against the horizon. The main aspects to take into account are the famous Figures of the nationally significant buildings that must not change by the installation of PV arrays. However, according to Robert Eriksson an optimistic perspective can be used for this thesis. As a general principle, Eriksson mentioned that the upper edge of the PV array must not be more than 1,5 meters higher than the rest of the roof surface. In addition, the arrays should not stand out from the roof surface when viewed from the street level. [35]

Eventually, regarding the interpretation of Otaniemi and Tapiola it was concluded that all the buildings that appear in publications of cultural history with relation to the area of Tapiola should be excluded from the potential buildings. In which case, they can be considered as significant cultural heritage and therefore it is reasonable to eliminate them from the potential roof surface areas in terms of solar electricity production. According to Robert Eriksson, Tapiola is currently under major changes, and therefore all the other buildings can be seen as potential buildings for solar electricity production except for the buildings that are considered as historically significant cultural heritage. [29] [31] [35] [36] [28] [37] [38]

4.3.4 Filter for mechanical barriers

The usability of the roof surface areas for solar electricity production is particularly limited by the physical barriers and surface profile of the roof surfaces which in practice can prevent the installation of PV arrays. The physical barriers may be caused by the structures related to the building technology, maintenance of the building and roof surface profiles. Such barriers can be for example ladders, skylights, ventilation equipment and other surface profiles that complicate the installation of the PV arrays. In order to be able to make the calculations of maximum solar electricity production potential more realistic, the third limiting filter for mechanical and physical barriers was defined. Requirements relating to the installation of solar panels were determined by interviewing Markus Andersén from Naps Solar Systems Oy. In addition, satellite and helicopter photos from the area of Espoo were utilized in the determination of the physical and mechanical barriers of the roof surface areas in T3. The final measurement and determination of the inappropriate roof surface areas from the SEES data was carried out manually one building at a time by using the measurement tool of Quantum GIS software. [39]

Regarding the structures of the buildings, only barriers that could be identified by using either satellite images or helicopter images were included. A more detailed

evaluation would require a visit to each roof. As a result, only those of the barriers that could be recognized as a serious barrier for installation of the PV arrays were eliminated from the SEES data.

In principle, solar modules can be installed on all buildings if only the roof area, inclination and roof materials are suitable for it. In the case of detached houses the installation is done, in principle, on inclined roof surface, and the modules are installed approximately 5–10 cm above the roof surface allowing an air gap between the modules and roof so that the rain fits to flow down to gutters between the panel and the roof, and for example snow and leaves can removed from the roof. However, in the case of flat roof surfaces, the roof edge must be often taken into consideration, and the module has to be raised above the edge so that the edge would not shade the module. [39]

Wind load, waterproof fastening of the arrays and the mechanical strength of the roof are the three most important features regarding the installation of the PV systems in existing buildings. The installation can also be done without drilling with the help of weights but it would increase the demands for mechanical strength of the roof. The biggest challenge is always associated with the water resistance of the attachment and the roof. Therefore, the installations must be done carefully in terms of waterproofness and mechanical strength. On the other hand, existing bridges and snow stops are already using similar mortgages on the roof, so it is not a problem but an issue which should be done always with great care. [39]

In order to avoid the snow load in Finland a useful solution is to raise the modules to a higher level, in which case the lower part of the module is at an altitude of 1,5 m. In addition, the increase of the tilt angle allows the snow to drip off. The snow load is not usually a problem in Finland, as the withstand capacity requirements of the roofs are very high. Similarly, the wind load is rarely a problem in Finland since the panels are usually mounted at the tilt angle of 30 degrees. Therefore, the amount of the wind-receiving surface area is less than in the case of higher tilt angles. The maintenance routes are made between the module rows according to the needed room. According to Andersén sun tracking PV systems are not recommended to be installed on the roof since the mechanical characteristics of the installation may lead to too high torques for the roof to endure because of the wind load. The reason for this is that in the tracking PV systems, the array is often installed on a long arm, whereby the wind can cause the torque on the point of attachment of the arm to exceed the duration of the roof. In addition, the tracking PV systems are significantly more expensive than usual roof-mounted PV systems. [39]

4.4 Results

All the calculations of solar electricity production were done according to the above mentioned assumptions. The main principle is that all the available roof surface areas are used for solar electricity production excluding such roof surfaces that do not receive enough solar radiation (profitability filter) or are considered as historically significant cultural heritage (city planning filter) or have mechanical barriers that prevent the installation of the PV modules on the roof (filter for mechanical barriers).

By using the building-specific information about actual roof surface areas, annual received solar radiation energy and the above mentioned three filters the annual insolation for all the roof surfaces of T3 could be calculated. Figure 34 illustrates the annual insolation that is received by the roof surface areas of Keilaniemi, Otaniemi, Tapiola and the whole T3. In addition, the Figure shows the effect of three filters.

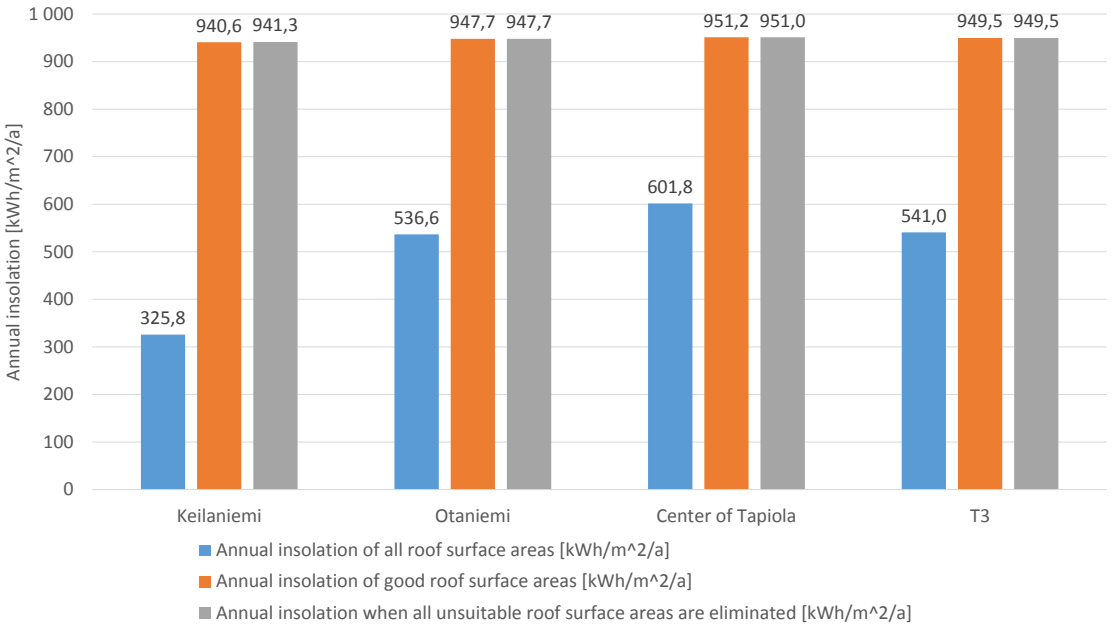

Figure 34: Annual insolation of the roof surface areas in Espoo T3 area.

In Figure 34, the blue bar depicts the result received by dividing the total solar radiation energy of all roof surface areas in the T3 area by the total roof surface area in T3. The impact of the profitability filter is illustrated by the difference between the blue and the red bars. The grey bar, in turn, represents the insolation received on the roof surface areas after eliminating the areas that are unsuitable for producing solar electricity based on the three above mentioned filters. Therefore, the outcome in the grey bar is obtained by filtering the result in the blue bar with both the city planning filter and the filter for mechanical barriers.

Figure 34 illustrates that the insolation is in principle the biggest in the buildings of the Tapiola area. Approximately 949,5 $\mathrm{kWh/m^2/a}$ solar radiation energy is received in the total T3 area when all unsuitable areas have been eliminated using the three filters. As insolation is calculated as energy in relation to area, it appears logical that the first filter improves the amount of solar radiation energy received per square meter. This is because the first filter excludes all roof surface areas that are less than $10\,\mathrm{m^2}$ in size and receive less than $900\,\mathrm{kWh/m^2/a}$ of solar radiation energy annually. From Figure 34 it can be seen that the impact of the last two filters (city planning filter and filter for mechanical barriers) on the amount of the annual insolation is rather small. The reason for this is most probably that the first profitability filter with its tight criteria already excludes most unsuitable areas for producing solar radiation energy. Therefore, it can be assumed that the remaining

roof surface areas carry good conditions for producing solar radiation energy, which is why the city planning filter and the filter for mechanical barriers are able to only marginally improve the average production conditions.

Eero Vartiainen has studied daylight modelling in Finland in his doctoral thesis (Daylight modelling and optimization of solar facades, Helsinki University of Technology, Espoo 2000). Hourly horizontal global and diffuse irradiance measurements in Helsinki-Vantaa airport, Jyväskylä airport and Sodankylä observatory between the years of 1971–1993 provided by the Finnish Meteorological Institute were utilized in the doctoral thesis. [40] These measurements of Helsinki-Vantaa airport can be considered as a reasonable reference for the calculation results of annual solar insolation in this thesis since the location of Helsinki-Vantaa airport is approximately ($60° 17' \mathrm{N}, 15° 58' \mathrm{E}$) and the location of T3 area is approximately ($60° 9' \mathrm{N}, 15° 48' \mathrm{E}$) [41]. The arithmetic mean calculated from the solar insolation measurements of Helsinki-Vantaa airport between the given period of time is 937,7 $\mathrm{kWh/m^2/a}$ with the maximum being at 1 040,7 $\mathrm{kWh/m^2/a}$ in the year of 1975 and the minimum being at 791,5 $\mathrm{kWh/m^2/a}$ in the year of 1977. [40]

The result obtained above, 949,5 $\mathrm{kWh/m^2/a}$, is very close to the arithmetic average, 937,7 $\mathrm{kWh/m^2/a}$, of the measurement data presented in Eero Vartiainen´s doctoral thesis. The difference can be interpreted as fairly small, especially when considering that the T3 area is located close to the sea, which might show as a difference in terms of weather conditions between these two locations. In addition, the result received in this thesis represents a result of mathematical modelling, which inevitably contains errors and inaccuracy. Therefore, it can be assumed that a significant part of the difference between the measured and calculated insolation is due to the presumptions and structure of the SEES model, whereby the result measured in the real world is in practice impossible to model perfectly. The error between the calculated and measured result is approximately 1,26 %, which can be interpreted as minor in terms of the usability of the calculations in this thesis.

4.4.1 Impact of filters on the amount of buildings

The usage of the above mentioned filters has an impact on the amount of buildings, where solar electricity eventually can be produced in the T3 area. Figure 35 illustrates the amount of buildings in the T3 area per building type, when the three filters specified in this thesis are used to eliminate roof surface areas unsuitable of producing solar electricity. The blue bar represents the total number of all building types in the entire T3 area. The difference between the blue and the red bar stands for how many buildings are eliminated from the potential building stock by the impact of the profitability filter. The grey bar, in turn, depicts the amount of buildings per building type that are left when all tree filters are used to exclude unsuitable roof surface areas. The yellow line reflects the amount of buildings from each building type left in relation to the original amount when all three filters are in place.

As can be seen, multi-storey garage is the only building type, where the share of final number of buildings ends up being zero. In addition, it is the only building

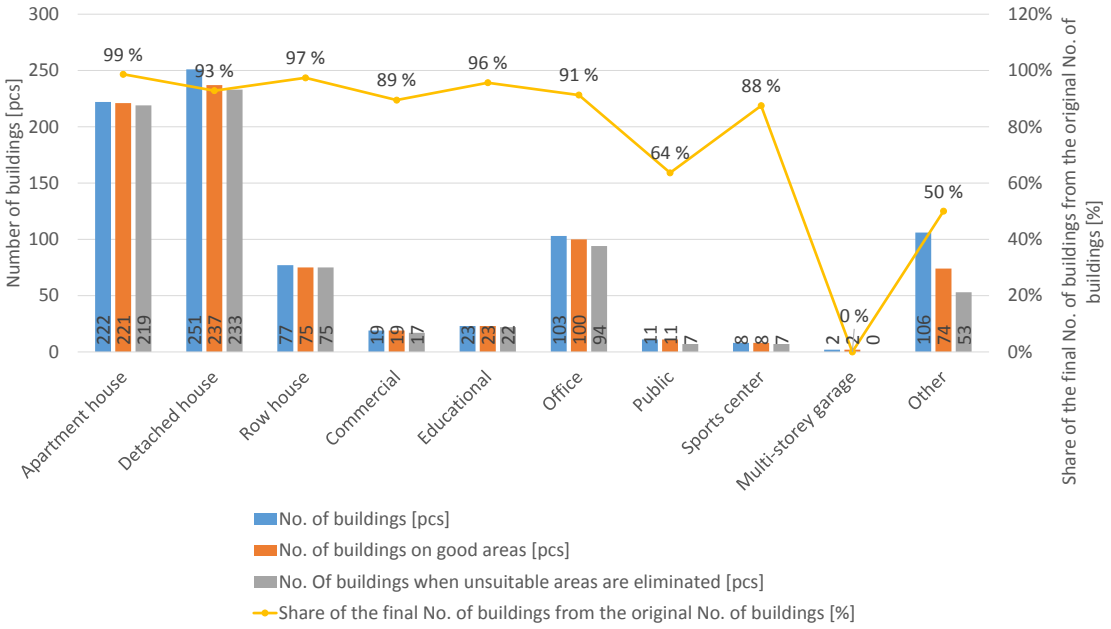

Figure 35: Impact of three filters on the different building types in T3 area.

type with a decrease of more than 50 % when it comes to the share of final number of buildings. However, the numerical reduction is only two buildings. The building type other ends up with only half of the buildings after the filtering. Also, this is the building type where numerically seen the biggest amount of buildings are eliminated, which partly can be explained by the fact that it contains various shelters and unoccupied buildings in which the conditions for sunlight probably has not been the main priority at the building stage. Moreover, in these kinds of buildings, the surface shape of the roofs can vary significantly. As the building type other comprises shelters and unoccupied buildings, it can be seen as a less probable location for installation in comparison to the other building types, which is why the lack of this building type is not a distressing issue for the potential of solar electricity production in the T3 area. To sum, it appears that the biggest amount of unsuitable roof surface areas in the entire T3 area can be found in the building type other.

In the so called residential buildings, i.e. apartment house, detached house and row house, the share of final number of buildings from the original number of buildings is over 90 % after using the three filters to delimit the roof surface area. Since it can be assumed that residential buildings represent commercial PV system customers, this outcome can be interpreted to mean that the potential of solar electricity production is rather big among residential buildings in the T3 area. Also for other building types the share of final number of buildings from the original number of buildings remains high even after the filtering. For commercial, educational and office buildings, as well as sports centres, the percentage is around 90 after the elimination using all three filters.

What is more, there are region-specific differences inside the T3 area considering the number of buildings. The amount of buildings per region are presented in

Figure 36. In addition, Figure 36 shows that the three filters have a reducing effect on the amount of buildings, when they are used to determine the realistic roof surface area suitable for real life solar electricity production. The number of buildings per region are illustrated by the blue bar. The size of the red bar describes the building amount having used the profitability filter to eliminate the weakest roof surface areas in terms of solar radiation energy. The grey bar reflects the number of buildings per region that in practice presumably can be used for solar electricity production assuming all three filters are used to eliminate unsuitable roof surface areas. Finally, the yellow line stands for the number of buildings left in relation to the original number of buildings for each area.

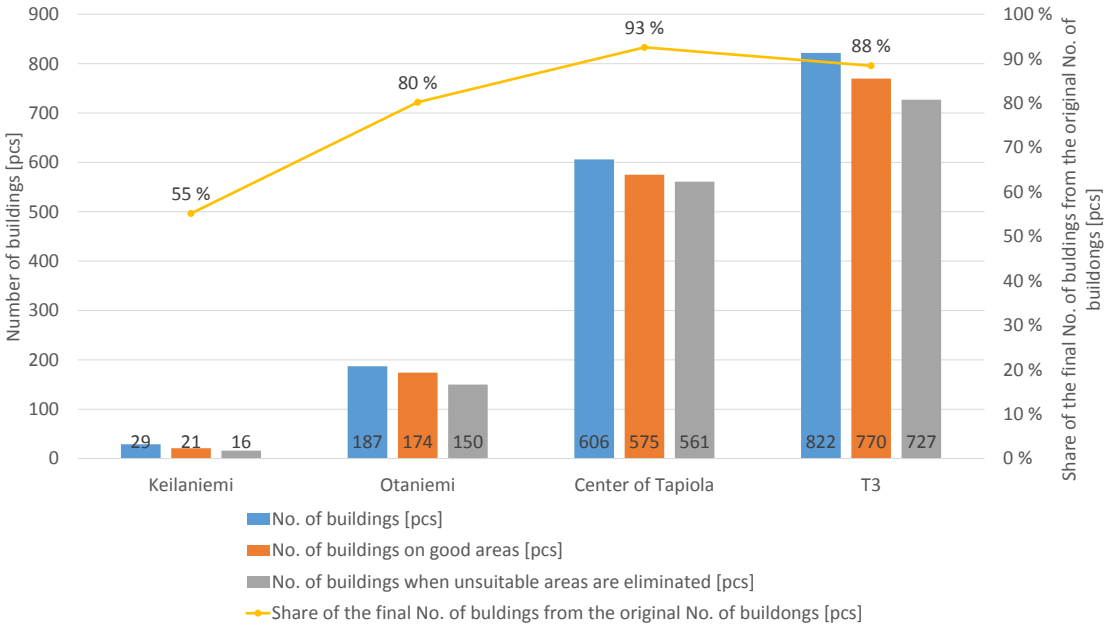

Figure 36: Change in the amount of buildings between the areas of T3 by the effect of three filters.

The number of buildings is greatest in Tapiola, which is logical as Tapiola has originally been planned as a garden city with a significant amount of residential buildings and a lively, constantly evolving city center [28]. In Tapiola, the decrease in the amount of buildings is relatively seen the smallest when the unsuitable roof surface area is eliminated using the three filters. However, when measured in numbers, the decrease is the biggest, which most probably is due to the fact that Tapiola has the biggest number of buildings. It is also worth noting that residential buildings do not in general get eliminated by the city planning filter, as culturally and historically significant buildings are often public buildings [36]. Of the buildings in Tapiola, approximately 93 % contain roof surface areas that are suitable for producing solar electricity.

In terms of percentage, the biggest decrease in the amount of buildings is seen in the area of Keilaniemi. However, in terms of number of buildings, the effect of the three filters is the smallest in Keilaniemi. In addition, Keilaniemi has the small-

est number of buildings to begin with, whereby the relative decrease is significant already when only a few buildings have been eliminated due to the usage of the filters. In Keilaniemi, the realistic amount of buildings suitable for solar electricity production is approximately 55 %.

The decrease of the number of buildings in Otaniemi was the second biggest in terms of both amount and percentage. As Otaniemi is characterized by campus and business premises, the area also holds a significant amount of bus stops and other shelters, for which the elimination effect of the filters is the biggest of all building types in Figure 35. Therefore, a significant amount of the building type other is eliminated specifically in the Otaniemi area, which explains partly both Figures 35 and 36. Of the buildings in Otaniemi, approximately 80 % include roof surface area suitable for solar electricity production.

When inspecting the buildings suitable for producing solar energy in the entire T3 area, it can be concluded that approximately 88 % of the building stock fulfils this criterion, which can be interpreted as a fairly significant percentage. The amount of unsuitable buildings is 95. From Figure 35 it can be observed that a big part of this amount consists of the building type other in addition to building type detached house.

4.4.2 Impact of filters on the amount of available roof area

In the examination area, there are several different kinds of buildings, which all have their own distinctive features when it comes to the roof surfaces and their usability. Figure 37 presents the formation of practical roof area for different building types, having eliminated unsuitable roof surface areas using the three filters. The yellow line shows the amount of roof surface area per building type that fulfils the demands of surface suitable for solar electricity production set by the three filters. The roof area per building type for the entire building stock in the T3 area is shown by the blue bar. The red bar reflects the roof area of which the roof areas unable to fulfil the limits set by the profitability filter have been eliminated. Furthermore, the grey bar shows the situation, where the prerequisites of all three filters have been considered as eliminating factors. In other words, the grey bar reflects the maximal roof area that in practice can be used for production of solar electricity.

In terms of percentage, it can be seen that the building type multi-storey garage stands for the biggest decrease, as was the case for the amount of buildings in Figure 35. The fierce decrease is again due to the fact that overground car parks are rare in the area, and they are not suitable for solar electricity production as their roof areas are commonly occupied for parking.

Office buildings represent the building type with by far the biggest total roof area. However, for office buildings the roof area lost as a consequence of the three filters is the biggest. Also relatively measured, office buildings together with public buildings are the ones losing second most roof area after filtering. The big amount of roof area lost in office buildings can partly be explained by the characteristics of the office buildings in the area, especially those common in Otaniemi. The office buildings in the area are commonly only two or three floors high, and horizontally

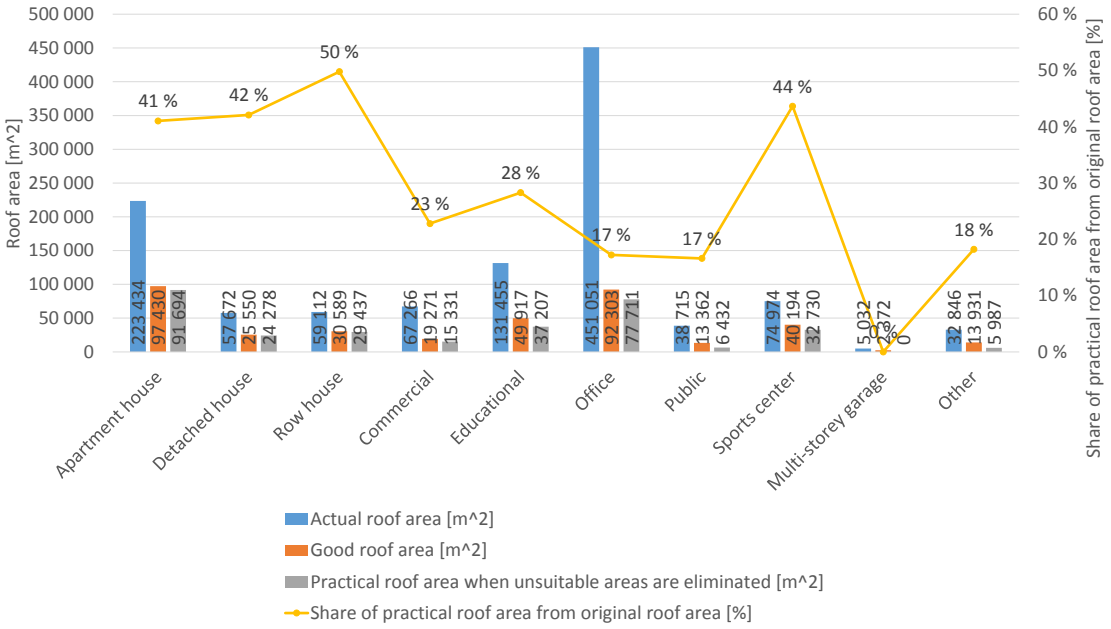

Figure 37: Formation of practical roof area between different building types.

extensive. Therefore, the roof area is extensive, but due to the character of office buildings, there are a lot of ventilation units, skylights and maintenance routes, which can prevent the installation of PV modules. Consequently, 83 % of the roof area is eliminated for offices and public buildings. The eliminated part is equivalent for the building type other. Also, commercial and educational buildings come up close to this, as the usable roof area is approximately a quarter of the original total roof area.

Apartment houses form the second biggest roof area. For the so-called residential buildings (apartment houses, detached houses and row houses) and sports centres, the decrease in the roof area is almost the same, i.e. the remaining practical roof surface area is 40–50 % of the original area. Relatively measured, the decrease in the original roof area is the smallest for row houses, for which approximately half of the roof areas are suitable for solar electricity production when taking into account the effect of the filters.

Figure 38 reflects how the roof surface areas of the T3 area react when the three filters are used to eliminate roof areas unsuitable for producing solar electricity. In the Figure 38, the blue bar equals the total roof surface areas of all buildings in each region. The red bar pictures the roof area received by reducing the areas that do not fulfil the limits set by the profitability filter. The practical roof area usable for solar electricity production is shown in the grey bar, the result of which is received by deducting the unsuitable roof areas from the total roof areas of all buildings with the help of the three filters. The relative effect of the three filters on the roof area of the entire building stock is presented with the yellow line, which shows what percentage of the roof area satisfies the criteria set by the three filters.

Tapiola has the biggest amount of roof area due to the fact that the building

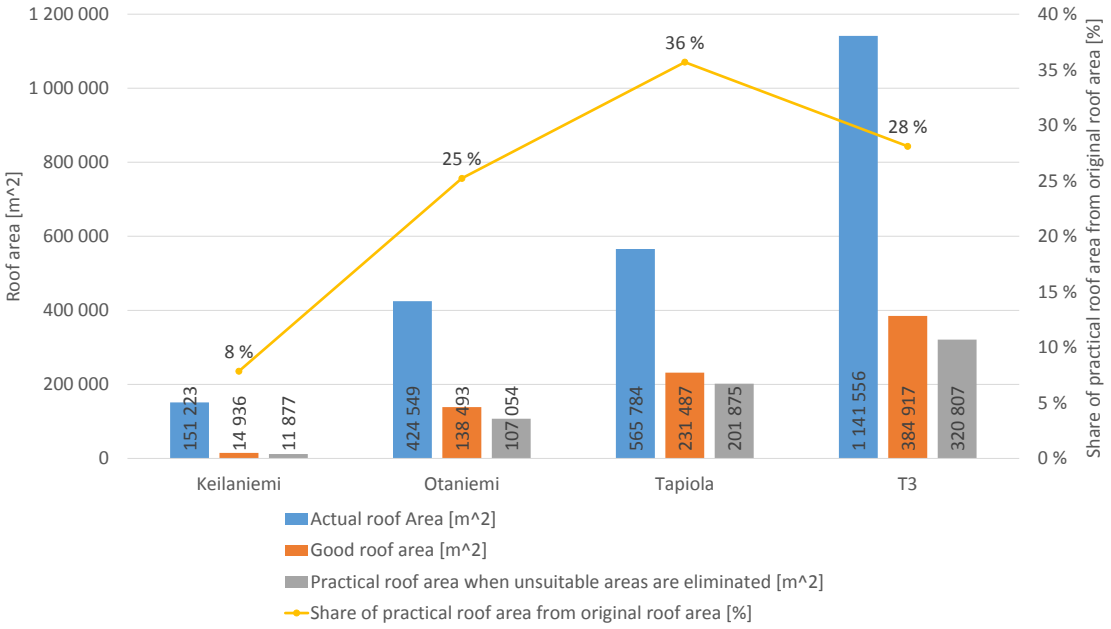

Figure 38: Formation of practical roof area between different areas of T3.

stock in Tapiola mainly consists of apartment houses, detached houses and row houses. This is illustrated in Table 1. The roof areas in these building types are generally extensive. Furthermore, when measuring the roof surface areas for the buildings mentioned above, no significant mechanical barriers were found. Especially apartment houses built in the 1960s in Tapiola are commonly only a few floors high and wide buildings with a lot of roof area. When eliminating unsuitable roof areas, the entire roof areas suitable for solar electricity production in Tapiola end up being approximately 36 %.

In the Otaniemi region there is a substantial amount of offices and educational buildings, many of which are low and wide containing a lot of roof area. Figure 38 clearly shows that a significant part of the roof area potential in Otaniemi is eliminated due to the three filters. The reason for this, as explained before, are the different barriers that prevent the installation of PV modules on these roof surfaces. However, as the campus area of the university of technology, Otaniemi makes a good target for renewable energy production, and solar electricity production could for instance be used for research purposes in the area. In Figure 38 it can be seen that the practical roof area for solar electricity production is about a quarter of the original area when considering all three filters.

The roof area available for solar energy production is the smallest to begin with in the Keilaniemi area. In this fairly small roof area, the biggest relative decrease in comparison to other areas can be seen. The big relative decrease is probably due to the fact that the buildings in Keilaniemi are generally multi-storey buildings, where the roof surface area is small in relation to the floorage. Due to the nature of the buildings, they are occupied by a big amount of people daily, and thereby have several ventilation units on the roof tops. In addition, there are often skylights

and even helicopter landing points, as the area houses the headquarters of many listed companies. When using satellite pictures to identify the roof areas unsuitable for producing solar electricity, it was discovered that only few office buildings in Keilaniemi had extensive uniform roof surface areas that could be used for installing wide rows of PV modules. After filtering away the unsuitable roof areas, the suitable areas left amounted to merely 8 % of the entire roof area of Keilaniemi, which can be seen as a significant decrease.

To sum, when inspecting the total roof areas of the entire T3 area, a prominent amount is eliminated due to the limits set by the three filters. Namely, 28 % of the T3 roof surface can be classified as practical roof area, i.e. the area left when unsuitable roof areas have been eliminated by the criterion of the three filters.

4.4.3 Impact of filters on the amount of maximum potential of solar electricity production

Although in real life approximately 28 %, as stated in Figure 38, of the roof surface areas of the existing buildings in T3 can be used for solar electricity production Figure 39 shows the effect of three filters on the solar electricity production potential. The blue bar in Figure 39 shows the solar electricity production potential when all possible roof surface areas of T3 are utilized for solar electricity production. The red bar, in turn, illustrates the situation when only so called good roof surface area eliminated by profitability filter is exploited for solar electricity production. The practical real life potential of solar electricity production in the T3 area is presented by grey bar. This is the amount of electricity that can be seen as practical potential of solar electricity production in T3 after using all the three filters in order to eliminate the roof surface areas that cannot be exploited for solar electricity production.

The practical potential of annual solar electricity production in the area of T3 is approximately 44 GWh/a. As can be seen from Figure 39 this amount is approximately 49,3 % of the theoretical maximum of solar electricity production if all possible roof surface areas of T3 were exploited. Therefore, it can be interpreted that approximately half of the theoretical maximum potential of solar electricity production can be realistically exploited for solar electricity production in real-life situation.

The potentials for solar electricity production between the three sub areas of T3 are arranged in such a way that both the highest theoretical and the highest real-life potential of solar electricity production can be found in Tapiola. The real-life potential is approximately 56,4 % of the theoretical maximum potential. The reason for this is most probably the biggest amount of residential buildings which usually have a large and clear roof structure to which even large PV module rows are rather easy to mount.

Otaniemi forms the second biggest practical potential for solar electricity production with approximately 44,5 % of the theoretical potential. The great potential is relatively easy to understand, since Otaniemi has a lot of only a few layers high, horizontally extensive buildings, which are mostly either use of educational purposes

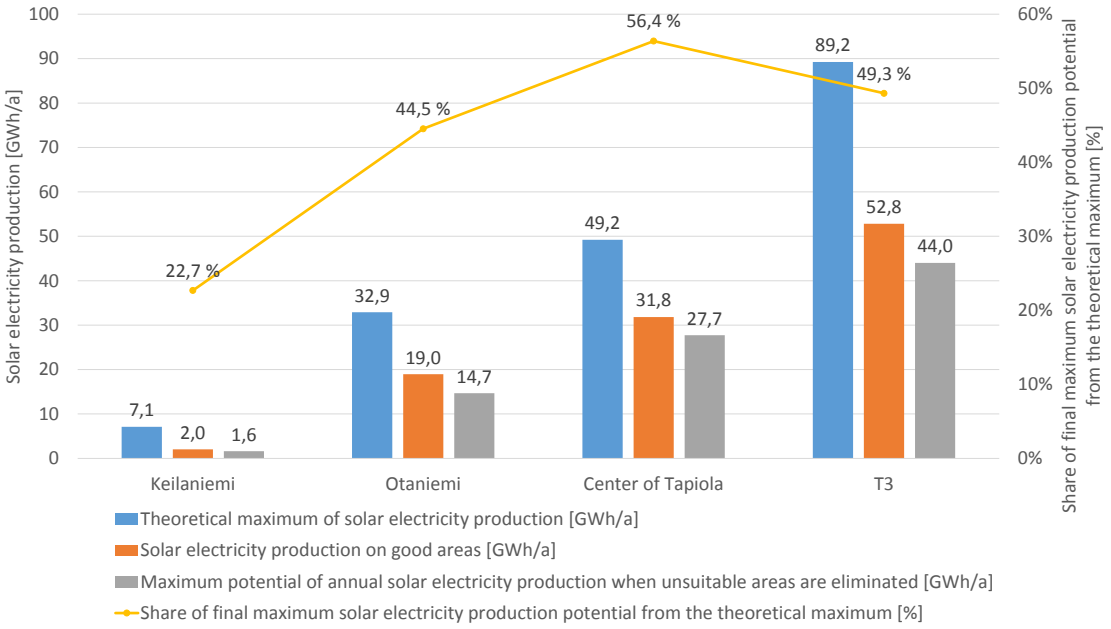

Figure 39: Effect of the three filters on the maximum potential of annual solar electricity production in T3.

or used as business premises. The roof surfaces of such buildings often contain a lot of air supply units and skylights in addition to other building automation, so a large part of the big potential eventually is eliminated off. Despite this, there remains extremely much suitable roof surface area for the solar electricity production in terms of square meters.

In the case of Keilaniemi the realistic potential of solar electricity production is approximately 22.7 % of the theoretical maximum production potential which makes it the smallest of the three. In addition the theoretical maximum potential of solar electricity production is the lowest. As mentioned above, this is probably due to the common high and narrow structures of the buildings in Keilaniemi which is why the floor area is big in relation to the roof area. In other words, the roof area is relatively small compared to the size of the building and the amount of people using the building.

It is also meaningful to compare the practical potential of the solar electricity production in T3, illustrated in Figure 39, with the existing electricity consumption of the area. The existing electricity consumption of the area was produced from the network information system PowerGrid of Tieto Oy. Figure 40 illustrates the situation where the previously provided maximum potential of annual solar electricity production is shown with the corresponding annual electricity consumption of the areas of Keilaniemi, Otaniemi, Tapiola and T3. The existing annual electricity consumption is presented with the yellow bar. The orange bar stands for the maximum potential of annual solar electricity production. The green line, in turn, stands for the percentage of the existing consumption that can be theoretically satisfied by the potential solar electricity production.

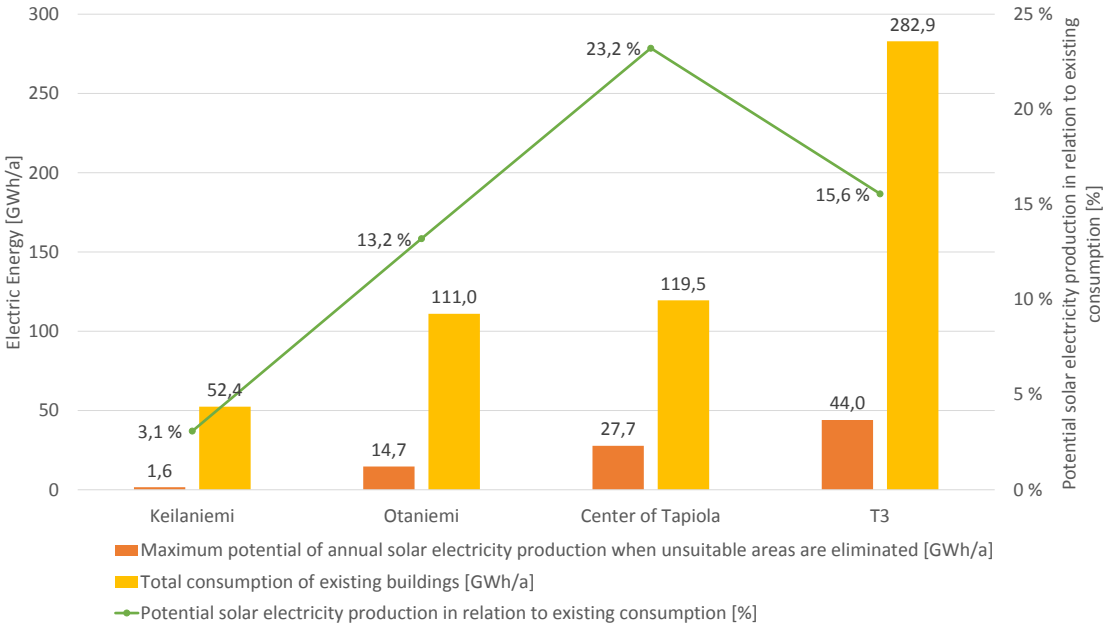

Figure 40: Practical maximum of annual solar electricity production in relation to existing annual electricity consumption.

It can be observed from the Figure 40 that the realistic potential of solar electricity production in the T3 area can theoretically satisfy approximately 15,6 % of the existing electricity consumption of the whole T3 area. However, it should be kept in mind that the percentage of potential solar electricity production from existing electricity consumption does not take into account how much of this solar electricity could be consumed by the producer of the solar electricity. In other words, what is the share of this solar electricity production that will be able to be consumed by the producer himself with the price of the investment of a grid-connected solar PV system, and how much of this solar electricity production is bought back from the distribution network by the customers of the area after feeding the extra solar electricity production, that can not be used by the producer, to the distribution network. As there is overlapping of consumptions inside an area, it is very likely that the surplus solar electricity production will be consumed by the other consumers of the area. However, the percentage of the potential solar electricity production in relation to existing electricity consumption presented in Figure 40 does not take into account how big the share of solar electricity production that can be used by producer is, and how much of the fed solar electricity production is bought back from the distribution network.

The biggest share, approximately 23,2 %, of the existing electricity consumption can be theoretically satisfied in Tapiola by utilizing solar PV arrays. The second biggest share can be found in Otaniemi. Approximately 13,2 % of the total consumption of the Otaniemi district can be theoretically produced by utilizing all practical roof area for solar electricity production. The third area of T3, Keilaniemi, has the lowest potential of solar electricity production when compared to the existing elec-

tricity consumption of Keilaniemi. Approximately 3,1 % of the existing electricity consumption could be theoretically produced by solar PV arrays. All the results in Figure 40 are practically consistent with the results presented in section 4.4.2, so also the remarks made on that section partially explain the differences between the subareas of T3.

5 Energy balance

The previous section provided the practical maximum potential of solar electricity production for the T3 area. However, it did not take into account the fluctuation of energy between the distribution network and the solar PV system when the solar PV system is assumed to be grid-connected without storage capabilities. In this section a model for solar electricity production is utilized along with the information about existing consumption in order to be able to model the behaviour of electric energy flows in the T3 area and between different building types by using the results of practical maximum potential of solar electricity production provided in the previous section.

5.1 Methods of energy balance simulations

It was assumed in all energy balance calculations that the PV system is grid-connected and the PV array is made of crystalline silicon as in the calculations of section 4. In addition it was assumed that the PV systems feed all the surplus solar electricity production straight to the distribution network without storing. All energy balance calculations are made with a presumption that all realistically potential roof surface areas, eliminated by the three filters, are exploited for solar electricity production. Therefore the results obtained in the section 4.4.3 can be used as initial values of annual solar electricity production.

The energy balance calculations were carried out by exploiting load curves and index series calculation based on the load study about the utilization of electric energy between the years 1984–1990 made by Suomen Sähkölaitosyhdistys r.y. A model of solar electricity production for horizontally mounted PV modules was obtained from Hannu-Pekka Hellman's conference paper Photovoltaic power generation modeling, Aalto University School of Electrical Engineering, 2011. This model was utilized in order to calculate solar electricity production powers for each hour of the year.

The load information and load curves were taken from the network information system PowerGrid. The most suitable load curve for each building type was chosen by carefully experimenting and analysing the results of each load curve. It is essential for the calculations that the load curve reflects the load as well as possible. Energy balance calculations were carried out by creating a spreadsheet template for calculations and analysis of results.

After the selection of the most suitable load curves, hourly powers for each hour of the year were calculated for selected loads. In addition, the hourly powers of solar electricity production were calculated according to Hellman's production model. The hourly powers were categorized into production and load in order to calculate the net hourly power. In addition, the calculation results were categorized according to point in time into four different seasons in order to be able to provide season-specific results. Table 4 illustrates the chosen dates from year 2007 to represent seasons in the results.

Table 2: Chosen dates for seasons in year 2007. [42]

Spring Workday (Equinox)	21.3.
Spring Sabbath	24.3.
Summer Workday (Solstice)	21.6.
Summer Sabbath	23.6.
Fall Workday	21.9.
Fall Sabbath (Equinox)	23.9.
Winter Workday	21.12.
Winter Sabbath (Solstice)	22.12.

5.2 Models for energy balance calculations

Energy balance calculations cannot be executed without a model for solar electricity production. In addition, a method for calculations of hourly energies is needed in order to be able to calculate both the hourly solar production and hourly electricity consumption for every hour of the year. A model for solar electricity production and principles of index series calculation are presented in this section.

5.2.1 Model for solar electricity production

In order to be able to calculate the energy balances of the buildings in the T3 area a model for solar electricity production was needed. Hannu-Pekka Hellman has defined a power output model for crystalline silicon solar module in the area of Southern Finland in conference paper Photovoltaic power generation modeling, Aalto University School of Electrical Engineering, 2011. The model is presented in Table 3. [43]

The model presented in the Table 3 has been calculated for the system power of 1 kW. This model was converted to correspond a system size of 1 W in order to be exploited in the energy balance calculations. Months from January to December are on the X axis. The Y axis reflects the hour of the day from 0 to 23. The corresponding index for each hour of each month can be found between the axes. For example, in January the PV module starts to produce at the hour number nine and ends the production at the hour number sixteen of the day.

Hannu-Pekka Hellman's model for solar electricity production has been made based on the observation measurement data of the Finnish Meteorological Institute. The model exploited in this thesis has been made for horizontally installed PV modules with a sunshine hour value of $t_{ssh} = 0,437$ for every month. According to Hellman the model provides an annual insolation of 985 kWh/m^2/a with this sunshine hour value. [43] The insolation for the area of T3 calculated in this thesis is, in turn, 949,5 kWh/m^2/a with an assumption that the PV modules are installed at the same level with the roof surface in each building. Considering the fact that Hellman's model represents the situation where the module is installed horizontally, and the assumption of the insolation calculated in this thesis is to install the modules

Table 3: A model of electricity production for horizontally mounted crystalline silicon photovoltaic system with sunshine hour value of $t_{ssh} = 0,437$ for every month made by Hannu-Pekka Hellman. [43]

M/h	J	F	M	A	M	Jn	Jl	A	S	O	N	D
0	0	0	0	0	0	0	0	0	0	0	0	0
1	0	0	0	0	0	0	0	0	0	0	0	0
2	0	0	0	0	0	0	0	0	0	0	0	0
3	0	0	0	0	0	0	0	0	0	0	0	0
4	0	0	0	0	36,2	67,3	48,5	0	0	0	0	0
5	0	0	0	19,6	93,3	122	96,3	38	0	0	0	0
6	0	0	1,45	84	165	193	163	98,7	26,4	0	0	0
7	0	0	45,2	158	244	269	237	170	90,8	14,3	0	0
8	0	17,3	121	239	319	339	307	244	160	74,5	1,49	0
9	7,79	84,7	196	311	382	399	368	309	228	129	50,5	0
10	66,5	142	261	368	430	444	414	360	282	179	92,6	57,1
11	96,6	188	306	405	461	473	446	394	317	213	122	83
12	115	213	329	421	473	486	460	410	332	226	134	97
13	115	214	327	416	467	482	457	407	325	216	125	92,4
14	95,6	192	303	391	444	461	438	385	299	186	98,5	71,2
15	65,7	148	256	346	403	425	403	346	253	138	63	28,2
16	11,1	91,1	191	283	347	373	352	291	191	84,1	6,15	0
17	0	24	117	208	278	310	290	224	123	23,4	0	0
18	0	0	41,3	129	202	238	219	152	56,1	0	0	0
19	0	0	0	59,5	127	164	148	85,5	7,72	0	0	0
20	0	0	0	4,42	67,2	99,2	85,8	28,7	0	0	0	0
21	0	0	0	0	13,1	54,5	39,7	0	0	0	0	0
22	0	0	0	0	0	0	0	0	0	0	0	0
23	0	0	0	0	0	0	0	0	0	0	0	0

at the same level with the roof surface, the difference between these two insolations is rather small. Thus, it can be interpreted that the result provided by Hellman's model can be exploited in the calculations of energy balance.

5.2.2 Load curves and index series

The hourly energies defined in the energy balance calculations are based on the load curves. The load curves are in turn based on the load measurements of the electricity consumption from years 1984–1990 made in the load survey of Suomen Sähkölaitosyhdistys r.y. in 1990. The starting point of the load survey is in the grouping of electricity users which divides the electricity user groups into such categories where the consumption of electricity can be assumed to be similar enough. Every load curve includes the following information:

- normal temperatures for each hour of the model
- sample size for each hour
- valid estimate of temperature coefficient from the period of the model definition
- standard deviation of average power corresponding to each hour of the model at the temperature in question
- estimate of average power corresponding to each hour of the model at the temperature in question [44]

The temperature dependence of the use of electricity is taken into account by a linear calculation model when forming the load models:

$$q_{tod}(t) = q_0(t) + \beta \cdot \Delta T(t), \tag{22}$$

where $\Delta T(t)$ stands for deviation of measured and normal outdoor temperature at time t. Parameter β is a coefficient describing the temperature dependence of electricity use which is valid for the entire model period. Parameter $q_0(t)$ means the use of electricity in normal outdoor temperature. And lastly $q_{tod}(t)$ stands for measured electricity use at time t. [44]

Index series is a relative manner of representation of the load data, in which the year is divided into 26 two-week periods. A so-called external index is calculated in index series for each period based on the average power of a two-week period. The external indices are used for describing the seasonal variation of electricity use. In addition, the external indices in the index series are scaled to a such a level that their sum becomes 2 600. So-called internal indices are used to illustrate the hourly variation of the day. The hourly variation is described in a 24-hour index separately for weekdays, Sabbaths and eves. Weekdays include all the days between Monday and Friday, eves include all Saturdays and Sabbaths include all Sundays. In the calculation of the index series internal indices are scaled to a such a level that the sum of the weekday indices multiplied by five plus the sum of the indices of Eves and Sabbaths will result in 16 800. All two-week periods have their own internal indexes in index series. The absolute value of the average hourly power for a given moment i can be calculated from the index series with the following:

$$P_{ri} = \frac{E_r}{8736} \cdot \frac{Q_{ri}}{100} \cdot \frac{q_{ri}}{100}, \tag{23}$$

where P_{ri} is the average hourly power of user group r at moment i, E_r stands for the annual energy of user group r, Q_{ri} is the external index of user group r at moment i and q_{ri} stands for the internal index of user group r at moment i. In the context of index series the standard deviations of hourly powers are also reported. The standard deviations are reported as percentage of the hourly power. In the calculations the winter period is presumed to be between 1.11. and 31.3. and the daytime is assumed to be between 7 and 22. [44]

Since the largest power needs do not always occur at the same time it causes the powers to overlap. The peak power of different objects' sum load is usually smaller than the sum of the individual objects' peak powers. The overlapping of powers is modelled with so-called coincidence factors. The coincidence factor can be calculated as follows:

$$K_r(n) = \frac{max\left(\sum_{k=1}^{n} P_k(t),\ t = 1, .., 8760\right)}{\sum_{k=1}^{n} max\left(P_k(t),\ t = 1, .., 8760\right)}, \tag{24}$$

where $K_r(n)$ is the coincidence factor of user group r with n amount of objects and $P_k(t)$ is the power of user k at moment t. [44]

The year 2007 was chosen to be the year for calculations of energy balance in this thesis since the first day of January was Monday in that year. This will make the interpretation of the calculation easier in terms of days.

5.3 Results

By using index series calculation it is possible to calculate the form of the solar electricity production model. Table 4 presents the relative amount of solar production between different seasons. It is assumed that winter consists of months from December to February, spring is from March to May, summer is from June to August and fall is from September to November.

Table 4: Relative amount of annual solar production according to season.

Season	Month	Relative amount of annual solar production
Winter	December January February	7,5 %
Spring	March April May	35,5 %
Summer	June July August	42,8 %
Fall	September October November	14,2 %

It can be seen from Table 4 that a significant part of the solar production occurs in the spring and summer months. The summer alone produces almost half of the total annual production. Together with the spring they form a half a year in terms of time and approximately 78,3 % of the annual solar electricity production.

A typical production curve of a detached house from Tapiola is shown in Figure 41 for all four seasons. Summer and winter are marked with an intact line and spring and fall are marked with a dashed line with four different colours according to the legend given in the chart. This notation will be used in upcoming Figures as well. It can be seen from the Figure that the production at winter time presented with yellow intact line starts at 9:00 and ends at 16:00. In other words, the PV modules produce only for seven hours a day at winter solstice. The difference between summer and winter is significant since the production at summer (summer solstice) starts already at 3:00 and continues all the way up to 22:00. Therefore, the time during which no solar electricity is produced amounts to merely five hours a day. Hence, Figure 41 explains the high production volume during the summer months presented in Table 4.

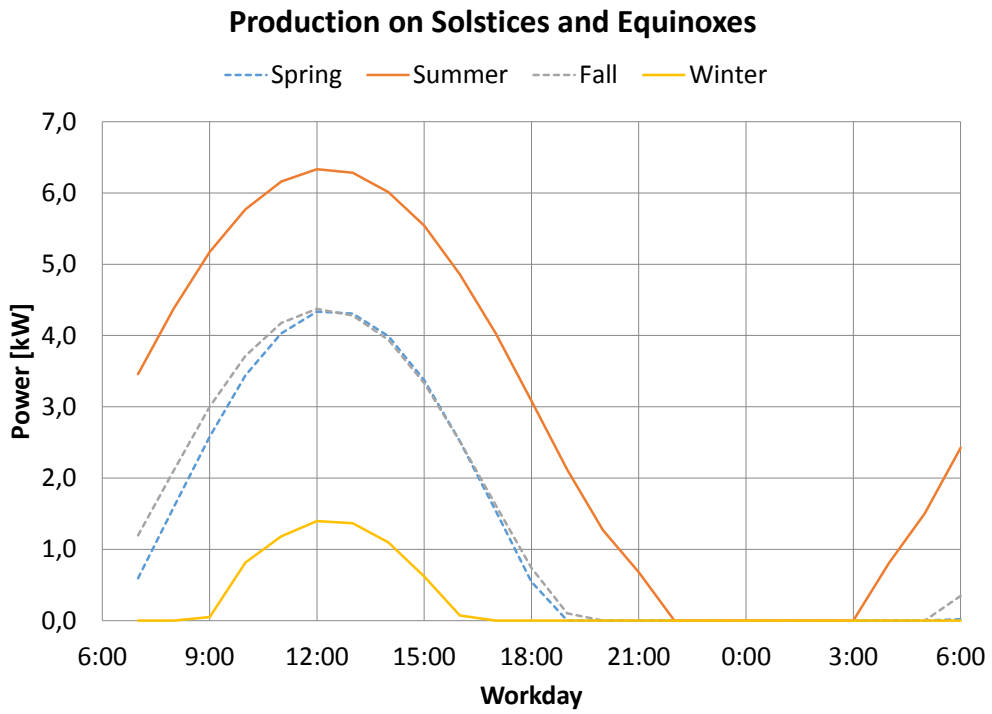

Figure 41: A typical solar electricity production curve of a detached house from Tapiola.

The shape of the production model stays the same every time because of the indices presented in Table 3. Only the height of the shape changes according to solar radiation circumstances. Therefore, the shape of the production curve is presented only once and for the most common building type, detached house, in the T3.

5.3.1 Results in case of single building

The energy balance calculations were carried out to a group of single building representatives from various building types which represent very ordinary features of

their own building types. The buildings that are covered in this section are detached house from Tapiola, apartment house from Tapiola, office from Keilaniemi and shopping centre from Tapiola.

Figure 42 presents the energy balance of a detached house from the Tapiola area. On the top left corner is a chart that illustrates the energy balance for the whole year in two-week periods. The blue line in this chart represents the existing electricity consumption before the PV system installation. The red line, in turn, stands for the electric energy that is bought from the distribution network when the PV system is in use with the assumptions made in the section 5.1. Finally, the green line presents the solar electricity production that is fed to the distribution network. The feeding appears intentionally as a negative value. The area between the blue and the red line is the amount of energy that can be consumed by the producer itself. This area also stands for the reduction of purchased energy from the distribution network. The area between the red and green lines represents the energy that flows through the energy meter during a year. This area is the amount of energy that could be controlled with a storage big enough or load control to enable a bigger share of own usage.

As can be seen from the top left corner of the Figure 42, the detached house feeds a significant amount of energy to the distribution grid annually. This is because of the big roof surface area in relation to the consumption, especially when all the surplus solar electricity is assumed to be fed to the grid. It was assumed that all possible roof surface areas are utilized for solar electricity production which in this case appears to result in an enormous amount of solar electricity production compared to the small consumption of the detached house.

The two charts on the right in Figure 42 are drawn exactly in the same way as the chart on the top left corner but they represent the situation for one workday on an hourly basis starting from 7:00 instead of two-week periods. The situation from the summer solstice, on the top right corner, is located exactly in the middle of the chart on the top left corner. Similarly, as in the chart on the top left corner, the blue line on the charts on the right-hand side is the existing electricity consumption before installation of the PV system. The red line is, similarly, the amount of electric energy bought from the distribution network and the green line presents the amount of solar electricity fed to the distribution network. The similar analogy of the areas between the blue and the red line, as the area between the red and the green lines, can be used in the charts on the right-hand side as explained above in the context of the chart on the top left corner. However, this time the areas stand for energies on a day level.

When looking at the two charts on the right in Figure 42 it can be seen that there is feeding to the distribution grid even at winter. An interesting observation is that the peak power at summer appears at different time when the solar electricity production is taken into account. The new peak power is also smaller. The previous peak power of approximately 0,7 kW appeared at 20:00, whereas the new peak power is approximately 0,5 kW in size and appears at 22:00.

On the bottom left corner in Figure 42 a chart of net power is presented. This chart illustrates the situation of four seasons in terms of hourly net power that is

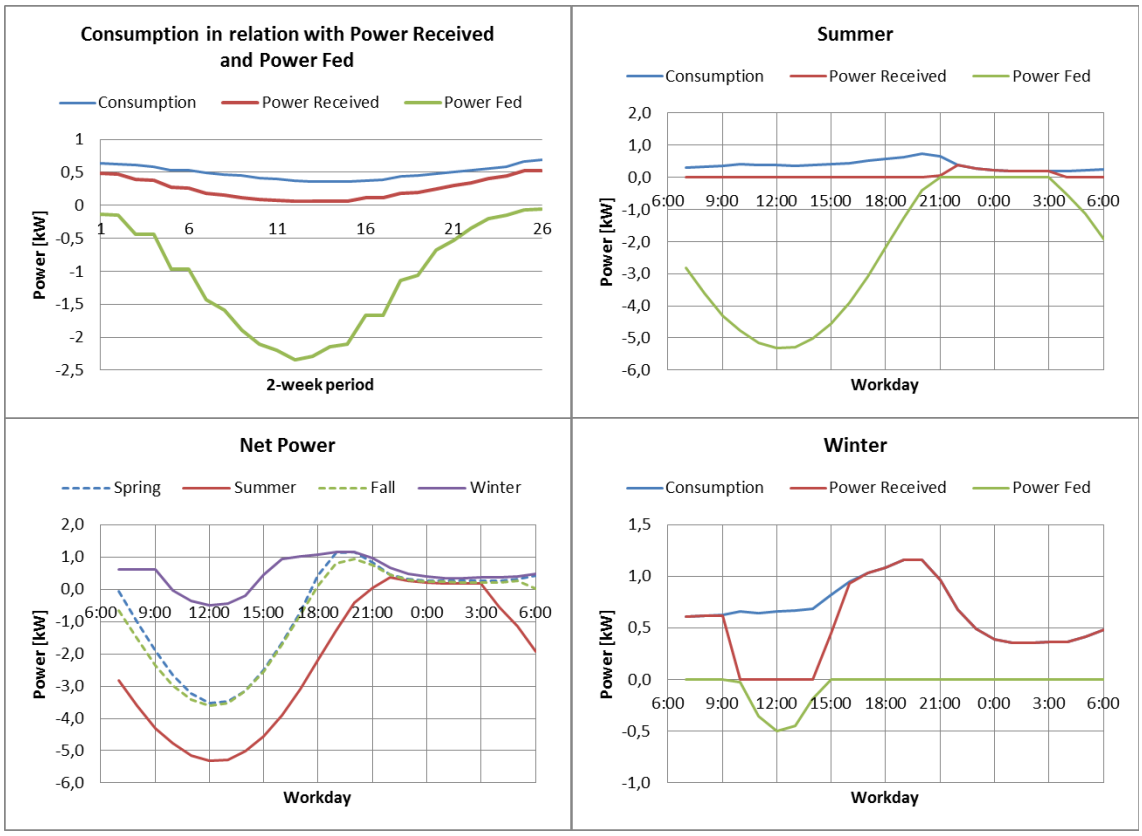

Figure 42: Energy balance of a detached house from Tapiola.

flowing through the meter. Therefore, power above the X axis stands for consumption and power below the x axis represents feeding to the distribution grid. From this chart it can be seen that feeding takes place during all seasons. The differences between winter and summer are probably due to the fact that the consumption tends to be bigger in winter time whereas the availability of solar radiation is at its worst. In summer the situation is completely reversed.

An identical manner of representation is used in the upcoming figures as well and therefore a similar approach applies to all of them. Thus, the interpretation of the four images has been described only in this first context.

The energy balance in the case of the apartment house is shown in Figure 43. It can be seen from the two-week period chart on the top left corner that feeding occurs during the summer time but not to the same extent as in the case of detached house. The solar electricity production significantly decreases the amount of annual energy bought from the distribution grid especially in the summer time.

From the net power chart it can be seen that feeding occurs at every season except for winter. From the right-hand side charts it shows that the only change in winter time is the decreased electricity purchase from the utility grid in the daytime. In the summer time, however, the peak power is reduced and delayed to an hour later from 19 to 20. The smaller annual feed to the distribution network compared to the case of detached house is probably due to the fact that the apartment building

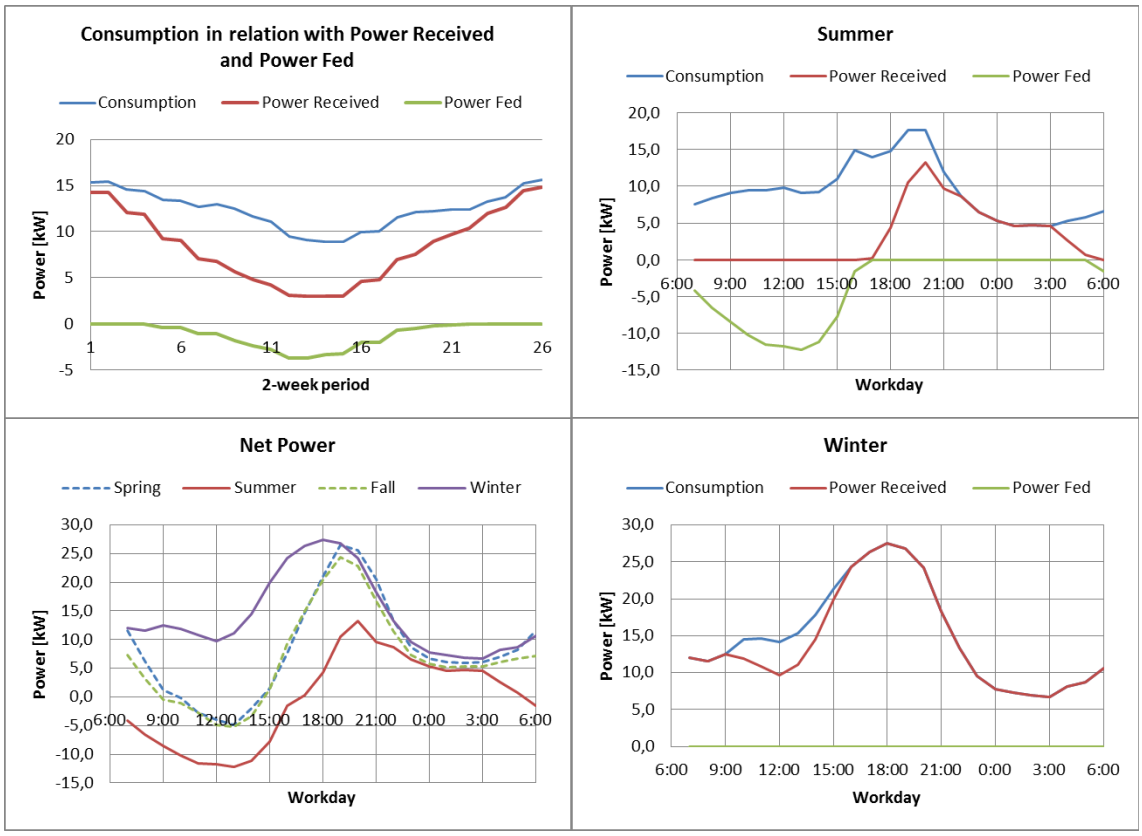

Figure 43: Energy balance of an apartment house from Tapiola.

has less roof surface area in relation to the annual electricity consumption.

A representative of an office building from Keilaniemi is shown in Figure 44. The two-week period chart on the top left indicates that feeding to the distribution network does not occur at all during the year. Instead, the peak power decreases and annually purchased electrical energy from the network is reduced especially in the summer time.

On a day level the existing load of the office building seems very flat without any major peaks. In the summer the peak load seems to decrease and shift from 15:00 to 19:00. In the winter time, however, the peak occurs approximately an hour later and the purchased energy is decreased at noon. From the net power chart on the bottom left it can be seen that the major effect of the solar electricity production is the decreased amount of purchased electrical energy around noon, the biggest decrease appearing in the spring. This is probably due to the bigger need of cooling energy in the summer, which rises the amount of purchased electricity from the grid despite the bigger amount of solar electricity production. Feeding to the distribution network does not take place at all, which is probably because tall office buildings tend to have large and even load combined with a relatively small roof surface area.

Figure 45 illustrates the energy balance of a shopping centre from the Tapiola area. Compared to the energy balance of the office building in Figure 44 the shapes of the charts have some similarities, even though the powers are considerably larger

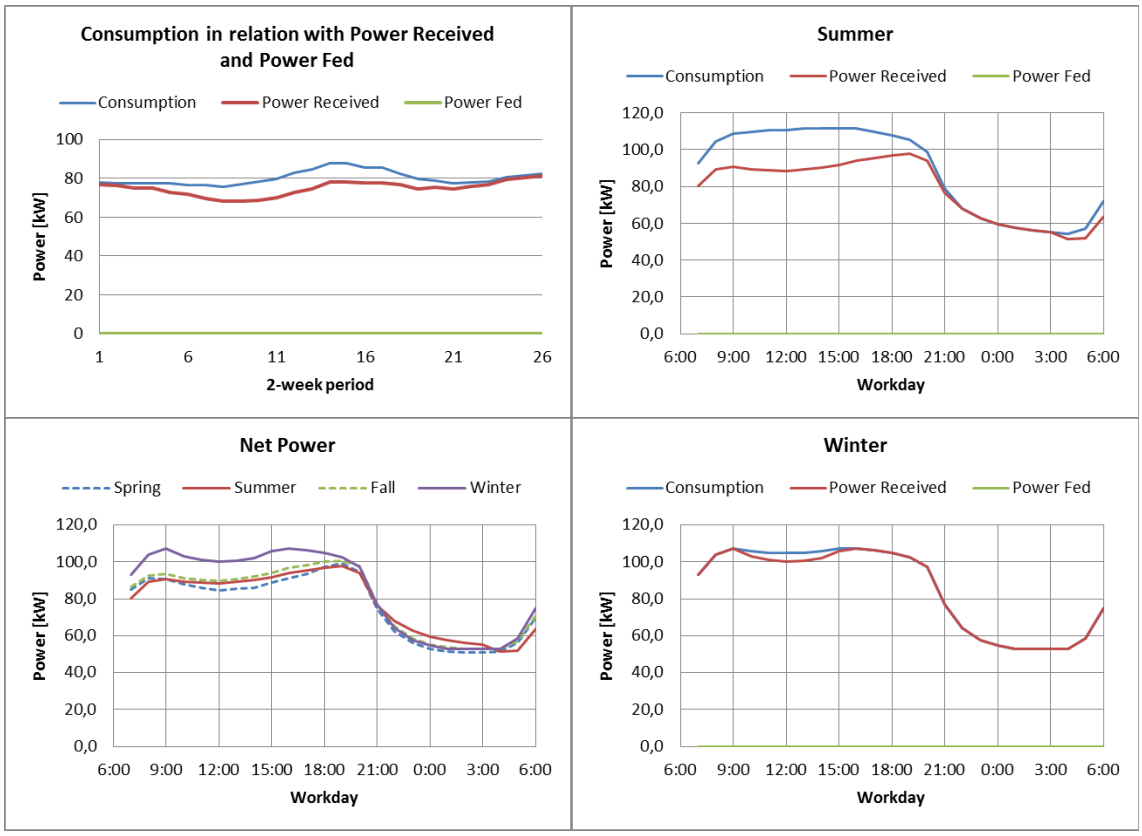

Figure 44: Energy balance of an office building from Keilaniemi.

in the case of the shopping centre. From the two-week chart it can be seen that there is no feeding to the distribution network. The high load in the summer is decreased, and it seems that the peak load is shifted from summer to winter. In this kind of building the reason behind the high load in the summer is probably a large need of cooling energy especially for frozen food in the grocery stores. For this reason the lowest demand for the purchased electricity from the grid occurs in the spring instead of the summer, when the solar electricity production is taken into account.

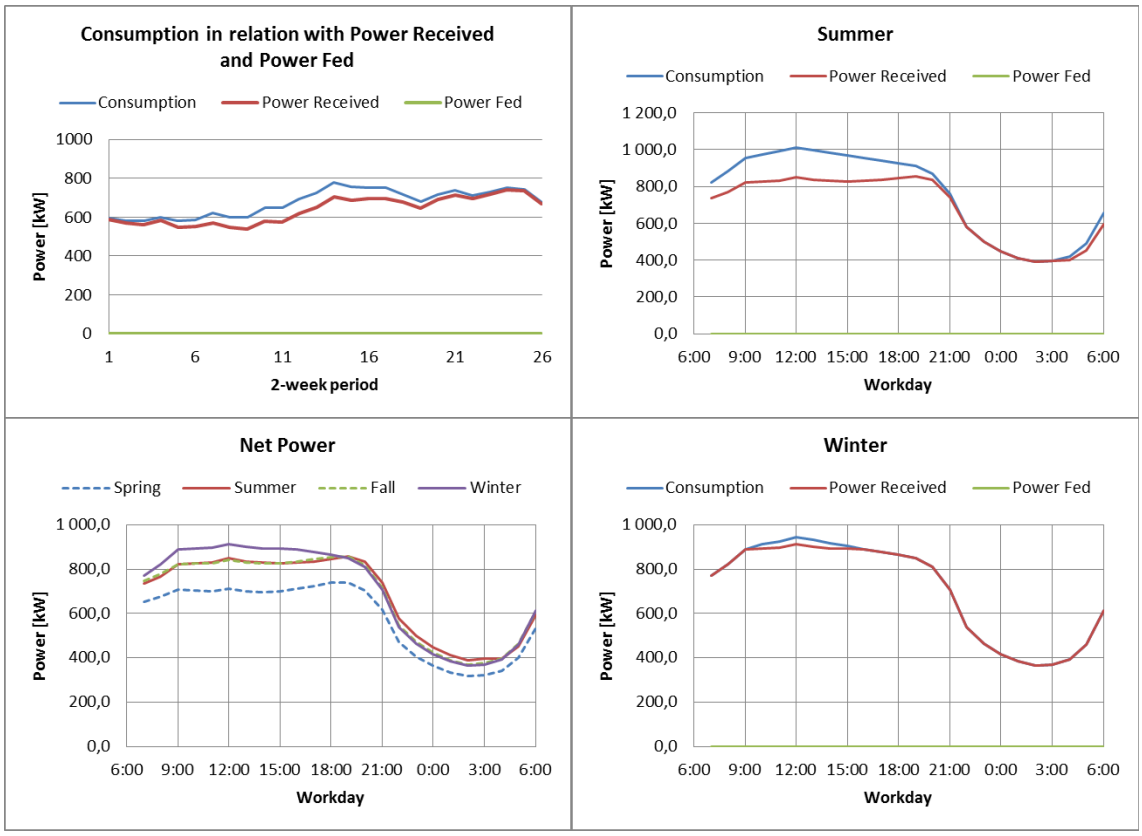

Figure 45: Energy balance of a shopping centre from Tapiola.

From the right side of the Figure 45 it can be seen that in the summer the peak power decreases approximately 150 kW and shifts from 12:00 to 19:00. The same relocation of the peak load occurs also in the spring and fall but the reduction in the peak power is slightly more moderate. In the winter the peak power occurs at the same time but decreases approximately 50 kW.

5.3.2 Results in case of block of buildings

This chapter covers the energy balance results of the building groups. The energy balances are now calculated for a little group of buildings that represent the same building type. In addition, the groups of similar buildings are treated as a single entity in energy flow sense and examined from an outside view.

The graphs presented in Figure 46 illustrate the energy balance of a group of detached houses. The group of detached houses consists of eleven houses that are situated next to each other. In terms of load curves there are small differences between the houses in order to be able to see the effect of the overlapping of powers. As in the case of the single detached house, the group of detached houses provide a large amount of feeding annually. This can be seen from the two-week period chart. In addition, the amount of purchased electrical energy from the grid decreases significantly over the year.

From the net power chart one can tell that feeding takes place at all seasons

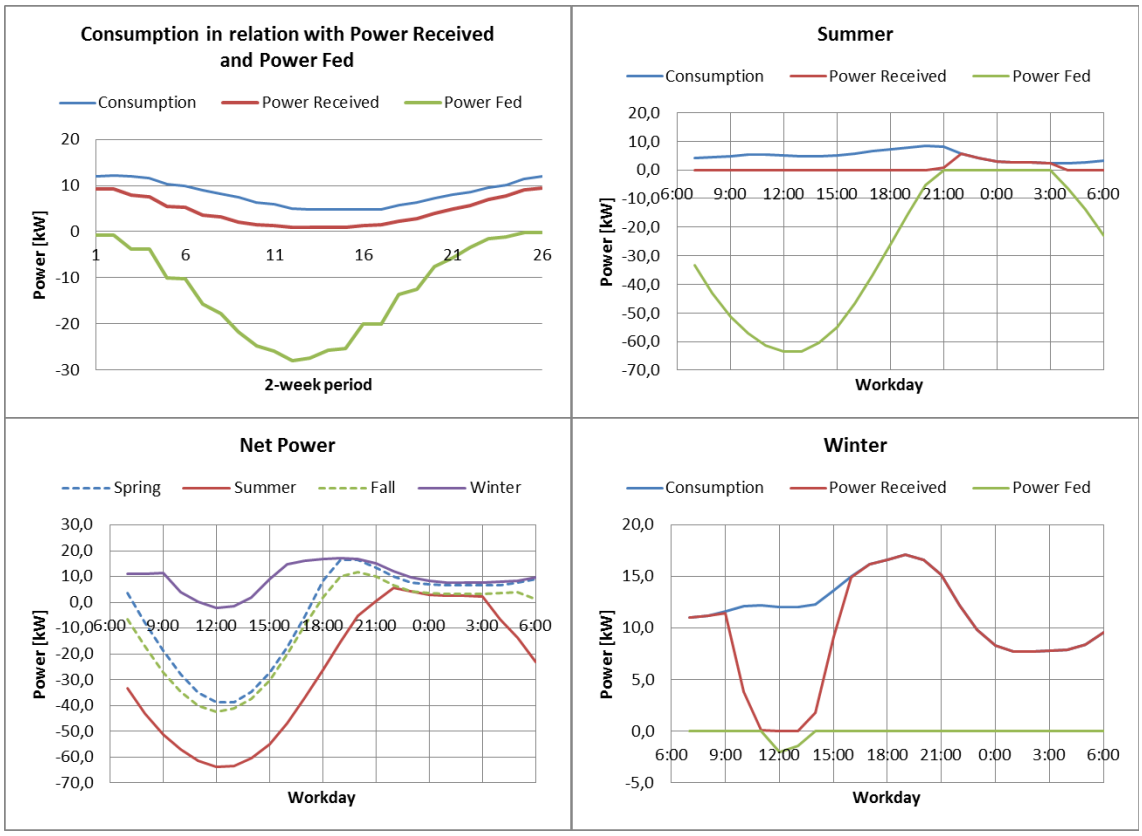

Figure 46: Energy balance of a group of detached houses from Tapiola.

in the same manner as for the single detached house above. Due to the similarity of the loads, the overlapping of powers does not seem to occur. As a result, the group of detached houses seems to behave in almost the same way as in the case of a single detached house. The peak load in the summer is shifted from 20:00 to 22:00 and reduced approximately in half. Especially in the summer time the feeding power towards the distribution network may exceed 60 kW, which is over six times the amount of the existing maximum power before the utilization of the PV system. Thus, power distribution companies may have to redesign the protection politics of the low voltage networks. However, one has to take into account that the assumption behind the calculation is to utilize all the roof surface areas available, and the option for the energy storages is not considered, making this the worst case scenario from the distribution network point of view.

The energy balance of the group of apartment houses is analysed in Figure 47. The apartment houses were examined as a group of six apartment houses of different sizes, located side by side in Tapiola. These six houses also have a small variation in the load curves. From the two-weeks period graph it can be seen that as a whole the group of apartment houses feed solar electricity to the distribution grid especially in the summer. The amount of purchased electrical energy from the distribution grid is significantly reduced during the entire year and especially in the summer time.

From the net power chart one can tell that feeding occurs in every season except

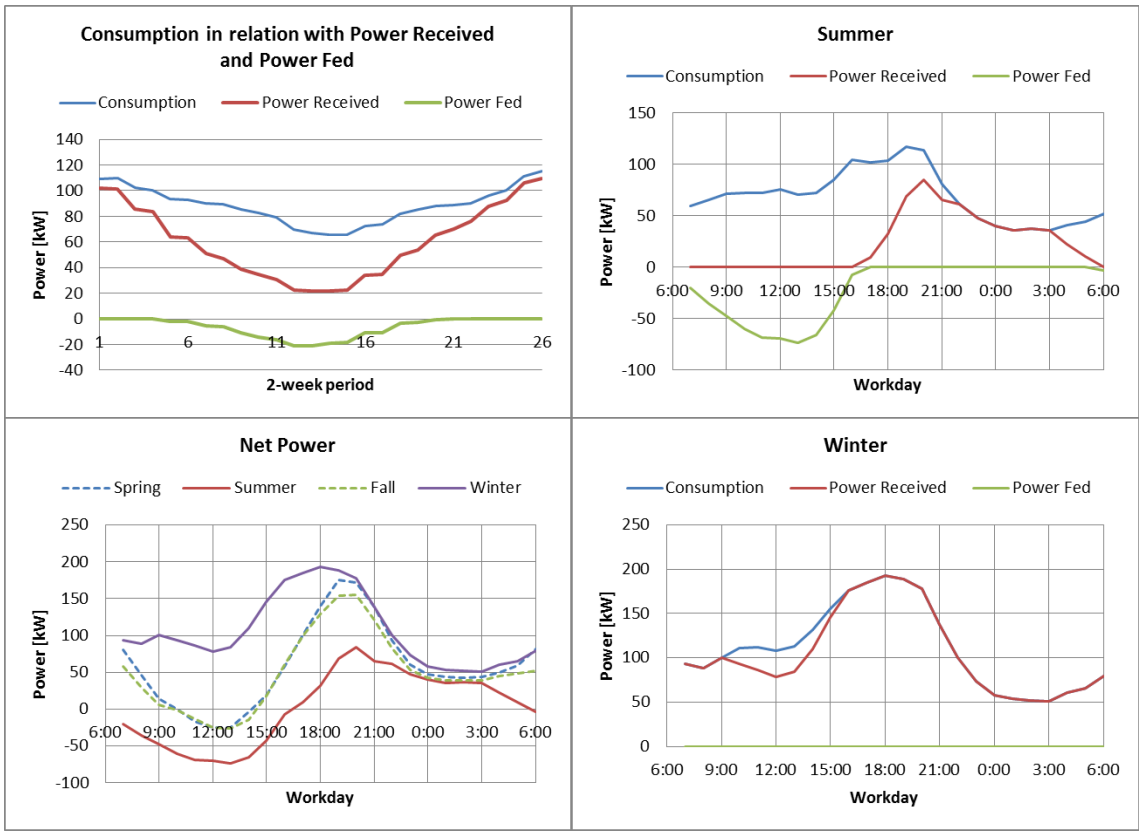

Figure 47: Energy balance of a group of apartment houses from Tapiola.

for the winter. This is most probably due to the worse sunlight conditions in the winter and the higher need of electricity. The peak power of the feeding in the summer is significantly smaller than the peak load in the winter, which is why the group of the apartment houses probably will not cause any notable problems from the protection of the low voltage network point of view. The peak load in the summer is reduced approximately from 120 kW to 90 kW and delayed by an hour. The feeding to the distribution network is significantly less compared to the group of detached houses, which is probably due to the higher consumption in relation to the roof surface area available. All in all, a group of apartment houses seems to behave in much the same way as a single apartment house, and a significant overlapping of powers is not clearly detectable from the results.

The group of shopping centres in Tapiola consists of ten different-sized buildings with their own specified consumption curve. The results of the energy balance of this group are shown in Figure 48. From the two-week period chart it can be seen that as a group the shopping centres do not feed any produced solar electricity to the utility grid. However, the amount of the purchased electric energy is notably reduced, except for the winter, when the solar radiation is clearly less available.

As in the case of a single shopping centre building the daily load remains very even and the benefits of the solar electricity production are particularly well visible in the summer time, when the volume of the purchased electricity from the network

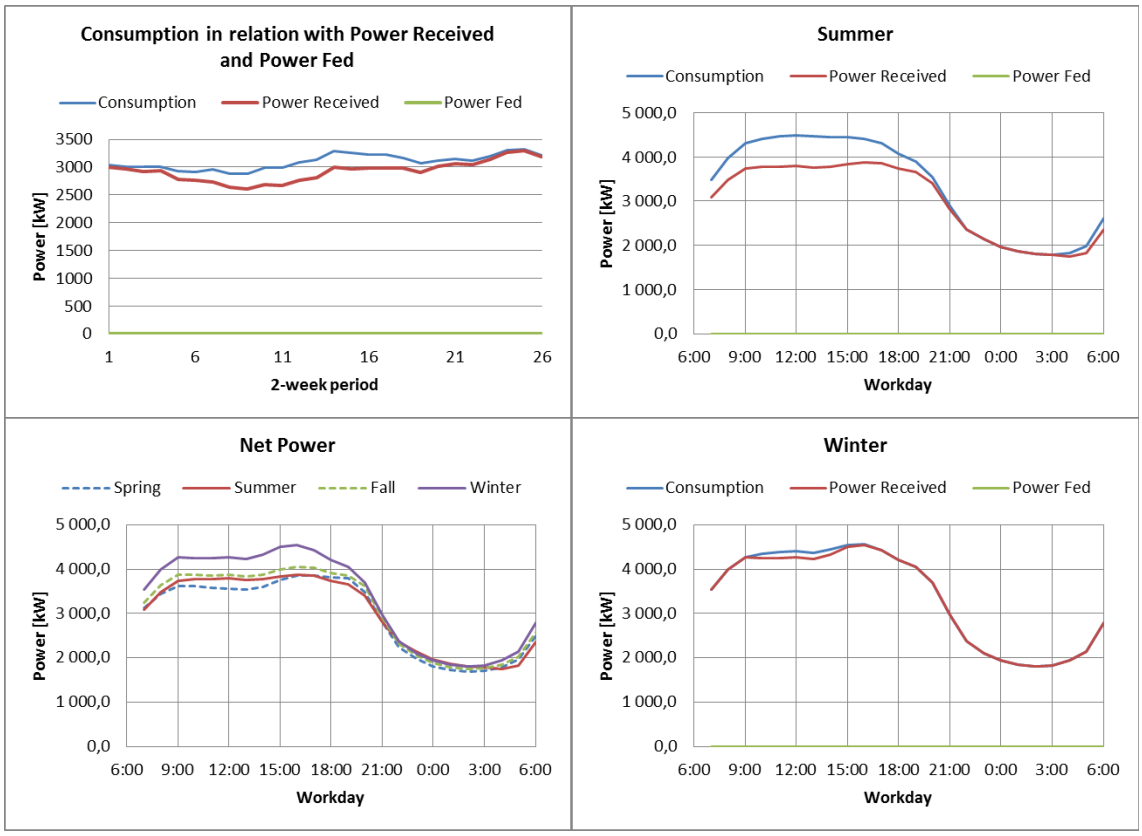

Figure 48: Energy balance of a group of shopping centres from Tapiola.

is reduced evenly throughout the day. In addition, any visible peak loads cannot be seen on the right-hand side of the Figure 48, although the peak load is reduced notably and shifted from 12:00 to 17:00. A steady reduction in the load during the entire day can be seen in the spring and in the autumn as well.

In conclusion, it can be noted that in the case of the shopping centres, significant benefits can be achieved by utilizing the solar electricity production. This is due to the lack of feeding to the distribution network and a high rate of own usage, caused by the overlapping of powers and the high and even consumption of electrical energy. What is more, these results can be achieved without the storage capabilities.

5.3.3 Results in case of district

This chapter examines the energy balances of Keilaniemi, Otaniemi, Tapiola and the whole T3 as separate entities. The energy balances are viewed from an outside point of view, in order to see how their energy balances appear from the distribution grid perspective.

The energy balance of Keilaniemi is presented in Figure 49. Keilaniemi is considered also as a group of office buildings in this context, so the results obtained here are comparable to those in the section of 5.3.2. First of all, it can be said that the entire area of Keilaniemi does not feed electric energy outwards. This is due to the overlapping of powers caused by the different load curves of each building.

From the two-week period graph it can be seen that the amount of the distributed electricity from the grid is reduced, especially in the summer.

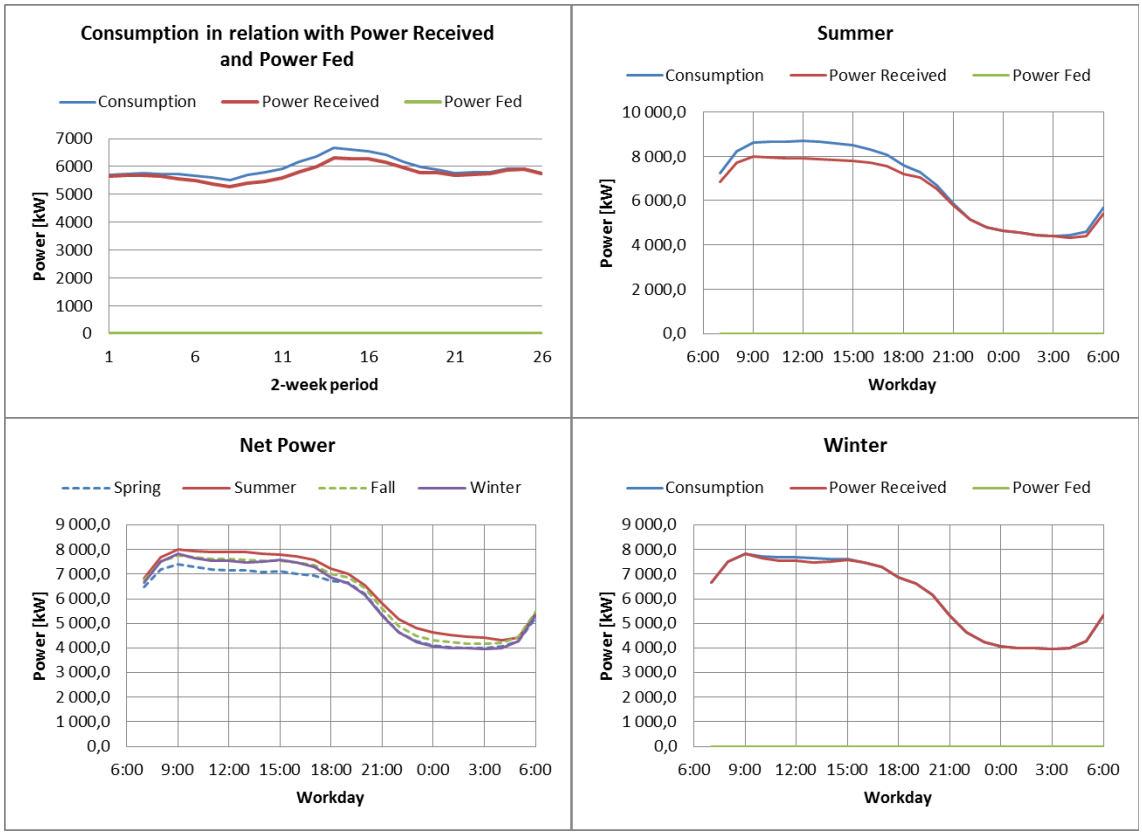

Figure 49: Energy balance of Keilaniemi as a group of office buildings.

The same observations can be seen from the other graphs as well in Figure 49. It is noteworthy to mention that the amount of the electricity purchased from the distribution grid is reduced the highest in the spring. The reason for this is probably the lower need for the cooling energy compared to the summer. Any significant change in the peak load is not clearly visible, since the consumption remains very even during every season throughout the day. However, the solar energy production reduces significantly the amount of the purchased electricity from the grid, except for the winter. In conclusion, all produced solar electricity is consumed within the area of Keilaniemi, and a notable decrease in the amount of the purchased electricity from the grid can be achieved by utilizing the solar electricity production, especially in the spring, summer and fall.

Figure 50 presents the results of the energy balance of Otaniemi. One can tell from the two-week period graph that feeding does not occur to the network at any season. However, the volume of the purchased electric energy from the distribution grid is significantly reduced. The largest decrease in the purchased electricity is experienced in the summer, but also during the winter one can see some benefits of the solar electricity production in the form of reduced need of the distributed electricity.

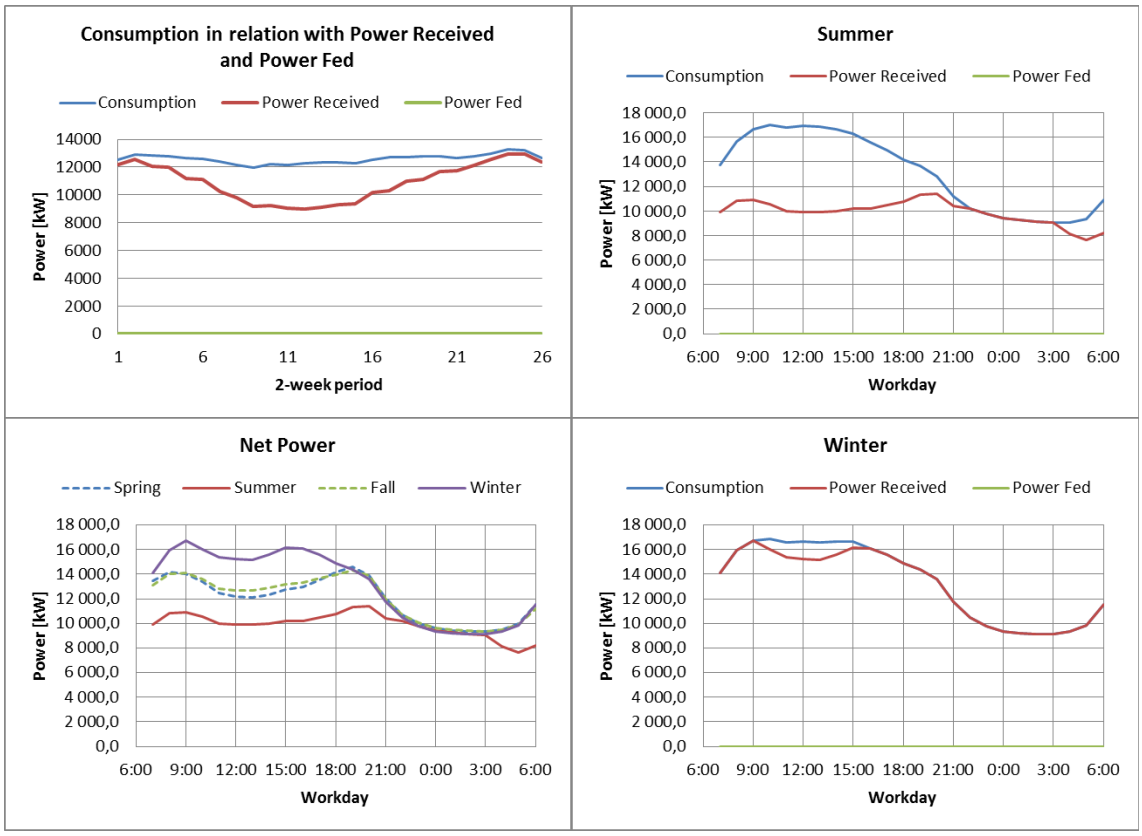

Figure 50: Energy balance of Otaniemi.

From the right-hand side of Figure 50 it can be seen that the peak power in the summer is significantly reduced. Also, the time of the peak load is transferred from 10:00 to 20:00. In spring and fall, the peak power is transferred from 10:00 to 19:00, but the reduction in the peak power is not as high as in the summer. In the winter, neither the peak load nor the time of the peak load is changed, but the demand for the distributed electricity will be reduced to some extent.

The benefits of the solar electricity production in Otaniemi are even higher than in Keilaniemi. The reason for this is most likely that the educational buildings and the business premises in Otaniemi are lower allowing larger roof surface area compared to the electricity consumption. All in all, Otaniemi has a significant potential for the exploitation of the solar electricity production, because all the produced solar electricity can be consumed within the region due to the overlapping of powers and the high rate of the electricity consumption.

The results of the energy balance calculations of Tapiola are shown in Figure 51. From the two-week period graph one can see that even if the demand of the distributed electricity from the distribution network is reduced considerably, the feeding does not take place. In addition, the benefits of the solar electricity production in terms of the decreased need of the distributed electricity are high.

One can tell from the net power and the day-level graphs that the need of the distributed electricity is notably reduced in the summer, spring and fall. In the

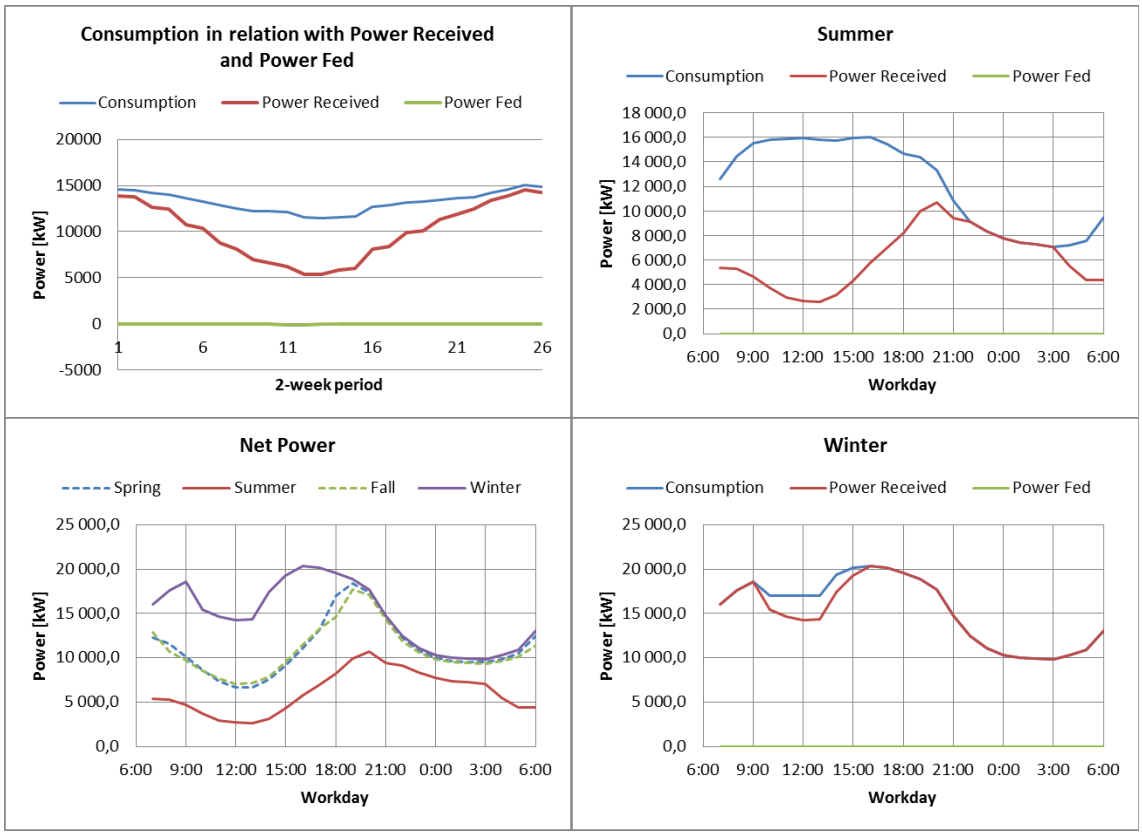

Figure 51: Energy balance of Tapiola.

summer the peak load is reduced approximately by 5 MW, and it is shifted from 16:00 to 20:00. In the spring and fall the peak load is reduced less than in the summer and the time of the peak load is transferred from 16:00 to 20:00. However, in the winter neither the timing nor the size of the peak load is changed, although the solar electricity production reduces the need of the distributed electricity from the distribution network.

Among all the three sub areas of T3 the greatest benefits of the solar electricity production can be achieved in Tapiola. The feeding outside the area does not occur, and all the solar electricity production is consumed within the region as a result of the overlapping of powers.

The results of the energy balance calculations for the whole T3 area are presented in Figure 52. When looking at the two-week period graph on the left it can be seen that feeding does not take place when the whole T3 area is analysed as an own entity. From the same graph it can be seen that all the produced solar electricity can be consumed by the loads within T3. This is very likely due to the overlapping of powers within the region. As one would expect, the biggest benefits from the solar electricity production are experienced in the summer.

From the net power and the day-level graphs one can tell that in the summer, spring and fall the amount of the peak load is reduced notably. In the summer the peak power is not only reduced from approximately 42 MW to 28 MW but is also

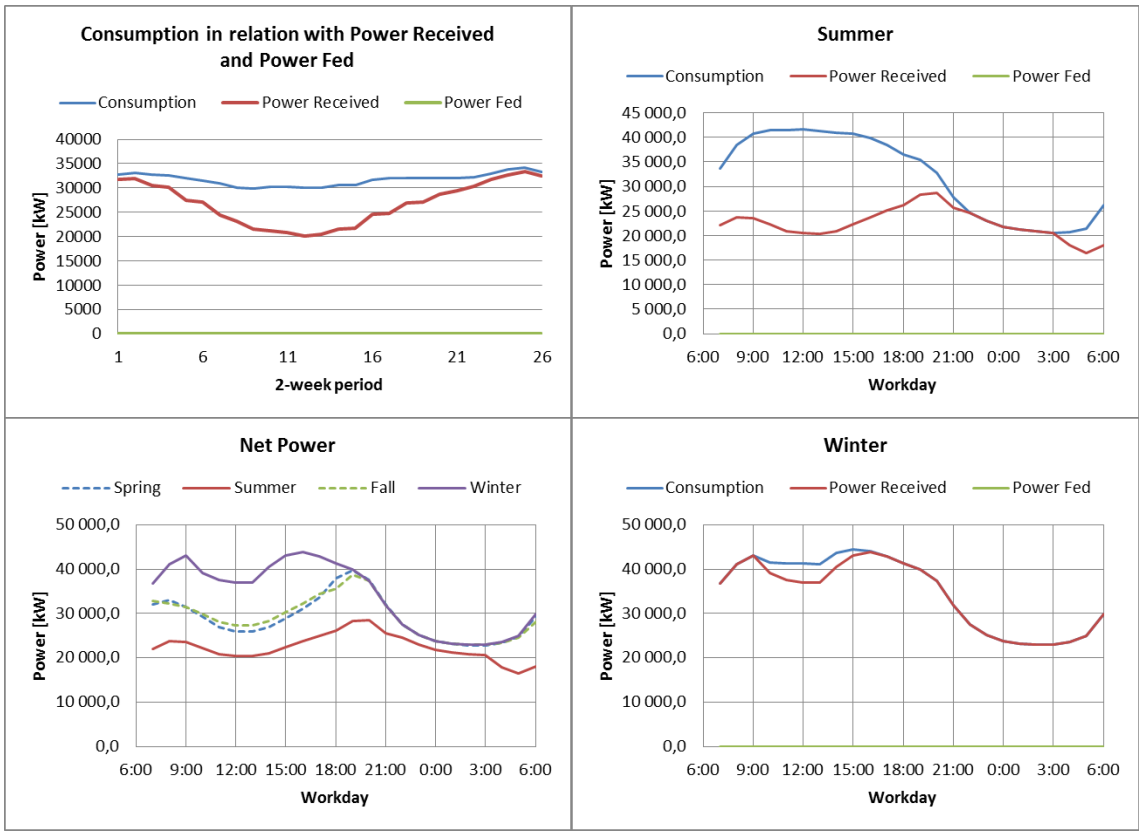

Figure 52: Energy balance of T3.

transferred from 12:00 to 20:00. A reduction of this size (14 MW) corresponds to almost the capacity of a single main transformer (16 MVA) of a substation. In the spring and fall the timing of the peak load is transferred from 12:00 to 19:00. In addition, the amount of the peak load is reduced significantly. Even in the winter time the benefits of the solar electricity production can be seen, although any changes in terms of the timing or the amount of the peak load are not seen.

It can be concluded that the T3 area is very suitable for the solar electricity production as an area, because of its very high utilization rate of the solar electricity production and the non-existence of the feeding outside the T3 area. Thus, it appears that the maximum potential of the solar electricity production in T3, described in the section 4.4.3, could be utilized in full extent inside the T3 area. The same also applies to Keilaniemi, Otaniemi and Tapiola as their own areas.

5.3.4 Energy balance characteristics of different building types

In this section the calculated characteristics of different building types are described. The building types under examination are the most common building types in the T3 area: detached house, apartment house, shopping centre and office. For each building type, calculated key Figures represent the results of a larger sample. Every graph to be presented includes maximum, minimum and average characteristics of each sample of the building types.

Figure 53 presents the ratio of the self usage from the solar electricity production on the left, and the annual reduction of the distributed electricity from the grid on the right. From the left-hand side it can be seen that the only building types that can use all the produced solar electricity are shopping centres, offices and apartment houses. The shopping centre is the only building type where this is the case for all buildings. In the case of the offices the average is 95,8 %. This is probably due to a few smaller office buildings in Keilaniemi with only one floor and smaller consumption. However, the average is significantly high, and as a general rule, all of the solar electricity production can be utilized by the producer in the office buildings without the storage capabilities.

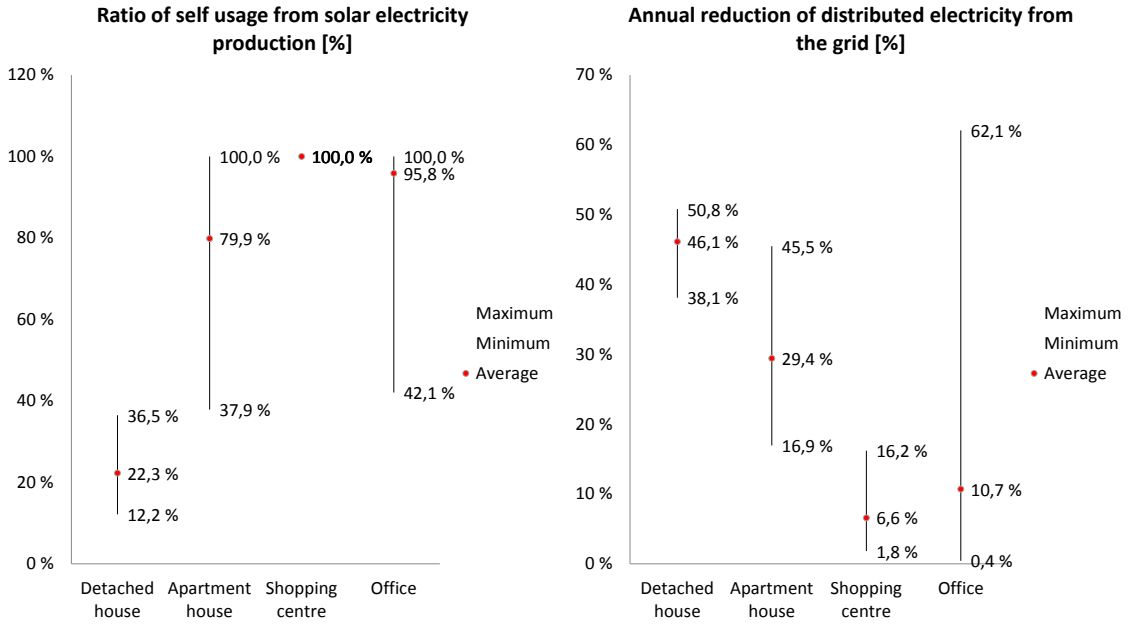

Figure 53: Ratio of self usage from solar electricity production on the left-hand side and annual reduction of distributed electricity from the grid on the right-hand side.

In the case of the apartment houses the average for the ratio of the self usage is 79,9 % which can be considered as a good result. The big difference between the maximum and the minimum is due to the big variation between the available roof surface areas in relation to the electricity consumption. The average ratio of the self usage for the group of the detached houses is 22,3 % being the lowest of the four building types. However, the variation in this building group is relatively small. In the light of the results, it appears that the worst in terms of the self usage of the solar electricity production are the detached houses if the storage is not used. On the other hand, detached houses usually have lower electricity consumption compared to the other building types presented in Figure 53, so the entire roof surface area does not necessarily have to be used to produce solar electricity, which can improve the ratio of self usage.

On the right-hand side of Figure 53, the annual reduction of the distributed electricity from the distribution network is presented. Somewhat unexpectedly, the

largest reduction, about 46.1 % on average, is experienced in the case of the detached houses. Once again, the difference between the maximum and the minimum is the lowest in the detached houses. The apartment houses experience a decrease of approximately 29,4 % on average. In this respect, the reduction of the distributed electricity from the grid is reduced the least in the cases of the shopping centres(6,6 % on average) and the offices (10,7 % on average). The results are likely to be explained by the fact that the consumptions of the detached houses and the apartment houses are often smaller in relation to the shopping centres and the offices. Thus, in relative terms a larger reduction in the office buildings and shopping centres would require significantly higher amounts of roof surface area.

Figure 54 shows the amount of the feeding hours per annum on the left, and the amount of the electricity fed in relation to the electricity distributed from the grid on the right. From the left one can tell that the shopping centre is the only building type with zero feeding hours per annum. This is easy to understand, since the amount of the own usage is 100 %, as presented in the previous Figure. The average amount of the annual feeding hours in the case of the office buildings can be considered as minor even if the number is not zero due to a few small office buildings in Keilaniemi, as explained in the context of the previous Figure. In the case of the apartment buildings the amount of the annual feeding hours is 1375 h on average. However, in the case of the detached houses the amount of feeding hours is approximately three times the amount of the apartment houses. It can be concluded that, the detached houses, in particular, can benefit from the storage capabilities in order to be able to increase the ratio of self usage and to reduce the amount of the annual feeding hours.

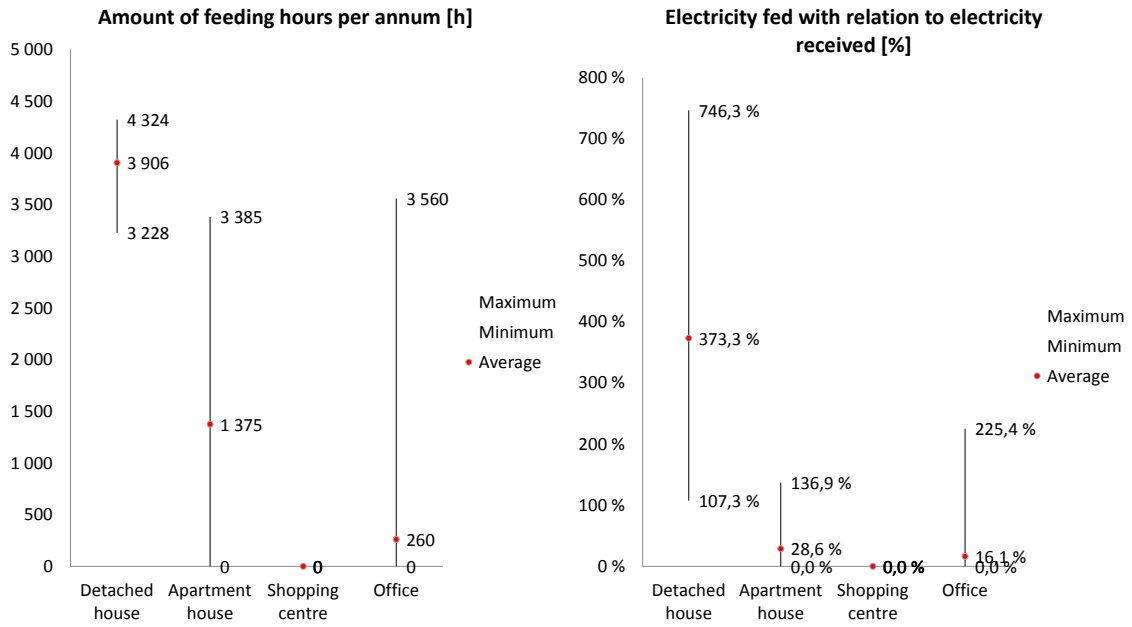

Figure 54: Amount of feeding hours per annum on the left-hand side and electricity fed with relation to electricity received on the right-hand side.

From the right of Figure 54 it can be seen that in the case of the detached houses the amount of the fed solar electricity to the distribution network in relation to the distributed electricity from the grid is 373,3 % on average. If the amount of the electrical energy fed to the grid is almost four times as big as the amount of the distributed electricity from the distribution network, it may cause harm to the power distribution companies in terms of the protection of the low voltage network. However, by using the storages the amount of feeding can be reduced. In addition, the assumption in these calculations is to utilize all the available roof surface areas for the solar electricity production, which makes this situation stand for the worst case scenario. In reality, the utilization rate of the roof surface area may be lower.

In general, the results for the other building types were not alarming on average. However, the offices and the apartment houses have some individual buildings, for which the amounts of the fed electricity exceed the amount of the distributed electricity from the grid. However, these are individual cases, from which one can not draw any conclusions about, as the average results are low in both cases.

Figure 55 presents the reduction of the maximum load estimate on the left-hand side and the maximum feed power estimate in relation to the original maximum load power estimate on the right-hand side. One of the best secondary effects of the solar electricity production from the distribution company point of view is its ability to reduce the peak loads depending on the load type. On average the greatest reduction in the peak load, 4,8 %, can be experienced in the case of the office buildings. The load curve of the office buildings is usually flat which enables a bigger and even reduction of the peak load. The shopping centres usually have a flat load curve as well, for which reason the estimate of the peak load is reduced by 2,7 % on average.

In the case of the detached houses and the apartment houses the load curves

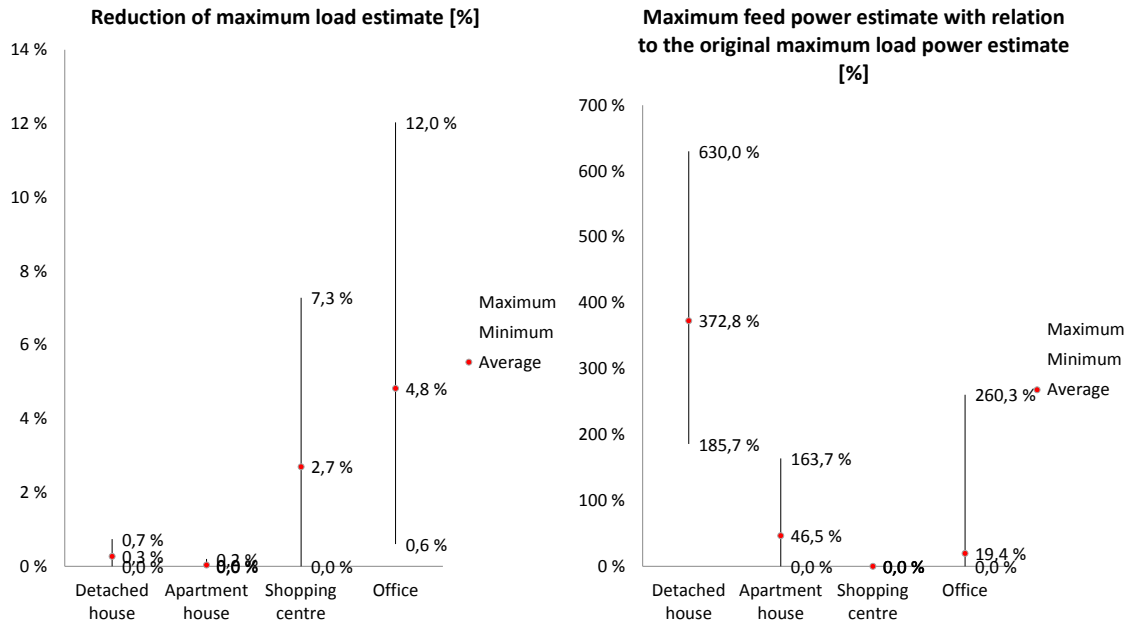

Figure 55: Reduction of maximum load estimate on the left-hand side and maximum feed power estimate with relation to the original maximum load power estimate on the right-hand side.

often include individual peaks in the evening which is why the peaks of the solar electricity production rarely hit the same point, if the storage is not in use. As a result, the reductions in the peak load estimates in these two building types are the lowest on the left in Figure 55.

From the right-hand side of Figure 55 it can be seen that the feeding power estimate of detached houses is approximately 372,8 % from the existing peak load. The relation this big can cause serious disadvantages to the power distribution companies, as they will have to redesign the protection politics on the level of the low voltage networks. Fortunately, the situation presented here stands for the worst case possible as the storage is not assumed to to be used, and all the available roof surface area is utilized for the solar electricity production. It is likely that in real life the entire roof surface area is not utilized for the solar electricity production, and the utilization of the storages equalizes the individual peaks.

In the case of the other building types in the chart on the right, any alarming average values can not be found. However, the apartment houses and the offices have a few individual buildings that exceed the limit of 100 % but as in the Figure 54 these most probably represent individual cases since the averages in both building types are 46,5 % for the apartment houses and 19,4 % for the offices.

5.3.5 Ratio of own usage and system size

The dependencies between the size of the PV system as a percentage from the existing electricity consumption and the ratio of own usage from the solar electricity

production can be examined based on the energy balance calculations made in this thesis. The dependencies were calculated by utilizing the the spreadsheet template made in for the energy balance calculations. The calculations were done to a group of different building types. The building types covered in the calculations are: detached house, detached house with partly accumulating electric heating, shopping centre and office.

The assumption in the calculations is that the storages are not used. In addition, it was assumed that the roof surface area is big enough to cover three times the existing consumption. This assumption is made based on the results presented in Figure 54.

The ratio of own usage from the produced solar electricity as a function of the PV system size in relation to the existing electricity consumption can be seen as an important factor in terms of profitability of the PV system. This is due to the fact that as long as the price of the purchased electricity from the distribution network is more expensive than the compensation paid from the solar electricity production fed into the grid, it is more profitable to use all the produced solar electricity directly on site without feeding.

The consumption of each building type was calculated as an average consumption between all the buildings of each building type in T3. From the electricity consumption data different system sizes between 0 % and 100 % could be calculated. From the different PV system sizes the amounts of solar electricity production could be calculated. After having the amounts of the solar electricity production for all system size combinations the energy balances were calculated in order to be able to calculate the amounts of annual feeding of solar electricity to the distribution grid. From these results the following charts were compiled.

The ratio of own usage as a function of the PV system size in relation to the existing electricity consumption is presented in Figure 56 in the case of the detached house. As it can be seen from the Figure the detached house is able to utilize all the produced solar electricity to a point where the PV system size is approximately 20 % from the existing electricity production. After this point the ratio of own usage decreases significantly being approximately 70 % with a system size of 50 % in relation to the existing electricity consumption. When the system size is exactly the same as the existing electricity consumption the ratio of own usage without storage is approximately 40 %.

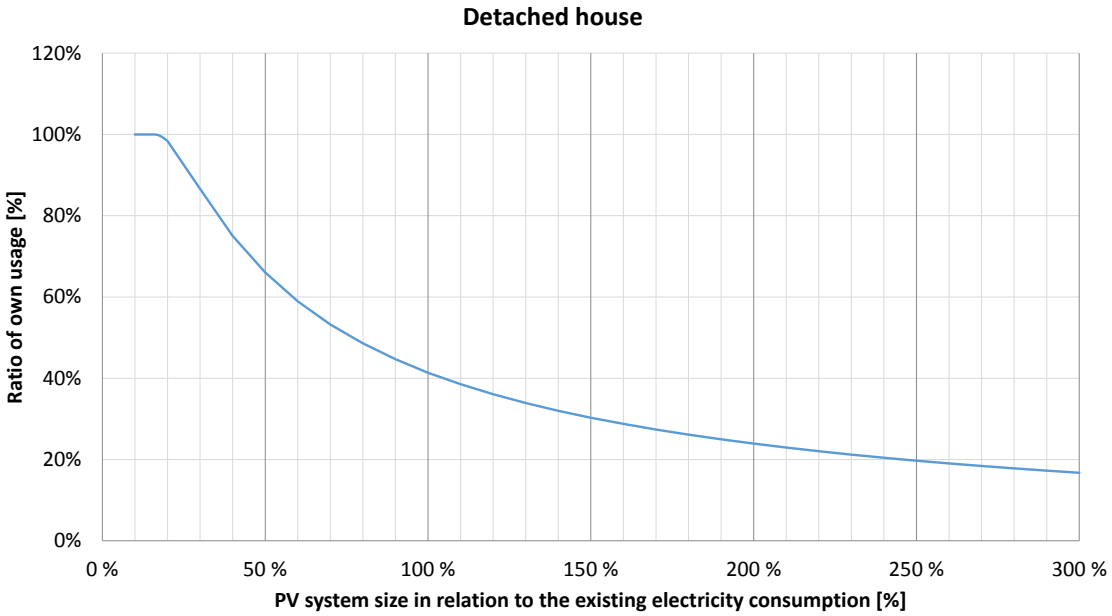

Figure 56: Ratio of own solar electricity usage in the detached house as a function of the size of the PV system in relation to the existing electricity consumption.

From the Figure 56 it can be concluded that the profitability of the PV system in the case of the detached house decreases after the PV system size exceeds 20 % of the existing annual electricity consumption. Therefore, the situation where all the available roof surface areas of the detached house is utilized for solar electricity production is not profitable if the storage is not used.

Figure 57 presents the calculation results for the ratio of own usage as a function of the size of the PV system in relation to the existing consumption for the detached house with partly accumulating electric heating. Unlike in the case of the normal detached house the ratio of own usage starts to decrease when the size of the PV system exceeds 10 % of the existing electricity consumption. This causes the profitability of the PV system investment to decrease if the system is over 10 % from the existing electricity consumption without the storage. It can be seen from the Figure that the ratio of self usage decreases very quickly. With the PV system size of 50 % from the electricity consumption the rate of own usage is approximately 45 %, and with the PV system of 100 % in size the rate of own usage is only about 27 %.

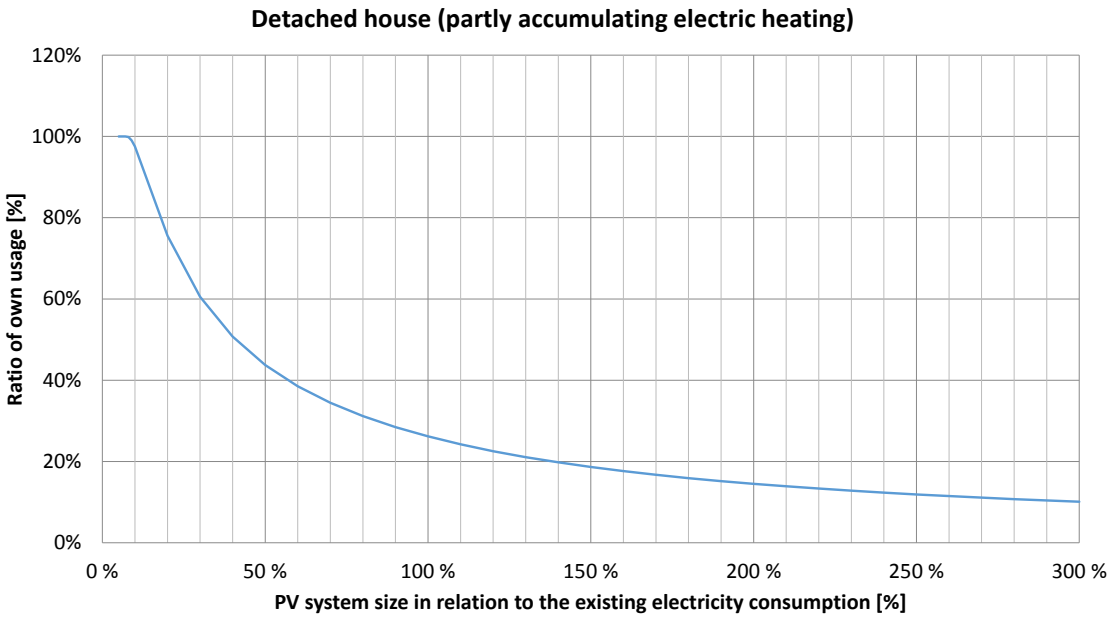

Figure 57: Ratio of own solar electricity usage in the detached house with partly accumulating electric heating as a function of the size of the PV system in relation to the existing electricity consumption.

Compared to the normal detached house the system sizes of the partly accumulating detached house is recommended to be under 10 % of the electricity consumption, while in the case of detached house with district heating the system size can be as much as 20 % of the electricity consumption from the profitability point of view. It should be noted, however, that this recommendation assumes that the price of the electricity purchased from the distribution network is higher than the price paid for the feeding of the surplus production. It is further assumed that the solar electricity storage is not in use.

The effect of the PV system size in relation to the electricity consumption on the ratio of self usage in the case of the office building is illustrated in Figure 58. One can tell from the Figure that the limit of the system size for the office building seems to be 20 % as in the case of the detached house. However, it should be noted that the annual consumption of the office building is usually much higher compared to the consumption of the detached house, which means that 20 % of the annual electricity consumption of the office building stands for a rather large system, and therefore the size of the PV system in the office buildings can be much higher in terms of the rated power than in the detached house, even though the relative limit for the system size is the same.

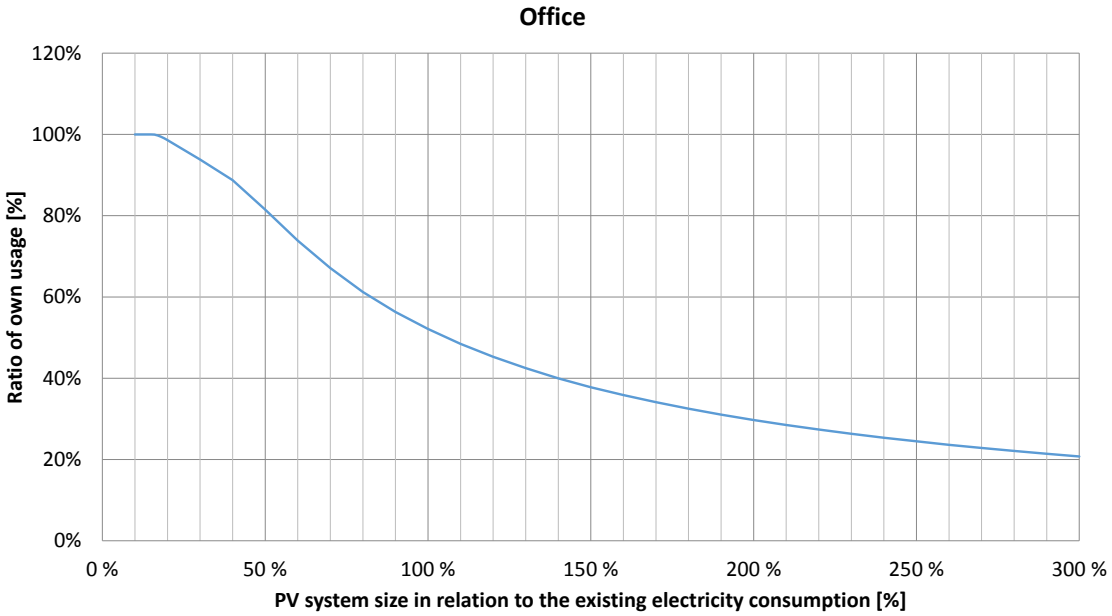

Figure 58: Ratio of own solar electricity usage in the office as a function of the size of the PV system in relation to the existing electricity consumption.

Compared to the chart of the detached house the ratio of self usage decreases slower in the case of the office building. When the relative system size is 50 % of the electricity consumption the rate of own usage is still over 80 %. Even with the systems size of 100 % of the electricity consumption the ratio of self usage is over 50 %.

Figure 59 illustrates the ratio of self usage for the shopping centre in relation to the electricity consumption. From the chart it can be seen that even with the PV systems of 30 % of the electricity consumption the rate of own usage stays at 100 %. In addition, the reduction of the ratio of own usage is slow as in the case of the office building.

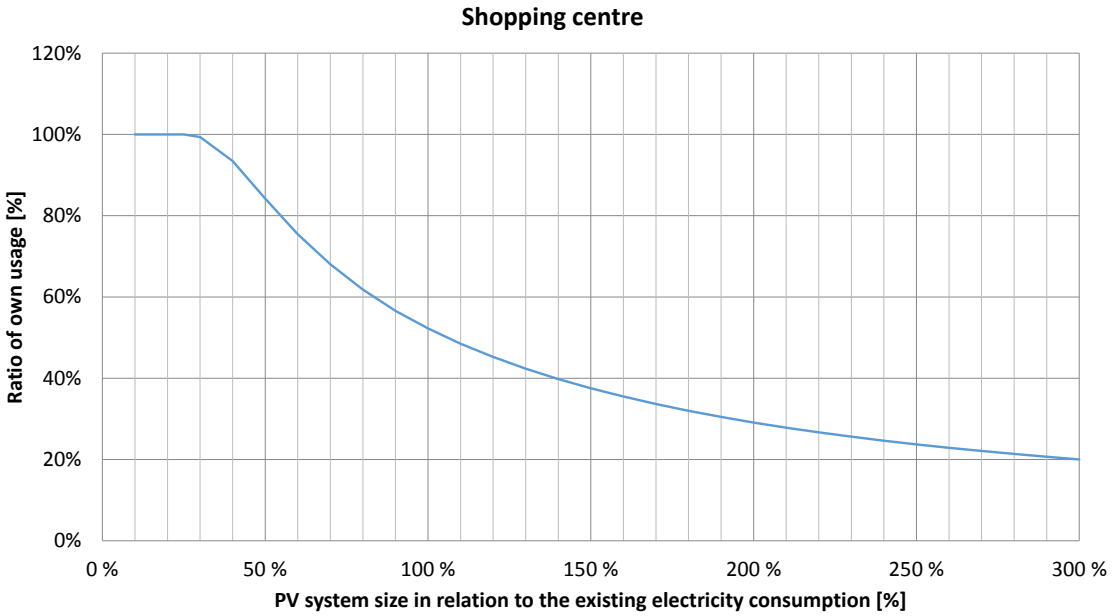

Figure 59: Ratio of own solar electricity usage in the shopping centre as a function of the size of the PV system in relation to the existing electricity consumption.

The ratio of self usage in the case of the shopping centre is the best of all presented building types. As the consumption of the shopping centre is usually high the relative size of 30 % for the PV system in relation to the existing electricity consumption leads to a very large PV system. In summary it can be said that shopping centres seem to be profitable targets for the solar electricity production, because in the case of the shopping centres the consumption is generally very high due to, for example, the need for cooling energy. Therefore, it may be difficult to build a PV system that would turn the ratio of own usage under 100 % without the storage. The same feature applies to the office buildings.

6 Conclusions

The main purpose of this thesis was to evaluate realistic solar electricity production potential of grid-connected photovoltaic systems in Tapiola district. The calculations were based on the SEES data delivered by the city of Espoo. In order to determine the most realistic maximum potential of solar electricity production, three filters were developed to eliminate all the roof surface areas unsuitable for solar electricity production. The three filters are: profitability filter, city planning filter and filter for mechanical barriers. It was found that the realistic potential of the annual solar electricity production in the T3 area is approximately 44 GWh/a. This represents approximately 15,6 % of the existing annual electricity consumption of the T3 area.

Based on the calculations of the realistic potential of the solar electricity production in the T3 area the energy balances of different building types were calculated. Calculations were carried out by utilizing load curves and index series calculation. In addition, a model for solar electricity production by Hannu-Pekka Hellman was utilized. The energy balances were calculated for individual buildings, blocks of buildings and for the sub-areas of T3. It was found that offices and shopping centres can be considered as highly potential targets for the solar electricity production because of the high rate of own usage and lack of feeding to the distribution grid. However, the detached houses were found to cause a lot of feeding to the distribution network due to the high amount of the roof surface area in relation to the electricity consumption. For this reason, it would be useful to further process the results obtained in this thesis by examining the possibilities of storage capabilities and load management opportunities in order to prevent possible difficulties from the protection of the distribution grid point of view. All the sub-areas of T3 were found to consume all the produced solar electricity within the region because of the overlapping of powers. For this reason it is possible to utilize the large potential of the solar electricity production of T3 to a significant extent.

Based on the results obtained from the energy balance calculations it was possible to examine the relations between the size of the PV system in relation to the annual electricity consumption and the ratio of own usage from the solar electricity production. It was found that for the detached houses the ratio of own usage begins to decrease when the size of the PV system exceeds 20 % of the existing annual electricity consumption. The shopping centres were found to be the best building types in this sense, since their ratio of own usage starts to decline slowly when the size of the PV system exceeds 30 % of the annual electricity consumption. In addition, the office buildings were found to perform well. The results of the ratio of own usage and the size of the PV system in relation to the electricity consumption can be exploited for a more precise profitability analysis in order to examine the current situation and the development of the Finnish photovoltaic markets.

The major criticisms with respect to the results of energy balance are associated with both the solar electricity production model and the load curves. The solar electricity production model assumes that each hour in a day has its own amount of production that stays the same one month at a time. As a result, there is only 12 variations for each hour of a day during a year. This is not the case in real

life. In reality the length of the day varies every day. In addition, the production conditions are constantly changing and can vary significantly even during one hour due to different weather conditions.

The other criticism, the load curves, assume that certain types of buildings behave in the same way in terms of the consumption. This reduces the overlapping of powers in relation to the real-world situation, because in fact, even within a single apartment building the behaviours of the consumptions of each apartment differ from each other. Therefore, in reality the impact of the overlapping of powers is likely to be even higher than the load curves modelling suggests. In the future, loads can be modelled in more detail by utilizing the hourly measurement data of AMR (Automatic Meter Reading) smart meters. Thus, the network effects of the decentralized production can be simulated more precisely and more reliably.

In the future, it would be beneficial to examine the effects of storage capabilities and load control on the energy balance and on the rate of own usage from the solar electricity production. In addition, the effects of the solar electricity production on the protection politics of the distribution network should be examined thoroughly, for example by exploiting simulations in the network information system in order to deepen the understanding of power distribution companies about the requirements of the decentralized production in the grid.

References

[1] European Photovoltaic Industry Association (EPIA) and Greenpeace International, "Solar generation 6." Available at: http://www.epia.org/index.php?eID=tx_nawsecuredl&u=0&file=/uploads/tx_epiapublications/Solar_Generation_6__2011_Full_report_Final.pdf&t=1385333524&hash=2a61ff48cc67da85ce51d38b1120b9799a1a847c, Feb. 2011. Accessed: Oct. 29, 2012.

[2] VTT, VATT, CEA, MDI, BOFIT, and TKK, *Energy Visions 2050*. Porvoo: WS Bookwell Oy, 2009.

[3] U.S. Energy Information Administration (EIA), "International energy outlook 2013." Available at: http://www.eia.gov/forecasts/ieo/, July 2013. Accessed: Dec. 29, 2013.

[4] European Commission, "Europe 2020 targets." Available at: http://ec.europa.eu/europe2020/pdf/targets_en.pdf, Apr. 2011. Accessed: Dec. 29, 2013.

[5] RYM Ltd, "Energizing urban ecosystems." Available at: http://rym.fi/fi/program/energizing-urban-ecosystems-eue-2/, 2012. Accessed: Dec. 29, 2013.

[6] National Aeronautics and Space Administration (NASA), "Solar system exploration." Available at: http://solarsystem.nasa.gov/planets/profile.cfm?Object=Sun&Display=OverviewLong, May 2012. Accessed: Aug. 1, 2012.

[7] National Aeronautics and Space Administration (NASA), "The solar interior." Available at: http://solarscience.msfc.nasa.gov/interior.shtml, Dec. 2012. Accessed: Aug. 1, 2012.

[8] Teollisuuden voima Oyj (TVO), "Olkiluoto 3 (OL3)." Available at: http://www.tvo.fi/OL3. Accessed: Aug. 1, 2012.

[9] S. A. Kalogirou, *Solar energy engineering: processes and systems*. Academic Press, 2009.

[10] M. Ross and J. Royer, *Photovoltaics in cold climates*. James and James Science Publishers Ltd, 1999.

[11] J. Ventre and R. A. Messenger, *Photovoltaic systems engineering*. CRC press, 2004.

[12] G. P. Smestad, *Optoelectronics of solar cells*. SPIE press, 2002.

[13] A. Luque and S. Hegedus, *Handbook of photovoltaic science and engineering*. John Wiley & Sons, 2011.

[14] S. R. Wenham, M. A. Green, M. E. Watt, R. Corkish, and A. Sproul, *Applied photovoltaics*. Routledge, 2011.

[15] B. Erat, V. Erkkilä, C. Nyman, K. Peippo, S. Peltola, and H. Suokivi, *Aurinko-opas - aurinkoenergiaa rakennuksiin*. Aurinkoteknillinen yhdistys ry, 2008.

[16] M. R. Patel, *Wind and solar power systems: design, analysis, and operation*. CRC press, 2006.

[17] C. F. Bohren and E. Clothiaux, *Fundamentals of atmospheric radiation*. Wiley-VCH, 2006.

[18] NOAA Earth System Research Laboratory, "NOAA solar calculator." Available at: http://www.esrl.noaa.gov/gmd/grad/solcalc/. Accessed: Aug. 1, 2012.

[19] PHOTON Publishing, "Solar Module Database." Available at: http://www.photon.info/photon_site_db_solarmodule_en.photon?ActiveID=5352. Accessed: Aug. 31, 2012.

[20] M. D. Archer and R. Hill, *Clean electricity from photovoltaics*. Imperial College Press, 2001.

[21] M. Šúri, T. A. Huld, E. D. Dunlop, and H. A. Ossenbrink, "Potential of solar electricity generation in the european union member states and candidate countries," *Solar energy*, vol. 81, no. 10, pp. 1295–1305, 2007.

[22] University of Gothenburg, "The SEES model." Available at: http://www.gvc.gu.se/Forskning/klimat/stadsklimat/gucg/software/sees/. Accessed: Oct. 15, 2012.

[23] WSP Analysis & Strategy and Urban Climate Group and Department of Earth Sciences from University of Gothenburg, "SEES - Solar Energy from Existing Structures, User manual for version 1." Available at: http://www.gvc.gu.se/digitalAssets/1366/1366440_sees_help_v11.pdf, Feb. 2011. Accessed: Oct. 18, 2012.

[24] O. Raunio, "SEES Espoo - Solar Energy from Existing Structures in Espoo," tech. rep., WSP Finland Oy, Apr. 2012.

[25] World Design Capital Helsinki 2012, "Espoo." Available at: http://wdchelsinki2012.fi/kaupungit/espoo, 2012. Accessed: Mar. 29, 2013.

[26] World Design Capital Helsinki 2012, "Faktat ja luvut." Available at: http://wdchelsinki2012.fi/sites/default/files/faktat_ja_luvut.pdf, 2012. Accessed: Mar. 12, 2013.

[27] Espoon kaupunki, "Tapiola." Available at: http://www.espoo.fi/fi-FI/Asuminen_ja_ymparisto/Kaupunginosat/Tapiola, Jan. 2012. Accessed: Mar. 12, 2013.

[28] Tapiolan tulevaisuusryhmä, *Tapiola huomenna–Tapiolan tulevaisuustyöryhmän raportti*. Espoon kaupunkisuunnittelukeskus, 2003.

[29] Museovirasto, "Valtakunnallisesti merkittävät rakennetut kulttuuriympäristöt - Tapiola." Available at: http://www.rky.fi/read/asp/r_kohde_det.aspx?KOHDE_ID=1359, Dec. 2009. Accessed: Mar. 13, 2013.

[30] Asiakirjahallinto-, käännös- ja tietopalvelut, *Espoon asukasluku vuodenvaihteessa 2011/2012*. Espoon kaupunki, 2012.

[31] Museovirasto, "Valtakunnallisesti merkittävät rakennetut kulttuuriympäristöt - Otaniemen kampusalue." Available at: http://www.rky.fi/read/asp/r_kohde_det.aspx?KOHDE_ID=1360, Dec. 2009. Accessed: Mar. 13, 2013.

[32] Espoon kaupunki, "Aluejakokartat." Available at: http://www.espoo.fi/fi-FI/Espoon_kaupunki/Tietoa_Espoosta/Tilastot_ja_tutkimukset/Aluejakokartat, Jan. 2012. Accessed: Mar. 13, 2013.

[33] Open Source Geospatial Foundation (OSGeo), "Quantum GIS." Available at: http://www.qgis.org/. Accessed: Jun. 16, 2013.

[34] Eero Vartiainen, Solar Technology Manager, Fortum Oyj. Private interview. Espoo, Aug. 31, 2012.

[35] Robert Eriksson, Architect, City Planning Department of Espoo. Private interview. Espoo, Jun. 18, 2012.

[36] Arkkitehtuurimuseo, "Tapiolan puutarhakaupunki - luettelo kohteista." Available at: http://www.mfa.fi/luettelokohteist, 2012. Accessed: Mar. 14, 2013.

[37] Espoon kaupunki and Museovirasto, *Tapiola - vanhojen asuntoalueiden korjauksen ja hoidon suuntaviivat*. Espoon kaupunki, Kaupunkisuunnittelukeskus, 2006.

[38] E. Härö, *Espoon rakennuskulttuuri ja kulttuurimaisema*. Espoon kaupunginmuseo, 1991.

[39] Markus Andersén, Sales Director, Naps Solar Systems Oy. Phone interview. Espoo, Sep. 12, 2012.

[40] E. Vartiainen, *Daylight Modelling and Optimization of Solar Facades*. Helsinki University of Technology, 2000. Doctoral thesis.

[41] Maanmittauslaitos, "Karttapaikka." Available at: http://kansalaisen.karttapaikka.fi/kartanhaku/osoitehaku.html?lang=fi. Accessed: Apr. 14, 2015.

[42] Yliopiston almanakkatoimisto, "Kalenterit 2000-." Available at: http://almanakka.helsinki.fi/fi/arkisto/kalenterit-2000.html. Accessed: Jan. 14, 2015.

[43] H.-P. Hellman, M. Lehtonen, and M. Koivisto, *Photovoltaic power generation modeling*. Aalto University School of Electrical Engineering, 2011. Conference paper.

[44] Suomen Sähkölaitos r.y., *Sähkön käytön kuormitustutkimus 1992*. Suomen Sähkölaitos r.y., 1992.